Vol.1, No.1, April 2010

Advances in Bioscience and Biotechnology

www.scirp.org/journal/abb

Scientific Research

Journal Editorial Board

http://www.scirp.org/journal/abb

TABLE OF CONTENTS

Volume 1, Number 1, April 2010

Advances in Bioscience and Biotechnology (ABB)

Journal Information

SUBSCRIPTIONS

The *Advances in Bioscience and Biotechnology* (Online at Scientific Research Publishing, www.SciRP.org) is published monthly by Scientific Research Publishing, Inc., USA.

Subscription rates:

Print: $50 per issue.
To subscribe, please contact Journals Subscriptions Department, E-mail: sub@scirp.org

SERVICES

Advertisements
Advertisement Sales Department, E-mail: service@scirp.org

Reprints (minimum quantity 100 copies)
Reprints Co-ordinator, Scientific Research Publishing, Inc., USA.
E-mail: sub@scirp.org

COPYRIGHT

PRODUCTION INFORMATION

For manuscripts that have been accepted for publication, please contact:
E-mail: abb@scirp.org

Advances in Bioscience and Biotechnology, 2010, 1, 1-6 **ABB**
doi:10.4236/abb.2010.11001 Published Online April 2010 (http://www.SciRP.org/journal/abb/).

The effects of neem [*Azadirachta indica A*. Juss (*meliaceae*)] oil on *Fusarium oxysporum* f. sp. *medicagenis* and *Fusarium subglutinans* and the production of fusaric acid toxin

Marcia Regina Ferreira Geraldo[1], Carla Cristina Arroteia[2], Carlos Kemmelmeier[2,*]

[1]Universidade Tecnológica Federal do Paraná, Campo Mourão, Brazil;
[2]Departamento de Bioquímica, Universidade Estadual de Maringá, Avenida Colombo, Maringá, Brazil.
Email: ccarroteia@uem.br; ckemmelmeier@uem.br; mperdoncini@ibest.com.br

Received 25 February 2010; revised 8 March 2010; accepted 10 March 2010.

ABSTRACT

Fungi of the genus *Fusarium* are well known plant pathogens, cause several vascular diseases and are producers of toxins. *In vitro* assays evaluated the effects of Neem (*Azadirachta indica*) oil on the diameter of colonies, dry weight, spore production, spore viability and production of Fusaric Acid toxin on *Fusarium oxysporum* f. sp. *medicagenis* and *Fusarium subglutinans* isolates. Effects of Neem oil were analyzed at concentrations 0.25%, 0.5% and 1% in Czapek Yeast Agar medium. The production of Fusaric acid was determined by Thin Layer Chromatography and quantified by UV spectrophotometry. Neem oil showed inhibitory effects on the isolates tested, although they varied according to type of isolate and oil concentration. Neem oil was efficient in reducing the colonies' diameter and dry weight in concentration-dependent manner. Neem oil was efficacious at higher concentration in the decrease of sporulation. Spore germination was affected by Neem oil when the spore was grown in Neem-contained medium as when the spore emerged from a culture in a Neem medium. Neem oil decreased and even inhibited the production of Fusaric acid by the assayed isolates. Since these isolates are plant pathogens and producers of Fusaric acid, Neem oil may be introduced as an integral item in the management of host plants.

Keywords: Fusarium; Azadirachta Indica; Fusaric Acid; Antifungal Activity

1. INTRODUCTION

Fungi of the genus *Fusarium*, known to be plant pathogens causing several vascular diseases, are largely distributed in soils, especially cultivated ones, and are active during the decomposition of cellulose material [1]. *Fusarium* spp. is the main colonizer of pre-harvest cereal grains, even though it may also occur in grain storage, especially under high humidity conditions [2]. *Fusarium oxysporum* f. sp. *medicagenis* is a important pathogen for alfafa (*Medicago sativa* L.), whereas *Fusarium moniliforme* f. sp. *subglutinans* = *Fusarium subglutinans* [3,4] is a pathogen for maize, sugarcane and other grasses.The above mentioned fungi are producers of mycotoxins with special reference to fusaric acid (5-butylpicolinic acid), which has a hypotension effect in several animals due to an increase in dopamine in the brain and to other peripheral effects in the tryptophan metabolism [5,6]. It not only interferes with animal food consumption, but also increases the toxicity of other mycotoxins [7]. Expectedly, the mycotoxin is rarely found alone in *Fusarium*-contaminated grains. This fact increases its importance in mycotoxicoses since this condition heightens the Fusaric acid's interactivity with other toxins, such as fumonisins and moniliformin [8,9]. Fusaric acid was one of the first fungus metabolites isolated from plants with Fusarium wilt and subsequently shown to be involved in the symptoms [9]. It is currently known to cause phytotoxic symptoms in several plants that develop Fusarium wilt. There are positive correlations between the production of the compound and the fungus virulence in the host [10]. Studies with several Fusaric acid-treated plants revealed that it inhibited respiratory activities [11-13]; decreased levels of adenosine triphosphate, increased the release of electrolytes [13], caused changes in the difference of transmembrane electrical potential [14]; disturbed nitrogen metabolism, decreased cell viability and induced apoptosis [12]; inhibited enzyme activities of plant defense [15-17]; induced plant's symptoms such as chlorosis, necrosis, inhibition and lengthening of roots [18,19]; and caused loss of weight in the plant [20].

Inhibiting chemical agents, mainly low molecular weight organic acids used in the preservation of stored grains [21], have exhibited several problems related to

the development of fungus resistance and the emergence of secondary pests owing to their indiscriminate use [22]. This fact has increased risks of high toxic residue levels, which damage the environment and put human and animal health at risk. Plants' natural extracts may be an alternative for the employment of these synthetic antifungal chemical agents since they may be easily acquired and employed, they are low cost and lack the problems inherent to synthetic chemical products [23].

The Neem (*Azadirachta indica* A. Juss) is a dense-leaved tree of the *Meliaceae* family whose biologically active extracts are obtained from its leaves, seeds, fruits and trunk, with acknowledged multiple therapeutic, insecticide, nematicide, anti-microbial and fungicide qualities [24-26]. Several studies show that Neem water and oil extracts are toxic to fungi [27-31] and may result in the reduction or inhibition of mycotoxin production [32-36]. Great interest exists in verifying the effects of the plant's extract on the fungi *Fusarium oxysporum* f. sp. *medicagenis* and *Fusarium subglutinans*, due to the fact that if there is an inhibitory activity, the extract may be tested in host plants for the control of this pathogen. This is the main purpose of the present study.

2. MATERIAL AND METHODS

2.1. Neem Oil

Neem Oil (NO) was commercial product (BioNeem®) extracted from the seeds of the neem plant.

2.2. Fungal Isolates

Isolates of *Fusarium oxysporum* f. sp. *medicagenis* UnB 201 and *Fusarium subglutinans* UnB 335 and UnB 327 were the test organisms used. They were stored in Potato Dextrose Agar (PDA) of the fungus collection at the Laboratory of Chemistry and Physiology of Microorganisms of the Biochemistry Department, State University of Maringá. Maringá. PR Brazil.

2.3. Effects of NO on the Colony Diameter, Dry Weight, Sporulation and Spore Viability

Assays were carried out according to technique described by Marques *et al.* [37]. Culture media employed were Malt Extract Agar (MEA) and Czapek Yeast Agar (CYA) [38]. CYA was prepared by adding NO to the medium to obtain concentrations of 0.25%, 0.5% and 1%, which were the test media. CYA without NO was the control medium. Isolates were pre-incubated in MEA during four days, at 25ºC. Plugs were retrieved from these colonies by a 5 mm-sterilized metallic ring and inoculated in 95 mm-Petri dishes with media control CYA (without NO) and with CYA tests (with NO at concentrations 0.25%, 0.5% and 1.0%).

Isolates were inoculated in media CYA control and tests at 25ºC, during seven days, to verify colonies' diameter. Colony's diameter was determined by measuring two diameters, in mm, of each colony on the seventh day of incubation.

Dry weight was determined after seven days of incubation of isolates, at 25ºC, in media CYA control and tests. Media were liquefied and mycelium was retrieved by a pincer and placed on a weighted filter paper. Papers with mycelia were dried at 70ºC. After 72 h, they were weighted daily until completely dried.

Spores production was evaluated by placing 10 mL of a 1:1 mixture consisting of a sterilized solution NaCl (0.89%, w/v) and Tween 80® (0.1%, v/v), on the incubated mycelium, after 7 days, at 25ºC, in media CYA control and tests. After spores were removed by scraping all the mycelia, they were transferred to a test tube and counted under a microscope in a Neubauer chamber. Dilution of suspension was employed when required. Results were given in spores/mm^2 of colony. Spores viability (germination) was evaluated by their cultivation in cellophane membranes, previously cut 2 cm × 2 cm size, dipped in distilled water in an Erlenmeyer flask and sterilized. Two situations were employed to verify spore viability: *Experiment* 1 - membranes were placed in CYA plates; each plate had one of the Neem oil concentrations mentioned above; they were then inoculated with spore suspensions from grown colonies in CYA without Neem oil, after incubation for four days, at 25 ºC; *Experiment* 2 - membranes were placed in plates with medium CYA without Neem oil. Inoculation was undertaken with spore suspensions from colonies grown in CYA with one of the different Neem oil concentration mentioned above, after incubation during four days, at 25ºC. Assays were undertaken by inoculating 0.1 mL of fungus suspension with 10^5 spores mL^{-1} on each membrane. Plates with incubated membranes were then incubated at 25ºC, in the dark, during 15 h. Drops of lactophenol cotton blue staining were then placed on grown membranes to impair germination and facilitate visualization of spores. By 400× microscope, 150 spores in each area of the lamina were counted. Germinated and non-germinated spores were counted and germination percentage established.

2.4. Effects of Neem Oil on the Production of Fusaric Acid (FA)

Assay was undertaken according to technique described by Eged [39]. Isolates were previously cultivated in MEA at 25ºC. After a four-day incubation, 5 mm diameter plugs of the culture were transferred to Petri plates with CYA control (without Neem oil extract) and tests (with 0.25%, 0.5%, 1.0% of Neem oil) and cultivated, during 7 days, within the same conditions. Media were liquefied after incubation and mycelia removed with a pincer. Liquefied medium was employed to extract FA since the mycotoxin is deposited in the extracellular me-

dium by the fungus.

2.5. Extraction and Quantification of FA

Hydrochloric acid at 2N was added to the medium to readjust pH to 3.9 - 4.0. Further, FA was extracted thrice with 30 mL of ethyl acetate in a separation funnel. The three extracts were put together and evaporated in a rotating evaporator at 50ºC, until complete dried. Residue was re-suspended in a 3 mL ethanol 80% water solution.

2.6. Detection and Quantification of FA by Thin Layer Chromatography (TLC), and UV Spectrophotometry

Basically the procedure described by Eged [39] was followed. In the case of TLC, 20 × 20 cm aluminium plates (Alugram®, Macherey-Nagel), coated with silica gel 60 (fluorescence indicator UV_{254}) were employed. Plates were first dipped in a chromatography development solution (n-butanol : acetic acid : ethyl acetate : water 3:2:2:2 v/v), dried and activated at 80ºC during 5-7 minutes. Further, 5-10 µL of the standard solution of Fusaric acid 0.2% (Acros Organics ®) and 30 µL of the fungus residue extract solution were spotted on the activated TLC plate. After development (*Rf* = 0.58 - 0.60), the plates were dried and observed under a 254 nm UV light. Sites with FA were cut from the plate and eluded with 3 mL ethanol liquid solution 80% (UV grade) during one hour. The contents of the FA in each sample were then determined by spectrophotometry (λ 270 nm absorbance - UV-VIS spectrophotometer Shimadzu mini 1240, Japan).

Quantification of FA was undertaken according to standard calibration of FA (1 g Fusaric acid / 10 mL distilled water). Resulting quantity of FA was calculated according to the quantity of sample applied in the TLC plate in µg FA per gram of mycelial dry weight. All described experiments were carried out four times. Treatment results were evaluated statistically by one-way variance analysis (ANOVA), probability 1% ($p < 0.01$); in the case of significant difference, means were analyzed by Tukey's test ($p \leq 0.05$), with the statistical program SAS (Statistical Analysis System. Sas Institute Inc., Cary, NC, USA, 2001).

3. RESULTS AND DISCUSSION

The effects of Neem Oil (NO) on the tested *Fusarium* isolates varied according to the isolate and NO concentrations (**Table 1**).

Neem oil was efficacious in reducing the diameter and dry weight in a concentration-dependent manner. Reduction of colonies' diameter occurred in all isolates: reduction was highest according to increase in oil concentration. In isolates 335a and 327, NO reduced the dry weight at the lowest concentration (0.25%). As NO con centration increased, the reduction of dry weight increased. Dry weight reduction in isolate 201 was effective in concentrations 0.5% and 1% of NO (**Table 1**).

NO at higher concentrations was efficient in sporulation decrease. The number of spores in isolates 201 and 335a were lower only in an oil concentration of 1%, but only statistically significant only for the isolate 327. An increase in sporulation occurred at lower concentrations. Sporulation of isolate 327 was reduced as from oil concentrations at 0.5% (**Table 1**).

When spores were collected in colonies grown in a NO-less medium and germinated in a medium with different oil concentrations (**Table 1**-VS 1), germination of spores was significantly influenced only in concentration 1%. Isolate 335a had its germination affected as from oil concentration 0.5%. On the other hand, when spores obtained from media with different Neem concentrations and germinated in NO-less medium (**Table 1**-VS 2), spore viability was not affected in isolate 327, which did not differ significantly from control. There was a decrease in spore viability in isolate 335a at all concentrations. This fact shows that spore germination is isolate-dependent and may be affected by NO either when the spore is grown in a medium with Neem or when the spore emerges in a medium with Neem. However, in the context of isolates tested in current assay (**Table 1**), the isolate 201 had the highest germination susceptibly to NO.

The production of Fusaric acid (FA) by the isolates (**Table 1**) was affected by NO Neem oil significantly reduced the production of FA, in proportion to oil concentration increase at all concentrations tested in isolate 327. Fusaric acid failed to be detected either in concentration 1% for isolate 327 or in all concentrations for isolate 335a. The latter, however, produced the lowest quantity of FA when compared to the other two isolates. Results show that NO may significantly reduce or even inhibit the production of FA by the isolates under analysis. Several assays with other fungi and toxins have shown similar results. Fungitoxic effects indicate that Neem extracts block the biosynthesis pathway of aflatoxin in *Aspergillus parasiticus* [31]; citrinin in *Penicillium citrinum* [35]; penicillic acid in *Penicillium cyclopium* [33]; patulin in *Penicillium expansum in vitro* [34] and in contaminated apples [32].

Although sporulation is typically followed by toxin production, its occurrence does not happen at all times. In fact, mycotoxins may be produced at high levels in growth conditions which inhibit sporulation [40]. In certain concentrations, as the current research showed, a sporulation stimulus occurred and, at the same time, a reduction in toxin production. Nevertheless, there was no relationship between sporulation and toxin inhibition

Table 1. Effects of Neem oil (NO) in *Fusarium oxysporum* f. sp. *medicagenis* (201) and *Fusarium subglutinans* (327 and 335a) isolates.

Isolates		Control	NO 0.25%	NO 0.5%	NO 1%
201	Diameter	82.5^{a} (±0.58)	65^{b} (±1.15)	57^{c} (±1.15)	49.5^{d} (±0.58)
	Dry weight	0.063^{a} (±0.01)	0.038^{ab} (±0.02)	0.035^{b} (±0.01)	0.018^{b} (±0.01)
	S (x10^{4}/mm^{2})	0.08374^{b} (±0.01)	0.114525^{ab} (±0.01)	0.128925^{a} (±0.02)	0.07735^{b} (±0.02)
	VS 1 (%)	93.77^{a} (±0.38)	87.11^{a} (±3.44)	86^{a} (±3.06)	70.22^{b} (±3.95)
	VS 2 (%)	84.89^{a} (±4.44)	48.88^{b} (±3.05)	40^{b} (±2.40)	37.33^{b} (±6.22)
	FA	24761.9^{a} (±35.24)	22500^{b} (±44.74)	21857.1^{b} (±41.43)	8333.3^{c} (±33.33)
327	Diameter	76.25^{a} (±0.96)	60^{b} (±1.41)	57.5^{b} (±2.38)	49.75^{c} (±1.26)
	Dry weight	0.087^{a} (±0.01)	0.05^{b} (±0.03)	0.02^{c} (±0.0001)	0.013^{c} (±0.0002)
	S (x10^{4}/mm^{2})	0.52145^{a} (±0.01)	0.475925^{a} (±0.07)	0.094405^{b} (± 0.01)	0.0463^{b} (±0.003)
	VS 1 (%)	89.55^{a} (±3.91)	86^{ab} (±3.46)	85.55^{ab} (±2.04)	75.78^{b} (±3.05)
	VS 2 (%)	88.44^{a} (±3.01)	87.55^{a} (±0.38)	86.66^{a} (±0.67)	85.33^{a} (±0.67)
	FA	25689.6^{a} (±34.48)	15537.2^{b} (±37.47)	11363.6^{c} (±39.09)	Nd
335a	Diameter	83.25^{a} (±2.99)	54.5^{b} (±2.38)	45^{c} (±0.82)	40.25^{c} (±1.71)
	Dry weight	0.15^{a} (±0.02)	0.062^{b} (±0.06)	0.047^{bc} (±0.03)	0.012^{c} (±0.001)
	S (x10^{4}/mm^{2})	5.478^{b} (±0.89)	8.2495^{a} (±0.29)	7.572^{a} (±0.75)	4.49675^{b} (±0.64)
	VS 1 (%)	97.77^{a} (±1.54)	94.66^{a} (±1.33)	81.11^{b} (±3.01)	18.89^{c} (±1.02)
	VS 2 (%)	90.66^{a} (±0.38)	84.44^{b} (±2.14)	80.22^{b} (±1.02)	79.55^{b} (±3.42
	FA	1900 (±20)	Nd	Nd	Nd)

Details of experiment described in the section 'Materials and Methods'. Diameter of colony (mm); Dry Weight (g); S: Number of spores x10^{4}/mm^{2} colony; FA: Fusaric Acid (µg/g dry weight); VS 1: Viability of spores (*Experiment* 1): germination percentage; VS 2: Viability of spores (*Experiment* 2): germination percentage; Nd: not detected. Means followed by the same small letter, on the line, do not differ among themselves by Tukey's test ($p > 0.05$). All above described experiments were carried out four times. Values between parentheses: standard deviaton.

when the fungus grows in media with Neem. Strain 335a in the control medium had the highest number of spores and the lowest FA production. Initially it showed a sporulation stimulus in media with Neem but FA production was inhibited.

Neem extract's capacity in inhibiting growth and sporulation was variable among isolates. Inhibition in mycelial growth is generally associated with sporulation inhibition [35,36]. However, Neem extracts decreased or increased sporulation according to extract concentration without showing the same effect when associated with mycelial growth.

Significant reduction of the colonies' diameter, dry weight, number of spores, viability of spores and the production of FA depended on NO concentration, as current research showed. For the inhibition of FA synthesis, however, the experiments cannot rule out that this inhibition of FA synthesis is merely a result from the growth inhibitory effects. Neem extracts have fungitoxic activity, although their mode of action is not understood very well. It is quit possible that the different chemical or different ratios of chemicals found in the Neem trees have varied effects on fungi. Several studies have shown that NO produced high negative effects on *Beauveria bassiana*, with inhibition in germination, colony diameter and conidiogenesis [28]. Also some sort of inhibition with Neem extracts was reported on *Phytophthora nicotianae*, *Aspergillus flavus* and *Aspergillus niger* [27,29,41].

Other researches reported antimicrobial activities from plant extract oils and showed inhibitory effects in the fungi tested, or rather; an increase in oil concentration produces an increase in inhibitory effects. Assays with essential oils confirm *in vitro* antifungal activity against *Fusarium* species [2,42].

Neem oil activities on the tested isolates show that the effects are concentration dependent and may vary according to the *Fusarium* species, fungal metabolisms, oil concentrations and anti-fungal activities.

Studies with oil from Neem seeds did not have any inhibitory effect on *F. verticillioides* [43], although it accelerated growth. On the other hand, complete inhibition of mycelial growth of *Fusarium oxysporum* f. sp. *lycopersici* was reported in a study with the dry extract of Neem seed in concentrations ranging from 5 to 30%. There were no spores in Neem incorporated media [44].

The different effects of NO on mycelial diameter, sporulation, spore viability and toxin production should

be attributed to Neem's active components and fungus metabolism. Although Azadiractin, known for its anti-fungus activities in *in vivo* and *in vitro* studies, may be isolated in small quantities from any part of the plant, mature seeds have the highest concentration of the compound [45].

The results of current research show that NO in the concentrations under analysis are effective on isolates of *Fusarium oxysporum* f. sp. *medicagenis* and *Fusarium subglutinans*. Since these isolates are plant pathogenic and producers of FA, further studies *in vivo* should be carried out with the same isolates and with host plants for the establishment of NO as an integral part of plant management.

4. CONCLUSIONS

The effects of Neem Oil extracts on growth, sporulation, morphology, and Fusaric acid production by Fusarum isolates were investigated. According to concentration, NO was efficacious in reducing the colonies' diameter, dry weight and sporulation. UV spectrophotometry analysis showed a reduction and even a complete inhibition of Fusaric acid production by using NO. The assays showed that NO has antifungal and anti toxin activity, even though their mode of action is not yet known. Evidence from the present and from other studies shows that fungal species react differently to compounds form the Neem oil. Additional research is needed to determine the potential usefulness of neem products in fungal control programs.

5. ACKNOWLEDGEMENTS

We would like to thank Dr. Thomas Bonnici for the grammatical review of the manuscript and to the Universidade Tecnológica Federal do Paraná for its support in this research.

REFERENCES

[1] Pitt, J.I. and Hocking, A.D. (1997) Fungi and food spoilage. 2nd Edition, Blackie Academic and Professional, London.

[2] Velutti, A., Marin, S., Gonzalez, P., Ramos, A.J. and Sanchis, V. (2004) Initial screening for inhibitory activity of essential oils on growth of *Fusarium verticillioides*, *F. proliferatum* and *F. graminearum* on maize-based agar media. *Food Microbiology*, **21**, 649-656.

[3] Booth, C. (1971) The genus fusarium. Commonwealth Agricultural Bureaux, England.

[4] Seifert, K.A., *et al*. (2003) The name *Fusarium moniliforme* should no longer be used. *Mycological Research*, **107**, 641-642.

[5] Porter, J.K., Bacon, C.W., Wray, E.M. and Hagler, W.M.J. (1995) Fusaric acid in *Fusarium moniliforme* cultures, corn, and feeds toxic and the neurochemical effects in the brain and pineal glands of rats. *Natural Toxins*, **3**, 91-100.

[6] Hidaka, H. and Nagatsu, T. (1969) Fusaric acid, a hypotensive agent produced by fungi. *Journal of Antibiotics*, **22**, 228-230.

[7] Nagatsu, T., Hidaka, H., Kuzuya, H., Takeya, K., Umezawa, H., Takeuchi, T. and Suda, H. (1970) Inhibition of dopamine β-hydroxylase by fusaric acid (5-butylpicolinic acid) in vitro and in vivo. *Biochemical Pharmacology*, **19**, 35-44.

[8] Bacon, C.W., Porter, J.K. and Norred, W.P. (1995) Toxic interaction of fumonisin B_1 and fusaric acid measured by injection into fertile chicken egg. *Mycopathology*, **129**, 29-35.

[9] Bacon, C.W., Porter, J.K., Norred, W.P. and Leslie, F. Production of fusaric acid by *Fusarium species*. *Applied and Environmental Microbiology*, **62**, 4039-4043.

[10] Luz, J.M., Paterson, R.R.M. and Brayford, D. (1990) Fusaric acid and other metabolite production in *Fusarium oxysporum* f. sp. *Vasinfectum*. *Letters in Applied Microbiology*, **11**, 141-144.

[11] Marrè, M.T., Vergani, P. and Albergoni, F.G. (1993) Relationship between fusaric acid uptake and its binding to cell structures by leaves of *Egeria densa* and its toxic effects on membrane permeability and respiration. *Physiological and Molecular Plant Pathology*, **42**, 141-157.

[12] Samad, L. and Behboodi, B.S. (1985) Fusaric acid induces apoptosis in savron root tip cells: roles of caspase-like activity, cytochrome *c* and H_2O_2. *Planta*, **225**, 213-234.

[13] Arias, J.A. (1985) Secretory organelle and mitochondrial alterations induced by fusaric acid in root cells of *Zea mays*. *Physiological and Plant Pathology*, **27**, 149-158.

[14] Bouizgarne, B., Brault, M., Pennarun, A.M., Rona, J.P., Ouhdouch, Y., El Hadrami, I. and Bouteau, F. (2004) Electrophysiological responses to fusaric acid of root hairs from seedlings of date palm-susceptible and -resistant to *Fusarium oxysporum* f. sp. *Albedinis*. *Journal of Phytopathology*, **152**, 321-324.

[15] Curir, P., Guglieri, L., Dolci, M., Capponi, A. and Aurino, G. (2000) Fusaric acid production by *Fusarium oxysporum* f.sp. *lilii* and its role in the lily basal rot disease. *European Journal of Plant Pathology*, **106**, 849-856.

[16] Wu, H.S., Yin, X.M., Zhu, Y.Y., Guo, S.W., Wu, C.L., Lu, Y.L. and Shen, Q.R. (2007) Nitrogen metabolism disorder in watermelon leaf caused by fusaric acid. *Physiological and Molecular Plant Pathology*, **71**, 69-77.

[17] Kuzniak, E. (2001) Effects of fusaric acid on reactive oxygen species and antioxidants in tomato cell cultures. *Journal of Phytopathology*, **149**, 575-582.

[18] Capasso, R., Evidente, A., Cutignano, A., Vurro, M., Zonno, M.C. and Bottalico, A. (1996) Fusaric and 9,10-dehydrofusaric acids and their methyl esters from *Fusarium nygamai*. *Phytochemistry*, **41**, 1035-1039.

[19] Barna, B. and Györgyi, B. (1992) Resistance of young versus old tobacco leaves to necrotrophs, fusaric acid, cell wall-degrading enzymes and autolysis of membrane lipids. *Physiological and Molecular Plant Pathology*, **40**, 247-257.

[20] Gapillout, L., Milat, M.L. and Blein, J.P. (1996) Effects

of fusaric acid on cells from tomato cultivars resistant or susceptible to *Fusarium oxysporum* f. sp. *Lycopersici*. *European Journal of Plant Pathology*, **102**, 127-132.

[21] Chao, S.C., Young, D.G. and Oberg, C.J. (2000) Screening for inhibitory activity of essential oils on selected bacteria, fungi and viruses. *Journal of Essential Oil Research*, **12**, 639-649.

[22] Cakir, A., Kordali, S., Kilic, H. and Kaya, E. (2005) Antifungal properties of essential oil and crude extracts of *Hypericum linarioides* Bosse. *Biochemical Systematics and Ecology*, **33**, 245-256.

[23] Mossini, S.A.G. and Kemmelmeier, C. (2005) A árvore Nim (*Azadirachta indica* A. Juss): Múltiplos Usos. *Acta Farmaceutica Bonaerense*, **24**, 139-148.

[24] Neves, B.P., Oliveira, I.P. and Nogueira, J.C.M. (2003) Cultivo e utilização do nim indiano. *Embrapa Circular Técnica*, **62**, Goiás.

[25] Locke, J.C. (1995) Fungi, H., Ed. In Schmutterer, The Neem Tree. VHC, Weiheim, Germany, 118-126.

[26] Martinez, S.S. (2002) *O Nim – Azadirachta indica. Natureza, Usos Múltiplos, Produção*. Martinez, S.S., Ed., IAPAR, Londrina.

[27] Bowers, J.H. and Locke, J.C. (2004) Effect of formulated plant extracts and oils on population density of *Phytophthora nicotianae* in soil and control of phytophthora blight in the greenhouse. *Plant Disease*, **88**, 11-16.

[28] Hirose, E., Neves, P.M.O.J., Zequi, J.A.C., Martins, L.H., Peralta, C.H. and Moino, A.J. (2001) Effect of biofertilizers and neem oil on the entomopathogenic fungi *Beauveria bassiana* (bals.) vuill and *Metarhizium anisopliae* (metsch.) sorok. *Brazilian Archives of Biology and Technology*, **44**, 419-423.

[29] Krishnamurthy, Y.L. and Shashikala, J. (2006) Inhibition of aflatoxin B_1 production of *Aspergillus flavus*, isolated from soybean seeds by certain natural plant products. *Letters in Applied Microbiology*, **43**, 469-474.

[30] Razzaghi-Abyaneh, M., Allameh, A., Tiraihi, T., Ghahfarokhi, M.S. and Ghorbanian, M. (2005) Morphological alteration in toxigenic *Aspergillus parasiticus* exposed to neem (*Azadirachta indica*) leaf and seed aqueous extracts. *Mycopathologia*, **159**, 565-570.

[31] Zeringue, H.J.J. and Bhatnagar, D. (1994) Effects of neem leaf volatiles on submerged cultures of aflatoxigenic *Aspergillus parasiticus. Applied and Environmental Microbiology*, **60**, 3543-3547.

[32] Arrotéia, C.C., Kemmelmeier, C. and Machinski, J.M. (2007) Efeito dos extratos aquoso e oleoso de Nim [*Azadirachta indica* A. Juss (*Meliaceae*)] na produção de patulina em maçãs contaminadas por *Penicillium expansum*. *Ciência Rural*, **37**, 1518-1523.

[33] Costa, C.L. and Kemmelmeier, C. (2008) Effect of aqueous and oily extracts from Neem [*Azadirachta indica* A. Juss (*Meliaceae*)] on the production of mycotoxins by the polyketide pathway (penicillic acid and sterigmatocystin). *Current Topics of Biotechnol*ogy, **4**, 35-40.

[34] Mossini, S.A.G., De Oliveira, K.P. and Kemmelmeier, C. (2004) Inhibition of patulin production by *Penicillium expansum* cultured with Neem (*Azadirachta indica*) Leaf Extracts. *Journal of Basic Microbiology*, **44**,106-113.

[35] Mossini, S.A.G. and Kemmelmeier, C. (2008) Inhibition of citrinin production in *Penicillium citrinum* by *Azadirachta indica* A. Juss (*Meliaceae*) in culture. *International Journal of Molecular Sciences*, **9**, 1676-1684.

[36] Mossini, S.A.G., Arrotéia, C.C. and Kemmelmeier, C. (2009) Effect of Neem leaf extract and Neem oil on *Penicillium* growth, sporulation, morphology and Ochratoxin A production. *Toxins*, **1**, 2-13.

[37] Marques, R.P., Monteiro, A.C. and Pereira, G.T. (2004) Crescimento, esporulação e viabilidade de fungos entomopatogênicos em meios contendo diferentes concentrações do óleo de Nim *(Azadirachta indica*). *Ciência Rural*, **34**, 1675-1680.

[38] Paterson, R.R.M. and Rutheford, M.A. (1991) A simplified rapid technique for fusaric acid detection in Fusarium strains. *Mycopathologia*, **113**, 171-173.

[39] Eged, S. (2005) Thin-layer chromatography – an appropriate method for fusaric acid estimation. *Biologia Bratislava*, **60**, 104.

[40] Adams, T.H. and Yu, J-H. (1998) Coordinate control of secondary metabolite production and asexual sporulation in *Aspergillus nidulans*. *Current Opinion in Microbiology*, **1**, 674-677.

[41] Pawar, V.C. and Thaker, V.S. (2006) In vitro efficacy of 75 essential oils against *Aspergillus niger*. *Mycoses*, **49**, 316-323.

[42] Soliman, K.M. and Badeaa, R.I. (2002) Effect of oil extract from some medicinal plants on different mycotoxigenic fungi. *Food and Chemical Toxicology*, **40**, 1669-1675.

[43] Fandohan, P., Gbenou, J.D., Gnonlonfin, B., Hell, K., Marasas, W.F.O. and Wingfield, M.J. (2004) Effect of essential oils on the growth of *Fusarium verticillioides* and fumonisin contamination in corn. *Journal of Agricultural and Food Chemistry*, **52**, 6824-6829.

[44] Agbenin, O.N. and Marley, P.S. (2006) In vitro assay of some plant extracts against *Fusarium oxysporum* f. sp. *lycopersici* causal agent of tomato wilt. *Journal of Plant Protection Research*, **46**, 215-220.

[45] Schaaf, O., Jarvis, A.P., van der Esch, S.A., Giagnacovo, G. and Oldham, N.J. (2000) Rapid and sensitive analysis of azadirachtin and relate triterpenoids from neem (*Azadirachta indica*) by high performance liquid chromatography - tmospheric pressure chemical ionization mass spectrometry. *Journal of Chromatrgraphy A*, **886**, 89-97.

Advances in Bioscience and Biotechnology, 2010, 1, 7-11 **ABB**
doi:10.4236/abb.2010.11002 Published Online April 2010 (http://www.SciRP.org/journal/abb/).

The effect of L-ornithine hydrochloride ingestion on human growth hormone secretion after strength training

Shinichi Demura[1], Takayoshi Yamada[2], Shunsuke Yamaji[3], Miho Komatsu[4], Koji Morishita[4]

[1]Kanazawa University, Kanazawa, Japan;
[2]Fukui National College of Technology, Fukui, Japan;
[3]Fukui University; Fukui, Japan;
[4]Healthcare Products Development Center, KYOWA HAKKO BIO CO., LTD.
Email: takay@fukui-nct.ac.jp; demura@ed.kanazawa-u.ac.jp; yamaji@u-fukui.ac.jp; miho.komatsu@kyowa-kirin.co.jp; koji.morishita@kyowa-kirin.co.jp

Received 26 February 2010; revised 8 March 2010; accepted 10 March 2010.

ABSTRACT

This study aimed to examine the effect of L-ornithine hydrochloride ingestion on serum growth hormone secretion response after strength training in young men who did not regularly engage in high intensity exercise. Ten healthy young males without workout habits (age: 22.2 +/- 1.0 yr). Subjects performed biceps curl strength training after L-ornithine hydrochloride and placebo ingestions. They participated in both of the above conditions randomly with a week interval in between. Serum growth hormone and ornithine levels were measured before L-ornithine hydrochloride or placebo ingestions and at 30 minutes after strength training. Serum growth hormone and ornithine level were measured. A change magnitude of serum growth hormone was significantly larger in the L-ornithine hydrochloride condition than in the placebo condition, and the effect size was also large ($t = 1.91$, $p = .044$, $ES = .75$). A significant interaction ($F = 280.98$, $p = 0.000$, $\eta_p^2 = 0.96$) was found in serum ornithine and a multiple comparison test showed that it was greater in the L-ornithine hydrochloride condition. Serum growth hormone level after strength training increases by L-ornithine hydrochloride ingestion in untrained young males.

Keywords: L-Ornithine Hydrochloride; Growth Hormone; Strength Training

1. INTRODUCTION

Many athletes ingest amino acids such as arginine, ornithine, methionine and lysine to make the secretion of growth hormone accelerate before training. The growth hormone is essential to gain benefits from training such as increasing muscle mass and strength due to causing anabolic action. In other words, ingestion of these special amino acids is based on the idea that training benefits can be effectively gained by stimulating growth hormone secretion.

Until now, the relatively larger growth hormone secretion effect (800-2200%) by intravenous infusion of special amino acids has been found [1-3]. However, all amino acids did not always show hormone secretion effect by intravenous infusion or oral ingestion. For example, it was reported that branched-chain amino acids (BCAA) such as leucine and varine showed a slight growth hormone secretion effect (10%), and isoleucine had no effect [1]. Moreover, it was reported also that aspartic acid, glutamic acid and cysteine stimulated little growth hormone secretion [4]. Of the amino acids which showed a growth hormone secretion effect, arginine, lysine and ornithine are believed to be superior in stimulating growth hormone secretion [3].

However, amino acids are not generally injected intravenously, but are instead ingested orally at training sites. Until now, arginine and ornithin have been mainly used to examine the effect on growth hormone secretion by oral amino acid ingestion [5-10]. However, there were mixed reports on the effect of growth hormone secretion by ornithine ingestion (negative reports: 5-9, Positive reports: 9, 10). One of the reasons for this large difference is considered to be the different ornithine amounts ingested. Subjects ingested over 170 mg per kilogram of body mass in Bucci *et al.* [10] and Cynober *et al.* [9]'s study, who reported positive effect, but subjects ingested no more than 100mg per kilogram of body mass in the other studies. Moreover, subjects in all studies were mainly body builders or weight lifters who routinely conducted high intensity strength training. Muscle fibers of these subjects were larger than average people and it is inferred that a size of their muscle cells had approached the biological limit. The degree of growth hormone effect causing muscle fiber hypertrophy depends on the level of growth hormone released in the blood and the activity level of the receptors. However, in

the body builders and weight lifters, because muscle fibers affected by growth hormone have approached the biological limit, receptor responses to an increase of growth hormone levels are small and the effect of ornithine ingestion on growth hormone secretion may be different.

Recently many people have begun conducting training for maintaining/enhancing health, and many of them actively ingest nutriceutical products to efficiently gain training benefits. Ornithine is also one of the typical nutriceutical products, and the growth hormone secretion effect has been expected by its oral ingestion. However, it has not been clarified whether a growth hormone secretion effect is also obtained in average people who do not have strenuous training habits as well as body builders and weight lifters.

This study aimed to examine the effect of L-ornithine hydrochloride ingestion on serum growth hormone secretion response after strength training in young men who do not regularly engage in high intensity exercise.

2. METHODS

2.1. Subjects

Ten healthy young adults who did not regularly engage in high intensity training participated in this study (age: 22.2 +/- 1.0 yr, height: 173.5 +/- 4.6 cm, body-mass: 72.5 +/- 12.5 kg). Written informed consent was obtained from all subjects after a full explanation of the experimental purpose and protocol. Moreover, experimental protocol in this study was approved by the inquiry committee of studies intended for humans" Kanazawa University Health & Sports Science Ethics Committee".

2.2. Experimental Design

The experimental design was a double blinded cross-over method. Namely, subjects participated in both conditions of L-ornithine hydrochloride and placebo (indigestible dextrin aqueous solution) ingestions. Due to the cross-over design, all subjects participated in both conditions at the same time with washing out period of a week. The test order was also counter balanced to eliminate order effect. In addition, subjects were prohibited from intensive exercise 2 days prior to, and to fast for at least two hours before, starting exercise in order to avoid a nutritional imbalance with eating and drinking. Subjects were also instructed not to consume food or beverages that contain caffeine throughout the experimental period.

2.3. Neutriceutical Products

Subjects ingested L-ornithine hydrochloride or indigestible dextrin aqueous solution with the same flavor (placebo) at the ratio of 0.1 g per body-mass. All neutraceutical products were made by KYOWAHAKKO BIO Co., LTD.

2.4. Procedure

2.4.1. Determination of 1 Repetition Maximum

One repetition maximum (RM) was measured for the subjects in advance in accordance with the procedure stated in **Table 1** [11,12] to determine the strength training intensity in this study.

2.4.2. Experimental Protocol and Procedure

Subjects entered the laboratory and consumed L-ornithine hydrochloride or a placebo after baseline blood drawing. They conducted bicep curl strength training with 60% of 1RM intensity (**Table 2**) an hour after ingesting nutraceutical products. In addition, all sets required 10 repetitions and a 90 second rest was set between trials. The range of elbow joint motions for the concentric part was fully extended from 145 to 155°, flexed and means velocities for one repetition including concentric and eccentric motions were in a range of 100-150°/s [13]. The second blood drawing was conducted 30 minutes after the strength training.

2.5. Parameters

Serum ornithine and growth hormone levels before ingestion and after strength training were measured. Changes after the strength training were subtracted from the baseline values and used for an analysis of the growth hormone.

Table 1. Procedure of 1RM measurement[11,12].

(1) Warm-up with a light resistance that easily allows 5-10 repetition; provide a 1 min rest.
(2) Load increased 10-20% more than point 1 to allow 3-5 repetitions to be completed; provide a 2 min rest period.
(3) Load increased 10-20% more than point 2 to allow 2-3 repetitions to be completed; provide a 2-4 min rest period.
(4) Male a load increased of 10-20% more than point 3. Instruct the subject to attempt a 1RM.
(5) If the subject is successful provide a 2-4 min rest and increase the load by 5-10% increase. If the subject is unsuccessful, provide a 2-4 min rest and decrease the load by 5-10%.
(6) Continue point 5 until the subject can complete one repetition with proper exercise technique at the highest possible load.

Table 2. Strength training protocol[13].

(1) Two sets of seated biceps curl at 60% of 2RM
(2) Two sets of seated biceps curl at 60% of 1RM – 1 kg
(3) Two sets of stamding biceps curl at 60% of 1RM – 2 kg
(4) Two sets of stamding biceps curl at 60% of 1RM – 3 kg

2.6. Statistical Analysis

The difference of serum ornithine level before ingestion and at 30 minutes after strength training between both conditions was tested by a paired two way analysis of variance. A Difference of variation in serum growth hormone in both conditions was tested by a paired t-test. Effect size was calculated by partial η2 (ηp2) and effect size (ES). In addition, an alpha level of .05 was used for all tests.

3. RESULTS

Figure 1 shows the results of the paired t-test between means of serum growth hormone in both conditions. A significant difference was found between both conditions, and the L-ornithine hydrochloride condition was greater than the placebo condition and this difference was larger ($t = 1.91$, $p = .044$, $ES = .75$). **Figure 2** shows the results of the two way analysis of variance for serum ornithine level. A significant interaction ($F = 280.98$, $p = 0.000$, $\eta_p^2 = 0.96$) was found in serum ornithine and a multiple comparison test showed that it was greater in the L-ornithine hydrochloride condition than in the placebo condition at 30 minutes after strength training. Moreover, serum ornithine level at 30 minutes after strength training was significantly greater than that before ingestion in L-ornithine hydrochloride ingestion.

4. DISCUSSION

The serum ornithine level at 30 minutes after strength training was greater in subjects ingesting L-ornithine hydrochloride than for subjects ingesting the placebo and this difference was large. Until now, it was reported that special amino acids such as ornthine and citruline were released and found at the peak level in the blood within 5-8 hours, being a relatively early time [8]. According to Cynober *et al.* [8], in the case of ornithine, blood concentration reaches a peak value at about 60 minutes after oral ingestion. Serum ornithine level after L-ornithine hydrochloride ingestion in this study was very high although 120 minutes elapsed after ingestion (about 300 nmol/l, 500% increase as compared with be-fore ingestion). Increasing the amount of growth hormone level before ingestion to 30 minutes after strength training was also significantly greater in subjects ingesting L-ornithine hydrochloride than in those ingesting the placebo and this difference was large (about 200%). Bucci *et al.* [10] compared blood growth hormone level before L-ornithine hydrochloride ingestion, 45 minutes and 90 minutes after ingestion under the conditions of 40, 100 and 170 mg/kg body-mass ingestion using body builders. They reported that blood growth hormone level at 90 minutes after ingestion in the 170 mg/kg condition was significantly greater than that of the other conditions (about 150-300%), and also significantly greater than that before ingestion (about 350%). Although the physical characteristics and training habits of subjects, and ingestion amount of ornithine hydrochloride differed between the present study and Bucci *et al.* [10]'s study, growth hormone secretion effect by ornithine hydrochloride ingestion was found in both studies and the degree of secretion was also similar. Meanwhile, Lambert et al. [5] measured the blood growth hormone level every 30 minutes for 3 hours for eight male body builders with a placebo, 2.4 g of arginine and lysine, 1.8 g of ornithine and tyrosine, and 20 g of beef extract ingestion after 8 hours of fasting to examine the influence of amino acid such as ornithine ingestion on blood growth hormone level. They reported that little change in growth hormone level was found in any case of amino acid ingestion. Fry *et al.* [7] conducted a weight lifting training experiment over a week with amino acid ingestion such as ornithine hydrochloride, arginine and branched-chain amino acid together for 28 weight lifters to examine the effect of high intensity training and ingestion of amino acid neutraceutical production on endocrine response and lifting performance. As a result, an increase of growth hormone was found by training with high intensity, but not by amino acid. Although experimental protocol differed between the former study 10 and the latter two studies [5,7], considering the similarity of subjects' characteristics, a difference in their results may be caused by the kind of ingested amino acid and/or the amount ingested. Until now, growth hormone secretion effect by intravenous infusion and oral ingestion was found by amino acid such as arginine, ornithine, methionin and lysine in previous studies [1-3], but little by branched-chain amino acids such as aspartic acid, glutamic acid, cysteine, cysteine, leucine, valine and isoleucine [1,4]. Fogelholm *et al.* [6] compared blood growth hormone level over 24 hours after 2 g of arginine, ornithine or lysine for weight lifters to examine the effects of a small amount of amino acid ingestion on growth hormone secretion. They reported an insignificant increase of blood growth hormone level was found after ingestion of any amino acid. Considering the above, studies by Fry *et al.* [7] and Lambert *et al.* [5], used not only amino acids such as ornithine, arginine, methionine and lysine, which indicate a growth hormone secretion effect, but also the branched-chain amino acids, glutamic acid and aspartic acid, which do not indicate such a growth hormone secretion effect. The former amino acids were reduced with the whole ingestion amount being less (less than 3 g). The amount administered may relate to the difference between Bucci *et al.* [10]'s results (over 10 g) and the results of Fry *et al.* [7] and Lambert *et al.* [5].

Meanwhile, although marked growth hormone secretion was not found after 100mg/kg body-mass ornithine hydrochloride ingestion in Bucci *et al.* [10]'s report, it should be noted that a significant increase was found

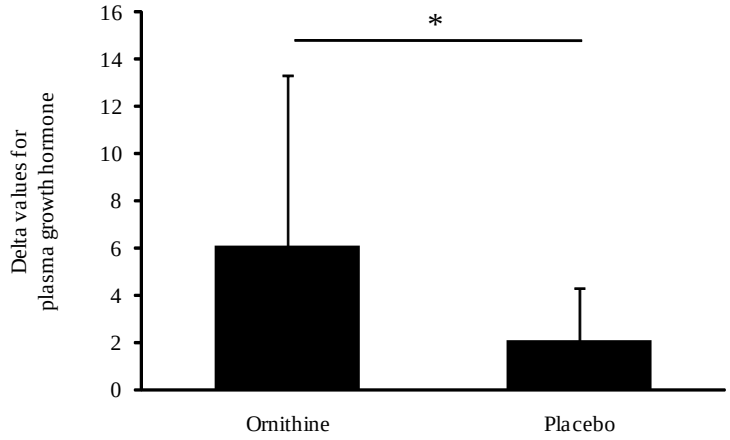

Figure 1. Variation of serum growth hormone level in both conditions*, significant difference was found between both conditions.

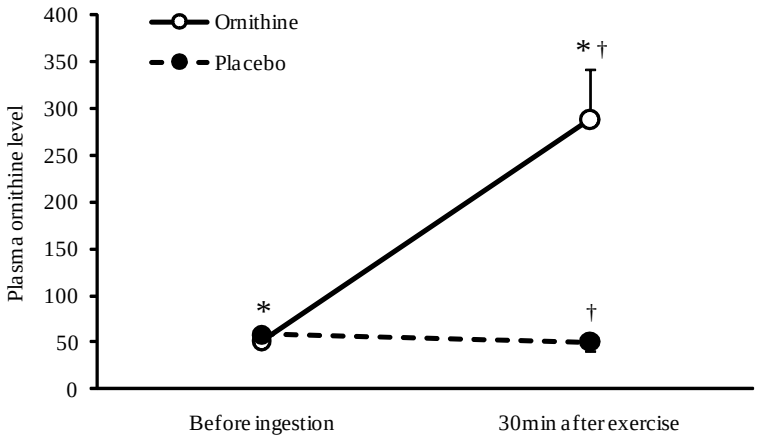

Figure 2. Serum ornithine level before ingestion and 30 min after strength training*, significant difference was found between before ingestion and 30 min after strengthe training, † significant difference was found between both conditions.

after ingestion of similar ornithine hydrochloride density in the present results. The difference between these results is inferred to be caused by the difference in the subjects' characteristics. Namely, although the present subjects had no exercise habits, the subjects in the previous studies that include Bucci *et al.* [10] were body builders or weight lifters who conducted strength training with high frequency and intensity. The difference in the subjects' characteristics in both studies may be related to the difference in adjustment and sensitivity of their muscle cells to training stimulation. Generally, hypertrophy of muscle fibers brought about by strength training is results from the following: effect of anabolic hormone such as growth hormone that secretes after strength training, and effect of satellite cells as stem cell existing between sarcolemmas assimirate with the existing muscle fiber [14,15]. Because muscle fibers of trained subjects are enlarged by repeated training stimulation, the size of muscle cells is inferred to be close to the biological limit. Strength of growth hormone effect regarding muscle fibers hypertrophy depends on the growth hormone level released into the blood and activity level of the receptors. However, responses of receptors to an increase of growth hormone level are inferred to be small in muscle fibers nearly enlarged to the biological limit. Namely, muscle hypertrophy of the trained subjects depends on the differentiation and disintegration of satellite cells with training stimulation rather than anabolic hormone secreted after training. Therefore, the present results may have been different from Bucci *et al.*'s results in spite of the same ornithine hydrochloride ingestion. Meanwhile, in the case of the present subjects without strength training habits, because activity level of receptors increases with an increase of blood growth

hormone level, adjustment to strength training may occur relatively smoothly. In addition, because the hypertrophy regarding satellite cells is expected, training effects can be obtained efficiently. From the above, it is considered that even in subjects without an exercise habit, a growth hormone secretion effect was obtained by ingestion of ornithine hydrochloride in lower amounts than the previous study (170 mg/kg body-mass) [10], which was reported to obtain a growth hormone secretion effect. However, Collier *et al.* [16] reported that gastrointestinal discomfort is often caused by special amino acids such as ornithine and arginine and the degree of this discomfort is related to the amount ingested. Although a growth hormone secretion effect was found by a lower ingestion amount as compared with Bucci *et al.* [10]'s report in this study, six out of ten subjects complained of gastrointestinal discomfort such as stomachache and diarrhea. Further studies may be required to examine the lower amount of ingestion that obtains growth hormone secretion effect without such gastrointestinal discomfort.

5. CONCLUSIONS

Blood growth hormone level increases after strength training by L-ornithine hydrochloride ingestion in untrained males.

5. ACKNOWLEDGEMENT

This work was supported by a KYOWA HAKKO BIO CO., LTD.

REFERENCES

[1] Knopf, R.F., Conn, J.W., Fajans, S.S., Floyd, J.C., Guntsche, E.M. and Rull, J.A. (1965) Plasma groeth hormone response to intravenous administration of amino acids. *The Journal of Clinical Endocrinology and Metabolism*, **25**, 1140-1144.

[2] Evain-Brion, D., Donnadieu, M., Roger, M. and Job, J.C. (1982) Simultaneous study of somatotrophic and corticotrophic pituitary secretions during ornithine infusion test. *Clinical Endocrinology*, 1982, **17**, 119-122.

[3] Chromiak, J.A. and Antonio, J. (2002) Use of amino acids as growth hormone-releasing agents by athletes. *Nutrition*, **18**, 657-661.

[4] Carlson, H.E., Miglietta, J.T., Roginsky, M.S. and Stegink, L.D. (1989) Stimulation of pituitary hormone secretion by neurotransmitter amino acids in humans. *Metabolism*, **38**, 1179-1182.

[5] Lambert, M.I., Hefer, J.A., Millar, R.P. and Macfarlane, P.W. (1993) Failure of commercial oral amino acid supplements to increase serum growth hormone concentrations in male body-builders. *International Journal of Sport Nutrition*, **3**, 298-305.

[6] Fogelholm, G.M., Näveri, H.K., Kiilavuori, K.T. and Härkönen, M.H. (1993) Low-dose amino acid supplementation: no effects on serum human growth hormone and insulin in male weightlifters. *International Journal of Sport Nutrition*, **3**, 290-297.

[7] Fry, A.C., Kraemer, W.J., Stone, M.H., Warren, B.J., Kearney, J.T., Maresh, C.M., Weseman, C.A. and Fleck SJ. (1993) Endocrine and performance responses to high volume training and amino acid supplementation in elite junior weightlifters. *International Journal of Sport Nutrition*, **3**, 306-322.

[8] Cynober, L. (2007) Pharmacokinetics of arginine and related amino acids. *Journal of Nutrition*, **137**, 1646-1649.

[9] Cynober, L., Coudray-Lucas, C., de Bandt, J.P., Guéchot, J., Aussel, C., Salvucci, M. and Giboudeau, J. (1990) Action of ornithine alpha-ketoglutarate, ornithine hydrochloride, and calcium alpha-ketoglutarate on plasma amino acid and hormonal patterns in healthy subjects. *Journal of the American College of Nutrition*, **9**, 2-12.

[10] Bucci, L., Hickson, J.F., Pivarnik, J.M., Wolinsky, I., Mc Mahon, J.C. and Turner, S.D. (1990) Ornithine ingestion and growth hormone release in bodybuilders. *Nutrition Research*, **10**, 239-245.

[11] Ball, N. and Scurr, J. (2010) An assessment of the reliability and standardisation of tests used to elicit reference muscular actions for electromyographical normalisation. *Journal of Electromyography and Kinesiology*, **20**, 81-88.

[12] Earle, R.W. (1999) Weight training exercise prescription. *Essentials of Personal Training Symposium Workbook.* SCA Certification Commission, Lincoln.

[13] Hansen, S., Kvorning, T., Kjaer, M. and Sjøgaard, G. (2001) The effect of short-term strength training on human skeletal muscle: the importance of physiologically elevated hormone levels. *Scandinavian Journal of Medicine & Science in Sports*, **11**, 347-354.

[14] Chesley, A., MacDougall, J.D., Tarnopolsky, M.A., Atkinson, S.A. and Smith, K. (1992) Changes in human muscle protein synthesis after resistance exercise. *Journal of Applied Physiology*, **73**, 1383-1388.

[15] White, T.P. and Esser, K.A. (1989) Satellite cell and growth factor involvement in skeletal muscle growth. *Medicine and Science in Sports and Exercise*, **21**, 158-163.

[16] Collier, S.R., Casey, D.P. and Kanaley, J.A. (2005) Growth hormone responses to varying doses of oral arginine. *Growth Hormone & IGF Research*, **15**, 136-139.

Advances in Bioscience and Biotechnology, 2010, 1, 12-25 **ABB**
doi:10.4236/abb.2010.11003 Published Online April 2010 (http://www.SciRP.org/journal/abb/).

On the orientation of plane tensegrity cytoskeletons under biaxial substrate stretching

Athanassios P. Pirentis, Konstantinos A. Lazopoulos*

Department of Mechanics, Faculty of Applied Mathematical and Physical Sciences, National Technical University of Athens, Athens, Greece.
Email: kolazop@mail.ntua.gr

Received 12 February 2010; revised 26 February 2010; accepted 6 March 2010.

ABSTRACT

Two different simple cases of plane tensegrity cytoskeleton geometries are presented and investigated in terms of stability. The tensegrity frames are used to model adherent cell cytoskeletal behaviour under the application of plane substrate stretching and describe thoroughly the experimentally observed reorientation phenomenon. Both models comprise two elastic bars (microtubules), four elastic strings (actin filaments) and are attached on an elastic substrate. In the absence of external loading shape stability of the cytoskeleton is dominated by its prestress. Upon application of external loading, the cytoskeleton is reorganized in a new direction such that its total potential energy is rendered a global minimum. Considering linear constitutive relations, yet large deformations, it is revealed that the reorientation phenomenon can be successfully treated as a problem of mathematical stability. It is found that apart from the magnitude of contractile prestress and the magnitude of extracellular stretching, the reorientation is strongly shape–dependent as well. Numerical applications not only justify laboratory data reported in literature but such experimental evidence as the concurrent appearance of two distinct and symmetric directions of orientation, indicating the cellular coexistence of phases phenomenon, are clearly detected and incorporated in the proposed mathematical treatment.

Keywords: Tensegrity; Cytoskeleton; Adherent Cells; Reorientation; Stability; Coexistence of Phases

1. INTRODUCTION

Active adherent cells alter their orientation direction, defined by their long axis, in response to substrate stretching. In absence of external strain field cells appear with random orientation; yet, the application of extracellular strain results to a concerted reorganization of the components of the cytoskeleton (CSK) in the new direction. The CSK is the intracellular network that consists of different types of biopolymers such as actin and intermediate microfilaments, microtubules, myosin and other filaments, and acts concurrently as a supporting frame and chief regulator of cell deformability. Constant remodelling of the CSK directly affects almost all functions of living cells like growth, differentiation, mitosis, apoptosis, motility, cell locomotion, etc. ([1] and references therein). In the case of cells adherent to an elastic substrate, the actin CSK disassembles and reassembles under stretching of the substrate in order to mechanically stabilize the cell by means of the so-called intracellular contractile mechanism, that is, the generation of tensile forces in the actin filaments by myosin motor proteins through the ATP-driven process of myosin crossbridge cycling. Experimental observations report that the direction of cellular orientation is primarily governed by the magnitude of the extracellular strain field and the strength of the contractile mechanism [2-5]. Depending on these agents, cells have been observed to align either with the direction of the maximum extracellular stretch component [6-9], or perpendicular to it [2-5,10-15]. Specifically, under the effect of static or quasi–static substrate stretch cells orient parallel to the direction of maximum stretch [6,7,9], whereas in response to dynamic stretching they align perpendicularly to the direction of maximum stretch [2-5,10-15]. However, there also exists a special case of cellular orientation behaviour; independent experiments have confirmed the discovery that under the same substrate stretching such a configuration is possible that two distinct orientation directions (*phases*) of the cells coexist [3,5].

In the present study the cellular orientation phenomenon is addressed by employing two simple mechanical models belonging to a family of structural systems known as *tensegrity*. Tensegrities are reticulated structures forming a highly geometric combination of bars

and strings in space. In fact, tensegrity is a portmanteau word for "tension-integrity" referring to the integrity of structures as being based in a synergy between balanced continuous tension (elastic strings) and discontinuous compression (elastic bars) components. Pre–existing tensile stress in the string members, termed prestress, is required even before the application of any external loading in order to maintain structural stability. There already exists extensive literature regarding the advanced mathematics and mechanics used for the integral description of these structures [16-20], as well as the successful identification of the principles of tensegrity architecture to cytoskeletal biomechanics [21-24]. In fact, some of the characteristic mechanical properties of the CSK were initially predicted by the *cellular tensegrity model* and were later verified in laboratory experiments as such [21,24].

Since reorganization of the CSK is observed at high extracellular strains (of the order 10%–110%), Finite Elasticity principles and methods will be followed. Adopting Maxwell's convention for stability [25,26], two different planar tensegrity CSK geometries are introduced and the stability of their orientation directions under the application of biaxial substrate stretching is studied. As it is the case for their biological counterparts, under the effect of stretching, the planar tensegrity models are considered to deform and reorient in a new direction. In concert to Maxwell's convention, it is assumed that this new orientation direction, out of all the available ones, renders the total potential energy function of the given tensegrity CSK model a global minimum. Recently, the same analytical methodology presented in this study was used to theoretically investigate the problem of stress fibre reorientation under both static and cyclic substrate stretching [27-29]. The current treatment is an extension of the previous work to the cellular scale, and enhances further the former effort that had not focused on the intracellular microstructure but considered the cell as a generalized Mooney–Rivlin elastic material [30]. The properties of the plane tensegrity models are discussed in detail in the next sections. However, it is pointed out that in the following and in terms of cell physiology, elastic string members correspond to actin microfilaments, elastic bar members correspond to microtubules and the tensegrity frames are anchored on the elastic substrate through their vertices, representing focal adhesions complexes on the extracellular matrix.

2. THE PLANE TENSEGRITY CYTOSKELETON MODELS

For the theoretical description of the reorientation phenomenon the CSK is modelled by two independent planar tensegrity frames of rectangular and rhombic shape, respectively (**Figure 1**). Both frames comprise four elastic strings and two elastic bars (not joint at their intersection) and are attached upon an elastic substrate through their vertices. It is apparent from **Figure 1** that the strings occupy the sides of the models while the bars are identified with the diagonals. In accordance to cellular physiology, the cross–section area of the bars is considered to be eight (8) times that of the strings [21,31], the elastic moduli of all members (both strings and bars) are assumed to be the same [21,31], and their constitutive equations are considered to be linear [21,31]. Albeit, nonlinear behaviour of the system may still be exhibited; it has been shown that it is mainly a result of geometrical rearrangement of the structural members under the effect of external loading, rather than intrinsic nonlinearity of the members themselves [32]. Further, in the initial configuration where no stretch is applied, it is assumed that all string members acquire the same prestrain due to the existing myosin–actin contractility motor systems. The prestrain of the strings is equilibrated entirely through reaction forces applied by the substrate at the vertices of the tensegrity model. Thus, the bars are considered to be initially unstressed. Finally, in the initial configuration, the origin of an orthogonal Cartesian coordinate system OX_1X_2 is defined to coincide with the geometric centre of the models, while their long axis is originally aligned with the X_1 axis of the coordinate system (**Figure 1**).

In absence of extracellular strain field the shape stability of the models is controlled by prestrain. Next, biaxial substrate stretching is applied in the directions defined by the angles β and ($\beta + 90^{\circ}$), cf. **Figure 2**. As mentioned above, due to the increased strain in the substrate the models deform and reorient to a new (current) orientation direction (**Figure 3**). The current direction is the one, out of all available orientation directions, that corresponds to the global minimum of the total potential energy of the models.

2.1. The Rectangular Model

The initial configuration of the rectangular tensegrity CSK model (henceforth simply rectangular model) is illustrated in **Figure 1(a)**. Assigning the index values: i = 1, 2 to the bars (*AC*) and (*BD*), i = 3, 4 to the strings (*AB*) and (*CD*) with initial length a_1, i = 5, 6 to the strings (*BC*) και (*DA*) with initial length b_1, and taking advantage of the model geometry, the initial deformation of every structural member due to prestrain is described by the deformation gradient tensors $\mathbf{F}_{0(i)} = \mathbf{I} + \nabla \mathbf{u}_{0(i)}$, in the fashion:

$$\mathbf{F}_{0(1)} = \mathbf{F}_{0(2)} = \mathbf{I} \tag{1}$$

$$\mathbf{F}_{0(3)} = \mathbf{F}_{0(4)} = \begin{bmatrix} 1+g^0 & 0 \\ 0 & 1 \end{bmatrix} \tag{2}$$

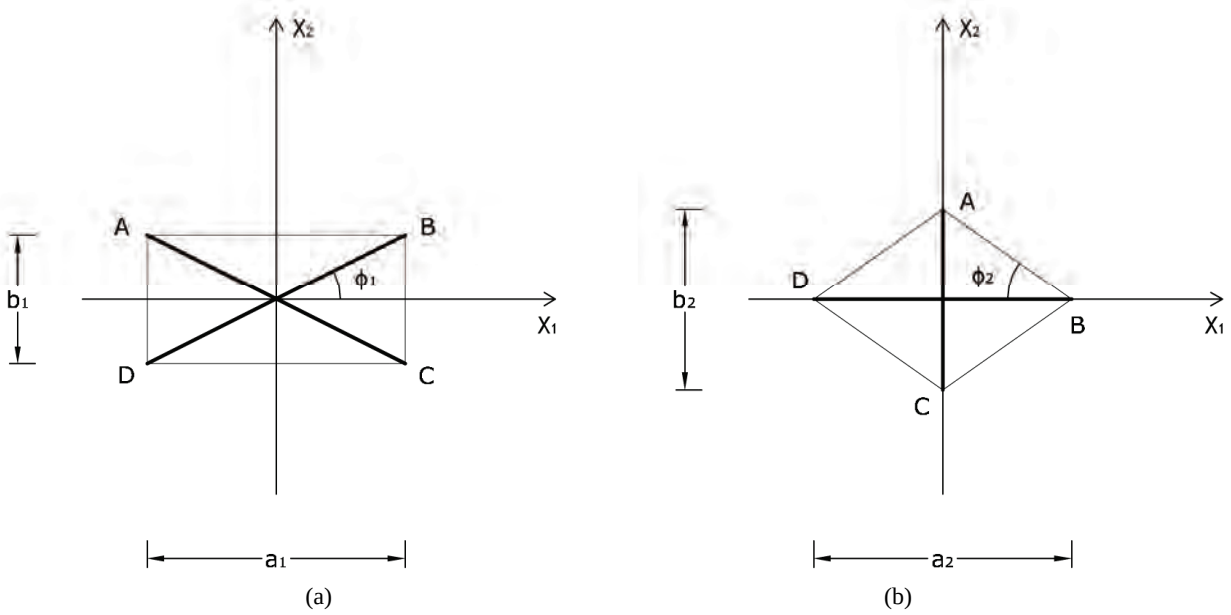

Figure 1. The initial prestrained placement of the: (a) rectangular plane tensegrity cytoskeleton; (b) rhombic plane tensegrity cytoskeleton.

$$\mathbf{F}_{0(5)} = \mathbf{F}_{0(6)} = \begin{bmatrix} 1 & 0 \\ 0 & 1+g^0 \end{bmatrix} \tag{3}$$

where $\mathbf{u}_{0(i)}$, g^0, *is* the initial homogeneous displacement and its gradient (prestrain) along the string members, respectively, while the (2×2) identity matrix 1 in **Eq.1** expresses the fact that at the initial configuration the bars are considered to be undeformed.

The deformation gradient of the biaxial substrate stretching with reference to the axis (Y_1, Y_2) of the maximum and minimum extracellular normal strain, respectively (**Figure 2**), is given as:

$$\mathbf{F}^{\beta} = \mathbf{R}_{\beta}{}^{\mathrm{T}} \cdot \begin{bmatrix} 1+g_1^{\beta} & 0 \\ 0 & 1+g_2^{\beta} \end{bmatrix} \cdot \mathbf{R}_{\beta}, \tag{4}$$

where g_1^{β}, g_2^{β}, with $g_1^{\beta} \geq g_2^{\beta}$, are the displacement gradients along the directions β and $(\beta + 90^{\circ})$, and:

$$\mathbf{R} = \begin{bmatrix} \cos\beta & \sin\beta \\ -\sin\beta & \cos\beta \end{bmatrix}, \tag{5}$$

is the rotation matrix of the coordinate system by the angle β. The superscript $(\,)^{\mathrm{T}}$ denotes the transpose matrix. The total deformation gradient of every member of the rectangular model as a result of the superposition of prestrain and biaxial substrate stretching is expressed through the product of the respective deformation gradient tensors as: $\mathbf{F}^{\mathbf{i}} = \mathbf{F}^{\beta} \cdot \mathbf{F}_{0(\mathbf{i})}$ for $\mathbf{i} = 1,...,6$.

The model responds to the increase of the substrate strain field by altering its initial configuration. Consequently, the reference placement has changed; in fact, it has been rotated through an angle θ (**Figure 3(a)**). In the θ direction the deformation gradient tensor of each member of the rectangular model due to prestrain is given as: $\mathbf{F}^{\theta(\mathbf{i})} = \mathbf{R}_{\theta}{}^{\mathrm{T}} \cdot \mathbf{F}_{0(\mathbf{i})} \cdot \mathbf{R}_{\theta}$, where the rotation matrix $\mathbf{R}_{\theta}$ is defined in the same fashion as $\mathbf{R}_{\beta}$. The total deformation in the θ direction as a result of biaxial substrate stretching and prestrain is expressed through the tensors: $\mathbf{F}_{\mathbf{i}} = \mathbf{F}^{\beta} \cdot \mathbf{F}^{\theta(\mathbf{i})}$. Now, if we call dx the deformed length of the initial length dX along the given member of the rectangular model, its displacement gradient is expressed in the form:

$$u_i = \frac{du_i}{dX_i} = \frac{dx_i}{dX_i} - 1 = \lambda_i - 1, \tag{6}$$

for $i = 1,...,6$, where $\lambda_i = \sqrt{\mathbf{n}_{\mathbf{i}}{}^{\mathrm{T}} \cdot \mathbf{C}_{\mathbf{i}} \cdot \mathbf{n}_{\mathbf{i}}}$ is the *stretch*, $\mathbf{C}_{\mathbf{i}} = \mathbf{F}_{\mathbf{i}}^{\mathrm{T}} \cdot \mathbf{F}_{\mathbf{i}}$ is the right Cauchy–Green tensor [33,34], and:

$$\mathbf{n}_{\mathbf{i}} = \begin{bmatrix} \cos t_i & \sin t_i \end{bmatrix}^{\mathrm{T}} \tag{7}$$

is the unit vector along the direction of each member in the new (reoriented) configuration. Specifically, defining the angle $\phi_1 = \arctan(b_1/a_1)$, see **Figure 1(a)**, it follows that in the reoriented configuration for $\mathbf{i} = 1$ to 6: $t_1 = \theta - \phi_1$, $t_2 = \theta + \phi_1$, $t_3 = t_4 = \theta$, $t_5 = t_6 = \theta + 90^{\circ}$, respectively. Hence, the analytical expressions for the displacement gradient along each member of the rectangular model are given in the form:

$$u_1 = -1+\frac{1}{\sqrt{2}}\cdot\left\{2+g_1^{\beta}\left(2+g_1^{\beta}\right)+g_2^{\beta}\left(2+g_2^{\beta}\right)+\left[g_1^{\beta}\left(2+g_1^{\beta}\right)-g_2^{\beta}\left(2+g_2^{\beta}\right)\right]\cdot\cos\left[2\left(\beta-\theta+\arctan\left(b_1/a_1\right)\right)\right]\right\}^{1/2}, \quad (8)$$

$$u_2 = -1+\frac{1}{\sqrt{2}}\cdot\left\{2+g_1^{\beta}\left(2+g_1^{\beta}\right)+g_2^{\beta}\left(2+g_2^{\beta}\right)+\left[g_1^{\beta}\left(2+g_1^{\beta}\right)-g_2^{\beta}\left(2+g_2^{\beta}\right)\right]\cdot\cos\left[2\left(\beta-\theta-\arctan\left(b_1/a_1\right)\right)\right]\right\}^{1/2}, \quad (9)$$

$$u_3 = u_4 = -1+\frac{1}{\sqrt{2}}\left(1+g^0\right)\cdot\left\{2+g_1^{\beta}\left(2+g_1^{\beta}\right)+g_2^{\beta}\left(2+g_2^{\beta}\right)+\left[g_1^{\beta}\left(2+g_1^{\beta}\right)-g_2^{\beta}\left(2+g_2^{\beta}\right)\right]\cdot\cos\left[2\left(\beta-\theta\right)\right]\right\}^{1/2}, \quad (10)$$

$$u_5 = u_6 = -1+\frac{1}{\sqrt{2}}\left(1+g^0\right)\cdot\left\{2+g_1^{\beta}\left(2+g_1^{\beta}\right)+g_2^{\beta}\left(2+g_2^{\beta}\right)-\left[g_1^{\beta}\left(2+g_1^{\beta}\right)-g_2^{\beta}\left(2+g_2^{\beta}\right)\right]\cdot\cos\left[2\left(\beta-\theta\right)\right]\right\}^{1/2}. \quad (11)$$

2.2. The Rhombic Model

The initial configuration of the rhombic tensegrity CSK model (henceforth simply rhombic model) is illustrated in **Figure 1(b)**. The deformation analysis of the model follows the exact same steps as in the previous section. Thus, we assign the index values: $\mathbf{j}=1$ to the bar (DB) with initial length a_2, $\mathbf{j}=2$ to the bar (CA) with initial length b_2, and $\mathbf{j}=3$ to 6 to the strings (AB), (BC), (CD), (DA), respectively, that constitute the rhombic model perimeter. The initial deformation of each member due to prestrain is described in terms of the deformation gradient tensors $\mathbf{F}_{0(j)}$ as:

$$\mathbf{F}_{0(1)} = \mathbf{F}_{0(2)} = \mathbf{I} \quad (12)$$

$$\mathbf{F}_{0(j)} = \mathbf{R}_{\omega_j}{}^{T}\cdot\begin{bmatrix}1+g^0 & 0\\ 0 & 1\end{bmatrix}\cdot\mathbf{R}_{\omega_j}, \text{ with } \mathbf{j}=3,...,6, \quad (13)$$

where g^0 is the initial homogeneous displacement gradient (prestrain) along the strings, $\mathbf{I}$ is the (2×2) identity matrix expressing, again, the fact that at the initial configuration the bars are considered to be undeformed, and $\mathbf{R}_{\omega_j}$ is the rotation matrix with explicit form:

$$\mathbf{R}_{\omega_j} = \begin{bmatrix}\cos\omega_j & \sin\omega_j\\ -\sin\omega_j & \cos\omega_j\end{bmatrix} \quad (14)$$

Defining the angle $\phi_2 = \arctan\left(b_2/a_2\right)$, see **Figure 1(b)**, from the rhombic model geometry follows that for $\mathbf{j}=3$ to 6: $\omega_3 = -\phi_2$, $\omega_4 = \pi+\phi_2$, $\omega_5 = \pi-\phi_2$, $\omega_6 = \phi_2$,

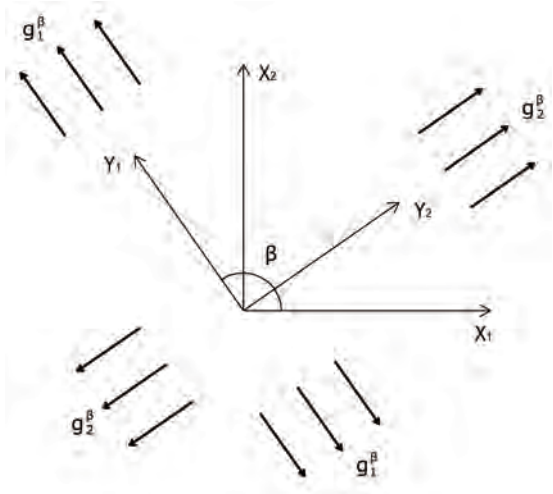

Figure 2. The geometry of the biaxial substrate stretching and its coordinate system.

respectively.

The deformation gradient of the biaxial substrate stretching is provided again from **Eq.4**. The total deformation gradient of the members of the rhombic model, as a result of prestrain and the strain field of the substrate, is given through the product of the respective deformation gradient tensors as: $\mathbf{F}^{j} = \mathbf{F}^{\beta}\cdot\mathbf{F}_{0(j)}$ with $\mathbf{j}=1,...,6$. In response to the increased strain the initial configuration of the model is changed to the new direction θ. In the θ direction the deformation gradient tensor of each member of the rhombic model due to prestrain is given as: $\mathbf{F}^{\theta(j)} = \mathbf{R}_{\theta}{}^{T}\cdot\mathbf{F}_{0(j)}\cdot\mathbf{R}_{\theta}$. Hence, the total deformation in the θ direction due to prestrain and the superimposed biaxial substrate stretching is expressed through the tensors: $\mathbf{F}_j = \mathbf{F}^{\beta}\cdot\mathbf{F}^{\theta(j)}$. Now, the displace-

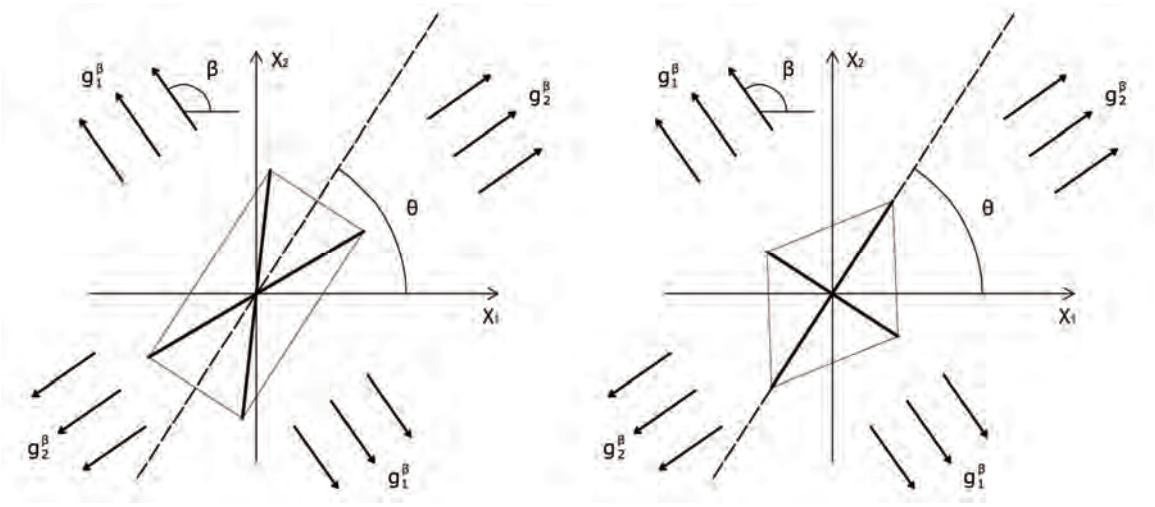

(a) (b)

Figure 3. The geometry of the reoriented plane tensegrity cytoskeletons. (a) the rectangular case; (b) the rhombic case.

ment gradient along each member of the model is given from **Eqs.6** and **7**, after the apparent interchange between indexes **i** and **j**. Specifically, for the unit vector $\mathbf{n}_j$ along the direction of each member in the new configuration (**Figure 3(b)**), follows that for $\mathbf{j}=1$ to 6 : $t_1=\theta$, $t_2=\theta+90^\circ$, $t_3=\theta-\phi_2$, $t_4=\theta+\pi+\phi_2$, $t_5=\theta+\pi-\phi_2$, $t_6=\theta+\phi_2$, respectively. Now, the analytical expressions for the displacement gradients of the rhombic model members are formulated as:

$$u_1=-1+\frac{1}{\sqrt{2}}\{2+g_1^\beta\left(2+g_1^\beta\right)+g_2^\beta\left(2+g_2^\beta\right)+\left[g_1^\beta\left(2+g_1^\beta\right)-g_2^\beta\left(2+g_2^\beta\right)\right]\cdot\cos\left[2\left(\beta-\theta\right)\right]\}^{1/2}, \tag{15}$$

$$u_2=-1+\frac{1}{\sqrt{2}}\{2+g_1^\beta\left(2+g_1^\beta\right)+g_2^\beta\left(2+g_2^\beta\right)-\left[g_1^\beta\left(2+g_1^\beta\right)-g_2^\beta\left(2+g_2^\beta\right)\right]\cdot\cos\left[2\left(\beta-\theta\right)\right]\}^{1/2}, \tag{16}$$

$$u_3=u_5=-1+\frac{1}{\sqrt{2}}\left(1+g^0\right)\cdot\left\{2+g_1^\beta\left(2+g_1^\beta\right)+g_2^\beta\left(2+g_2^\beta\right)+\left[g_1^\beta\left(2+g_1^\beta\right)-g_2^\beta\left(2+g_2^\beta\right)\right]\cdot\cos\left[2\left(\beta-\theta+\arctan\left(b_2/a_2\right)\right)\right]\right\}^{1/2}, \tag{17}$$

$$u_4=u_6=-1+\frac{1}{\sqrt{2}}\left(1+g^0\right)\cdot\left\{2+g_1^\beta\left(2+g_1^\beta\right)+g_2^\beta\left(2+g_2^\beta\right)+\left[g_1^\beta\left(2+g_1^\beta\right)-g_2^\beta\left(2+g_2^\beta\right)\right]\cdot\cos\left[2\left(\beta-\theta-\arctan\left(b_2/a_2\right)\right)\right]\right\}^{1/2}. \tag{18}$$

3. EQUILIBRIUM OF THE PLANE TENSEGRITY CSK MODELS

For the reasons of physiological compatibility mentioned in Section 2, it is assumed for both model geometries that the constitutive equations of all members are linear. Thus, the strain energy density per unit length function for each member may be written as:

$$W_k=\frac{1}{2}\cdot E_k\cdot A_k\cdot e_k^2 \quad \text{with} \quad k=1,...,6, \tag{19}$$

where E_k is the Young modulus, A_k is the cross–sectional area, and:

$$e_k=u_k+\frac{1}{2}u_k{}^2 \tag{20}$$

is the nonlinear Lagrangian strain. Again for the physiological reasons of Section 2—and recalling that index *i* corresponds to the rectangular model, whereas index j to the rhombic—it is considered that $E_k=E$ for $k=i=j=1$ to 6, $A_k=8A$ for $k=i=j=1,2$ (bars), and $A_k=A$ for $k=i=j=3$ to 6 (strings). With no harm of the generality, in what follows it is assumed that $E=1$ and $A=1$. Evidently, the strain energy density,

through the Lagrangian strain of **Eq.20**, may be expressed as a function of the displacement gradient u_k. Then, the total potential energy of each model is written as:

$$V = \sum_{k=1}^{6} \left(W_k - P_k \cdot u_k \right) \cdot l_k \qquad (21)$$

where $P_k = \partial W_k / \partial u_k$ is the first Piola–Kirchhoff stress along each member, and l_k is its natural (unstressed) length. In the case of the rectangular model $(k = i)$, from the geometry of the initial configuration, **Figure 1(a)**, follows that:

$$l_1 = l_2 = \sqrt{a_1^{\,2} + b_1^{\,2}}\,, \quad l_3 = l_4 = \frac{a_1}{1+g^0}\,, \quad l_5 = l_6 = \frac{b_1}{1+g^0}\,, \qquad (22)$$

whereas for the rhombic model $(k = j)$, from **Figure 1(b)**:

$$l_1 = a_2\,, \quad l_2 = b_2\,, \quad l_3 = l_4 = l_5 = l_6 = \frac{\sqrt{a_2^{\,2} + b_2^{\,2}}}{2\left(1+g^0\right)}\,. \qquad (23)$$

The combination of **Eqs.8** to **11**, **19** for $k = i$, and **Eq.22** yields the analytical expression of the total potential energy density function of the rectangular model. Similarly, the combination of **Eqs.15** to **18**, **19** for $k = j$, and **Eq.23** yields the analytical expression of the total potential energy density function of the rhombic model. The explicit form of both functions is not given here due to their large representations; albeit, in compact form they are expressed as:

$$V = V\left(a, b, g^0, g_1^{\beta}, g_2^{\beta}, \beta, \theta\right) \qquad (24)$$

where $a = a_1$, $b = b_1$, for the rectangular model, and $a = a_2$, $b = b_2$, for the rhombic model. Furthermore, it should be stressed that after some elementary algebraic manipulation and factorization, the potential energy functions show a very strong dependence on the ratio (b/a) rather than on the individual lengths themselves. It is straightforward that the value of this ratio directly controls the shape geometry of the two plane tensegrity models. Assuming that $b \le a$, as already implied in **Figure 1**, from the geometrical point of view, low ratio values correspond to elongated tensegrity frames, whereas at the limiting case where the ratio assumes the value equal to unity the shape of the frames degenerates to exactly square. As it will become evident in the following, the value of the *elongation ratio* (b/a) (henceforth simply ER) strongly affects the orientation direction of the models.

Finally, the stable equilibrium directions are detected from the minimization of the total potential energy of both models, *i.e.*, when the following two conditions are met simultaneously:

$$\frac{\partial V}{\partial \theta} = 0 \quad \text{(a)} \qquad \text{and} \qquad \frac{\partial^2 V}{\partial \theta^2} > 0 \quad \text{(b)} \qquad (25)$$

4. GLOBALLY STABLE EQUILIBRIUM DIRECTIONS OF THE PLANE TENSEGRITY CSK MODELS

It is evident that there exists a number of equilibrium directions for the plane tensegrity models that emerge as solutions to **Eq.25(a)**; among them, the ones that additionally satisfy **Eq.25(b)** are stable. The investigation of the stability of the equilibrium requires the definition and adoption of the appropriate explicit stability criteria for the given problem. The orientation of active adherent cells, or even of stress fibres within them, is experimentally established to be one of the natural phenomena that exhibit *coexistence of phases*. Here, coexistence of phases is translated to the emergence of two distinct and concurrent orientation directions in a two–dimensional culture of cells or stress fibres, under the application of the same substrate stretching [3,5]. This kind of behaviour can be met at many different fields of the physical sciences, e.g., the melting of ice, or the coexistence of crystallographic systems in solids [35,36]. In order that our present framework is compatible to this behaviour, we adopt Maxwell's convention for stability which allows coexistence of phases phenomena and declares that the system state is such that globally minimizes the potential [25]. In this context, the fundamental physical reasoning behind cellular reorientation is that when the strain field under the substrate anchored CSK changes, the orientation direction that renders the total potential energy minimum, with respect to all equilibrium directions θ, will be chosen. Accordingly, under the application of substrate stretching, the plane tensegrity models will equilibrate at such a placement where their total potential energy value is a global minimum.

For the integral study of the reorientation phenomenon, the mechanical response of both tensegrity frame geometries will be examined for a broad range of the problem parameters. The general outline is sketched through numerical inspection of the stability of the equilibrium solutions of **Eqs.25**. To this end, a series of graphs is produced that illustrate the variation of the total potential energy density function of each model with respect to the orientation direction θ. Specifically, for a given set of the parameters (g^0, g_1^{β}, g_2^{β}, β) the potential energy is plotted for selected, increasing values of the ER until its maximum value equal to unity. In this fashion, the differences in mechanical behaviour between the two shape geometries, and between more or

less elongated frames of the same geometry, are both successfully detected. Moreover, comparison between graphs that correspond to the same ER value, yet different substrate stretching or prestrain conditions, allows the interpretation of the individual parameter effect on the stability of the orientation direction and on the control of the phenomenon in general. Finally, in this way, the direct cross–examination between experimental data and theoretical predictions is also possible.

4.1. Globally Stable Equilibrium Directions of the Rectangular Model

The graphs comprising **Figure 4** illustrate the total potential energy density as a function of the orientation direction θ for the case of the rectangular model. For the reasons reported above the graphs are arranged in the following fashion. Every column corresponds to a given set of the parameters (g^0, g_1^β, g_2^β, β), and differs from the next one in the value of a single parameter. Further, for each individual column the descending graph order corresponds to discreet increasing ER values, see **Figure 4**. On the other hand, every individual row corresponds to the same ER value.

The graphs of the first (reference) column, **Figures 4(1)** to **4(8)**, have been produced for the set of parameter values: $g^0 = 0.10$, $g_1^\beta = 0.50$, $g_2^\beta = 0.25$, $\beta = 2$, and outline the general behaviour of the rectangular model under biaxial substrate stretch with respect to the geometry of the frame shape. From this sequence it is deduced that for elongated rectangular frames (low ER values), relatively low prestrain and minimum stretch component values, only one global minimum exists at the direction $\theta = \beta$; that is, the rectangular model is reoriented and aligned with the direction of the maximum substrate stretch, see **Figures 4(1)** to **4(3)**. For intermediate ER values, *i.e.*, moderately elongated rectangular frames, the stability character of this direction is maintained (**Figures 4(4)** and **4(5)**). However, as ER tends to its limiting value equal to one, the $\theta = \beta$ solution is destabilized and the emergence of two new globally stable solutions is evident (**Figures 4(6)** to **4(8)**). The direction of maximum substrate stretch, $\theta = \beta$, evolves initially to a local, and finally to a global maximum at the square configuration of the frame. Moreover, the two new, globally stable equilibrium directions located at $\theta = \beta \pm 45^\circ$ are obviously symmetric with respect to the direction of the maximum substrate stretch.

The second column graphs of **Figure 4** have been produced after doubling the value of the maximum displacement gradient of the substrate ($g_1^\beta = 1.00$), while all the other parameter values are the same as in the reference column. The general behaviour of the model is essentially the same as in the previous case. It is easy to identify that rectangular models with low ER values are still aligned with the direction $\theta = \beta$ of the maximum stretch (**Figures 4(9)** to **4(12)**). Albeit, comparison of **Figures 4(5)** and **4(13)** reveals that now the maximum stretch direction is destabilized and the symmetric global minima appear even for intermediate ER values.

The third column graphs of **Figure 4** have been produced after increasing the value of the minimum displacement gradient of the substrate to $g_2^\beta = 0.40$, while all the other parameter values are the same as in the reference column. Again, the same general orientation evolution of the model is observed as in the previous cases. Yet, by cross–examining the sequences of the first three columns, especially for the intermediate and high ER values (e.g., **Figures 4(6)**, **4(14)** and **4(22)**), it is observed that the increase of the minimum stretch results to a delay (in terms of increasing ER value) in the destabilization of the maximum stretch direction and the consequent appearance of the two symmetric global minima at $\theta = \beta \pm 45^\circ$.

The same conclusions hold for the case where prestrain is the parameter increased with respect to the first column value set. For $g^0 = 0.40$, and all the other parameter values the same as in the reference column, the fourth column graphs are produced. Comparing **Figures 4(6)**, **4(14)**, **4(22)**, and **4(30)** (that is, the sixth row of **Figure 4**), it is evident that high prestrain value delays the destabilization of the $\theta = \beta$ solution and favours the orientation parallel to the direction of the maximum substrate stretch, even for high ER values. However, when the rectangular model tends to its limiting configuration (ER→1), the symmetric global minima at $\theta = \beta \pm 45^\circ$ appear again.

It should be pointed out that the four parameters sets reported above and used to construct the graphs of **Figure 4** are representative, and were chosen in order to clearly define both the general behaviour of the model as well as the individual parameter effect on this particular behaviour. Apart from these specific sets, other possible combinations of substrate stretching and prestrain were applied on the rectangular model for an extended range of parameter values (e.g., simultaneous gradual variation); nevertheless, no deviation from the general behaviour exposed above was observed whatsoever. The stability investigation reveals that the final orientation direction depends strongly on the shape geometry of the model as expressed through the ER. Thus, upon the application of biaxial substrate stretch, for the quite elongated rectangular models (low ER values), there exists a single globally stable orientation direction parallel to the direction of the maximum substrate stretch ($\theta = \beta$), independently of the magnitude of the stretch or prestrain. Regarding the other extreme value of the ratio

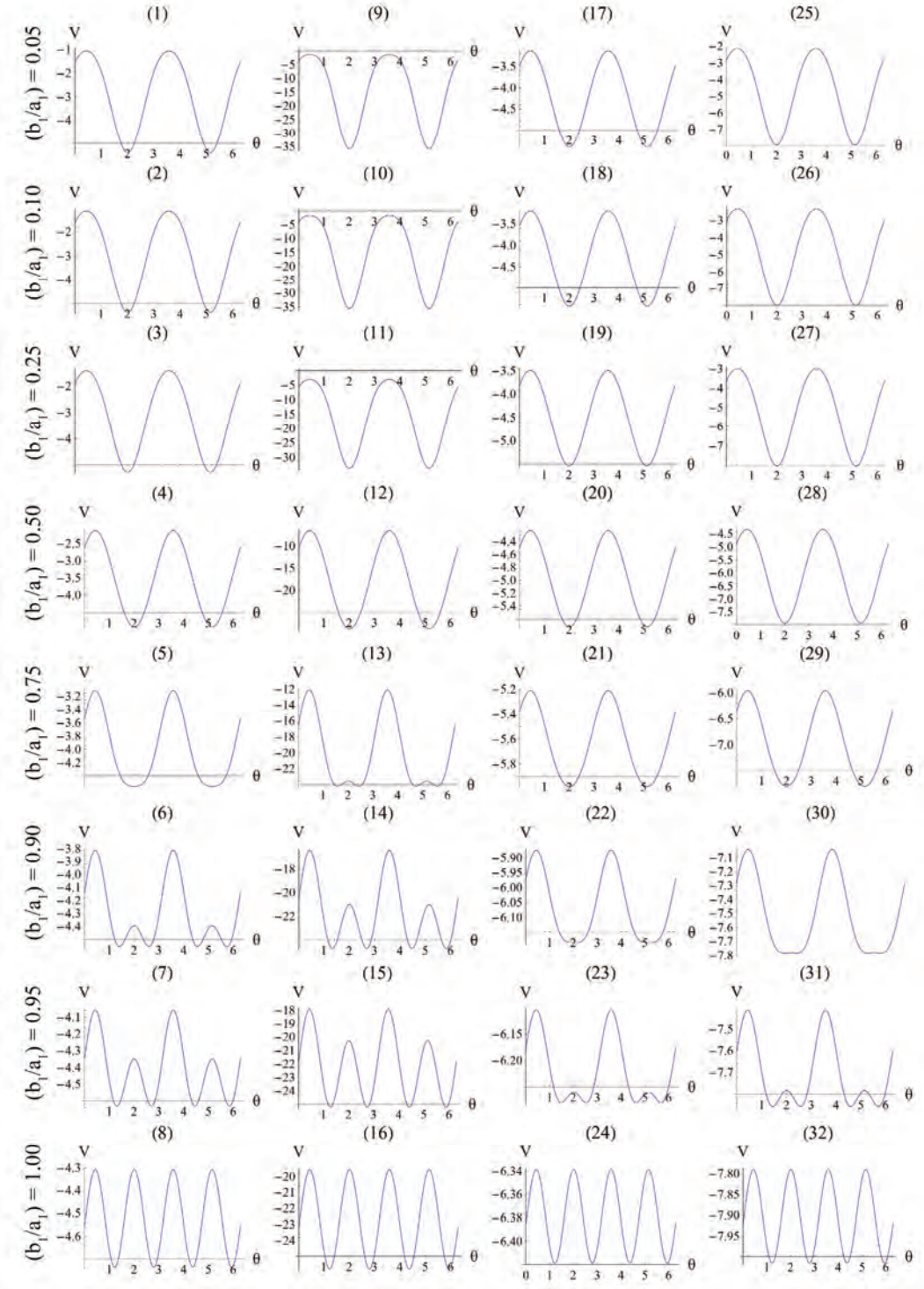

Figure 4. Graphs illustrating the variation of the total potential energy function with respect to the reorientation angle θ for the rectangular tensegrity cytoskeleton. For graph parameters and thorough description see Subsection 4.1.

(ER = 1), where the rectangular frame evolves to square, there exist two globally stable orientations ($\theta = \beta \pm 45^{\circ}$), symmetrically arranged with respect to the direction of the maximum substrate stretch, again independently of the magnitude of the stretch or prestrain. The stability character for intermediate ER values is determined primarily by the magnitude of the maximum substrate stretch component. Initially, the direction of the maxi-

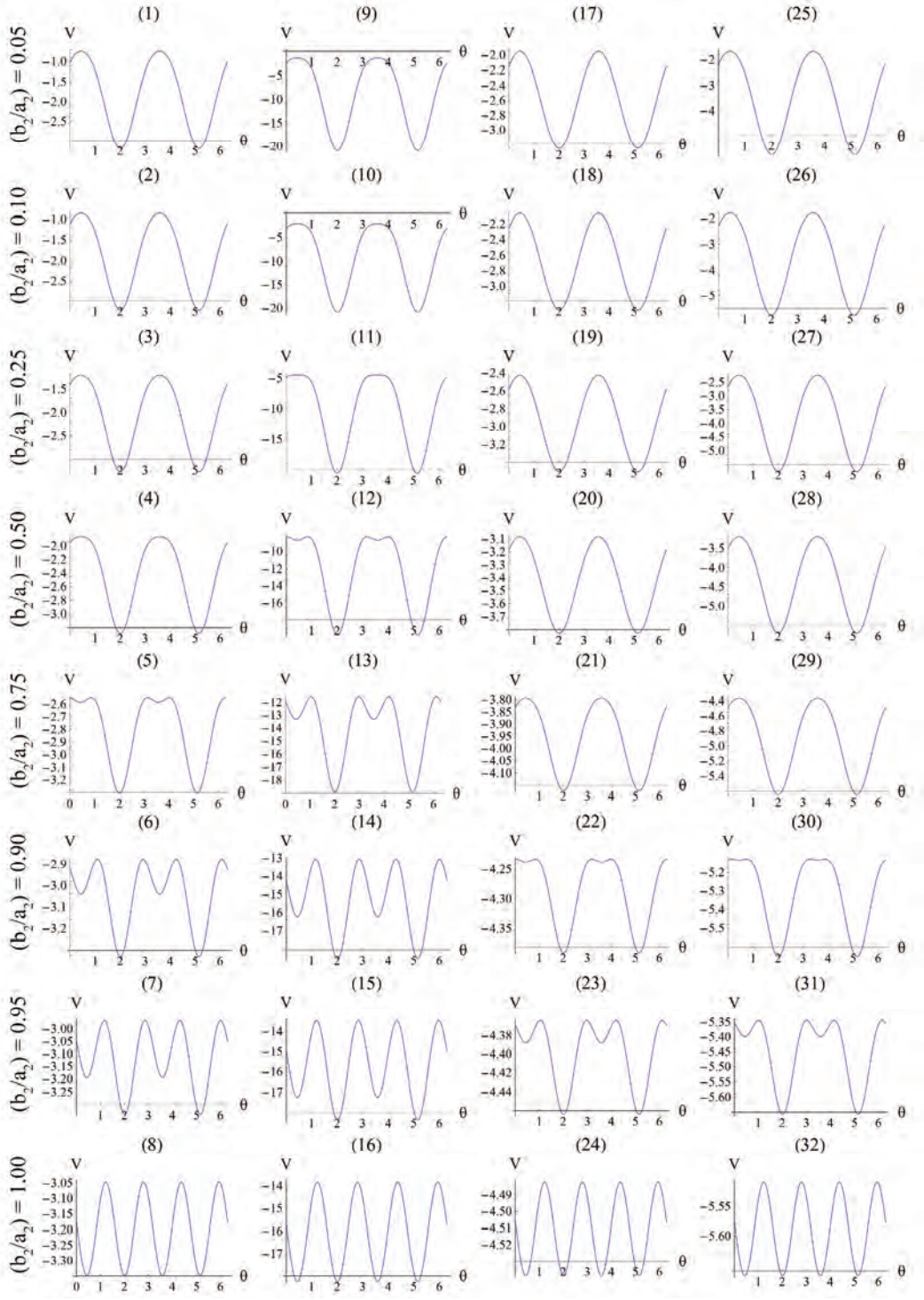

Figure 5. Graphs illustrating the variation of the total potential energy function with respect to the reorientation angle θ for the rhombic tensegrity cytoskeleton. For graph parameters and thorough description see Subsection 4.2.

mum stretch $\theta = \beta$ is globally stable, but as the value of g_1^β increases, the aforementioned direction destabilizes and the new, symmetric globally stable minima emerge. On the other hand, increase of the minimum stretch or prestrain with respect to, either constant or increasing, maximum stretch, delays the destabilization and the appearance of the symmetric global minima until relatively higher ER values only when the values of g_2^β

and g^0 are comparable to the value of g_1^β. In any case, the increase of g_2^β, g^0, values does not prevent the destabilization from happening, and their effect is observed to diminish for high g_1^β values. Hence, as it is concluded by the preceding analysis of the rectangular model, its stability is strongly shape dependent and it is affected by other agents as well, of which the magnitude of the maximum substrate stretch is the primary one.

4.2. Globally Stable Equilibrium Directions of the Rhombic Model

The graphs comprising **Figure 5** illustrate the total potential energy density as a function of the orientation direction θ for the case of the rhombic model. The arrangement of the graphs follows the same fashion as in **Figure 4** (cf. Subsection 4.1 for details).

The graphs of the first (reference) column, **Figure 5(1)** to **5(8)**, have been produced for the set of parameter values: $g^0 = 0.10$, $g_1^\beta = 0.50$, $g_2^\beta = 0.25$, $\beta = 2$, and outline the general behaviour of the rectangular model under biaxial substrate stretch with respect to the geometry of the frame shape. From this sequence it is deduced that for elongated rhombic frames (low ER values), relatively low prestrain and minimum stretch component values, only one global minimum exists at the direction $\theta = \beta$; that is, the rhombic model is re-oriented and aligned with the direction of the maximum substrate stretch, see **Figures 5(1)** to **5(4)**. In contrast to the rectangular frame case, here, as the ER value increases, equilibrium direction β maintains its globally stable character for the entire range of the ratio values, even for the limiting square configuration (**Figures 5(5)** to **5(8)**). Nevertheless, increase of ER values generates the change of stability character in other θ directions-solutions. Specifically, directions $\theta = \beta \pm 90^\circ$, which initially corresponded to global maxima, **Figures 5(1)** to **5(4)**, are gradually developed to local minima, **Figures 5(5)** to **5(7)**, and at the limit case (ER = 1), their stability becomes global, **Figure 5(8)**.

Doubling the value of the maximum displacement gradient of the substrate ($g_1^\beta = 1.00$), while keeping all the other parameter values the same as in the reference column, the second column graphs of **Figure 5** are produced. The general behaviour observed above for the reference column is identically traced here as well, the only actual difference being that the stability transition of directions $\beta \pm 90^\circ$ from unstable global maxima to stable local minima takes place even for intermediate ER values (compare **Figures 5(4)** and **5(12)**).

The exact opposite case holds when the parameter values that are increased with respect to the reference column correspond to the minimum displacement gradient of the substrate (third column, $g_2^\beta = 0.40$), or prestrain (fourth column, $g^0 = 0.40$). Upon comparing **Figures 5(5)** with **5(21)** and **5(29)** it is concluded that increased values of the aforementioned parameters allow the stability transition of directions $\beta \pm 90^\circ$ only for high ER values.

It is pointed out once again that the parameter sets reported above for the construction of the graphs of **Figure 5** are representative, in order to clearly define both the general behaviour of the rhombic frame as well as the individual parameter effect on this behaviour. Other possible combinations of parameter variation were also tested for an extended range of values, yet the frame response was essentially the same in every respect. The stability investigation for the case of the rhombic tensegrity model reveals that the dominant orientation direction strongly depends on the shape geometry also. Thus, upon the application of biaxial substrate stretch, elongated rhombic frames (low ER values) are always aligned parallel with the maximum stretch direction, which corresponds to the unique global minimum of the total potential energy, independently of the stretch or prestrain magnitudes. In the limiting configuration where the rhombus evolves into a square (ER = 1), apart from the globally stable direction $\theta = \beta$, there exists concurrently a second globally stable direction at $\theta = \beta \pm 90^\circ$, that is, perpendicular to the maximum stretch direction. The stability character for the intermediate shape geometries is dominated, again, by the magnitude of the maximum stretch component. Increasing the magnitude of g_1^β not only does not affect the globally stable character of the $\theta = \beta$ solution for any feasible ER value, but new–normal to the initial stable direction–local minima appear at formerly unstable directions. The emergence of the new minima takes place for intermediate or even low ER values provided that the magnitude of g_1^β is sufficiently high. On the other hand, increase of the minimum stretch or prestrain with respect to, either constant or increasing, maximum stretch does not affect the stability character of the maximum stretch direction $\theta = \beta$, and delays the emergence of the new symmetric minima until relatively higher ER values, only when g_2^β and g^0 values are-comparable to g_1^β. In any case, the g_2^β or g^0 value increase does not prevent the emergence of the new minima and their transition from local to global. Further, the influence of g_2^β and g^0 is observed to diminish for high g_1^β values. Consequently, it is deduced from the analysis of this section that the orientation stability of the rhombic model is strongly shape dependent, and that it is controlled secondarily by the magnitude of the

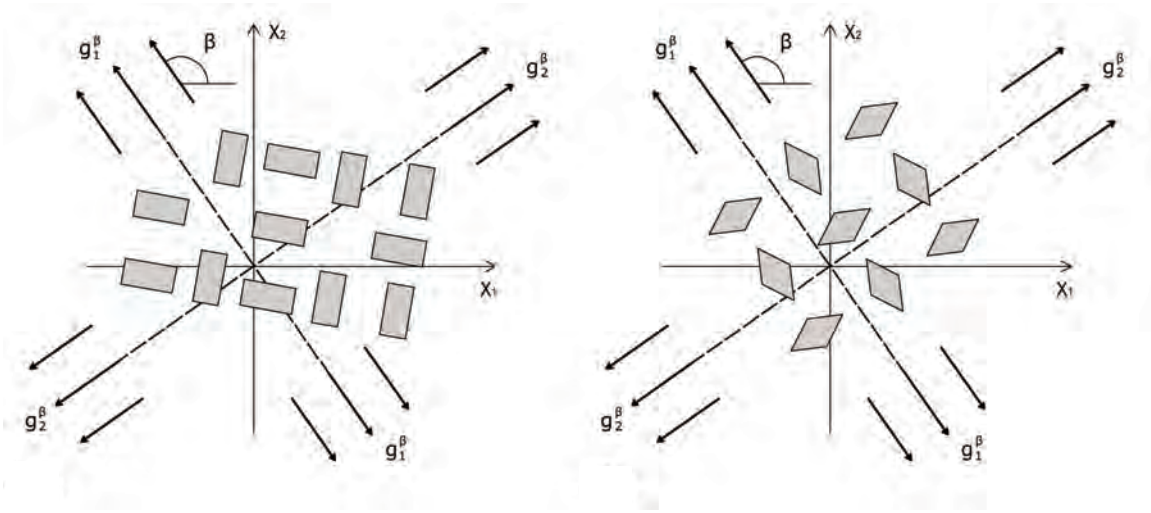

Figure 6. The cellular coexistence of phases phenomenon. (a) the rectangular cytoskeleton case; (b) the rhombic cytoskeleton case.

maximum substrate stretch.

5. DISCUSSION

Summarizing the findings of the stability investigation of both plane tensegrity models in the context of Maxwell's convention, the following can be said. The orientation direction is defined primarily by the shape geometry of the models (ER value), and secondarily the magnitude of the maximum substrate stretch. The similar contribution that present the minimum stretch and prestrain is rather negligible and is only detected when their values are comparable to the maximum stretch component. The rectangular model, for the greatest part of the ER value range, is aligned parallel to the direction β of the maximum substrate stretch, while for the high ER or maximum stretch values it is symmetrically aligned $\pm 45^{\circ}$ away from the aforementioned direction. The rhombic model is oriented parallel to the direction of the maximum stretch for all ER values; albeit, in the liming configuration where it degenerates to a square (ER = 1), it can also align perpendicular to the β direction. In terms of increasing ER values, the orientation of both models evolves from a single, globally stable orientation direction, to the appearance of multiple stable directions, **Figure 6**. In conjunction to previous studies [27,28], it should be pointed out that even though the strain energy of individual structural members of each model has been assumed to be convex, multiple stable equilibrium solutions appear here too, and the total potential energy of both models may be a non–convex function of the orientation direction. This fact affects the shape geometry the models as well.

The discords in the described above orientation evolution of the two models may be attributed both to the different initial shape geometries, and the slightly different definitions of the ER. Although ER expresses essentially the same thing for both frames, it is evident that in the case of the rectangular model it is a ratio of length of elastic strings, whereas for the rhombic model it is a ratio of length of elastic bars, **Figure 1**. Furthermore, in the initial configuration of the rectangular model the two bars are of the same length, while the length of the strings differs in pairs. On the other hand, in the initial configuration of the rhombic model the length of all strings is equal and of the two bars different. However, all these differences are eliminated at the limit–case $(b_1/a_1) = (b_2/a_2) = 1$, where both initial geometries degenerate to precisely square. At this special configuration, the "rectangular–square" and the "rhombic–square" identify with each other provided that either one of them is rotated by $\pm 45^{\circ}$ with respect to its geometric centre. This can be independently confirmed upon qualitative inspection and comparison of the last row graphs in **Figure 4** and **Figure 5**. It is found that the locations of the global minima in the "rectangular–square" case coincide with the locations of the global minima in the "rhombic–square" case if either one of the plot families is translated parallel to the θ–axis by $\pm 45^{\circ}$.

For the low and intermediate ER values, that correspond to physiologically more compatible cellular configurations, the stability analysis of the two models predicts orientation parallel to the direction of the maximum substrate stretch. This response is consistent to the experimental observations of the behaviour of active adherent cells cultured on an elastic substrate under the effect of static or quasi–static stretching [6-9]. For low ER values (ER→0), it is reasonable to consider that the models now represent stress fibres, rather than the entire

CSK [24]. In this case, the analysis predicts alignment with the direction of the maximum substrate stretch, again, in concert to the experimental observations for static stretch [6,8,14]. Further, according to the performed stability analysis, for a certain range of parameter values the concurrent existence of more than one orientation directions is possible, **Figure 6**, a fact that has also been certified experimentally (*cellular coexistence of phases phenomenon*) [3,5]. In the case of the rectangular model, increase of the maximum substrate stretch value results to alignment away from the direction of maximum stretch. The same response to stretch increase is observed for adherent cells under the effect of cyclic substrate stretch [2,4,5,10-13,15], in order to avoid the excessive stretching that may cause rapid disassembly of the cytoskeletal filament network [11,14,37]. Nevertheless, this kind of behaviour is not presented during the orientation evolution of the rhombic model. For this frame type, the increase of the maximum substrate stretch results to a stability transition of the perpendicular to the maximum stretch direction from globally unstable to locally stable. This direction continues to correspond to local only minima until the limit square–configuration, where its stability is rendered global. Hence, according to Maxwell's convention, the rhombic model orients parallel to the direction of the maximum substrate stretch, since in the perpendicular to the latter direction the total potential energy is not globally minimum (except, of course, when ER = 1).

Apart from this last discrepancy between theoretical predictions and experimental observations there appears to be another one related to the effect of prestrain. For both model geometries, increase of prestrain while keeping all the other parameter values constant seems to promote alignment parallel to the maximum stretch direction. Nevertheless, experimental observations for the case of cyclic substrate stretching report a different response [11]. Since in previous theoretical work on the subject, [27,28], model predictions were in concert to experimental data regarding the prestrain effect, it is possible and reasonable to ascribe this discrepancy to the assumption of linear elastic strings. Quite often, in two–dimensional cultures of stationary cells on artificial substrata, actin filaments are bundled to form stress fibres (in fact, in such cases stress fibres are the prominent cytoskeletal feature). If instead of actin filaments we assume that the elastic strings of the two plane tensegrity models correspond to stress fibres, then the strain energy function of **Eq.19** should be modified (e.g., by adding a higher order term), since experimental data suggest that for strains exceeding 40% their behaviour is nonlinear [38]. However, such a consideration would only be in expense of mathematical calculations without improving the physical motivation. In any case, the general behaviour of the two plane tensegrity models is in good agreement with experimental data reported in literature for the cellular orientation under static biaxial substrate stretching, whereas the detected inconsistencies are related to cyclic stretching observations (which are not examined here).

6. CONCLUSIONS

A general integral stability analysis of two plane tensegrity frames used for the description of cellular reorientation under biaxial substrate stretching has been presented. Adopting Maxwell's convention for stability, the analysis was performed in the context of Finite Elasticity Theory. It has been shown that the reorientation is controlled by such parameters as the magnitude of the extracellular stretch components, of which the maximum component is the primary one, and the strength of the intracellular contractile mechanism. This dependence is consistent to numerous well documented laboratory reports (see Refs. in Introduction). It is also in accord with previous theoretical modelling of the reorientation of cellular stress fibres as well [27,28]; yet, the present study focuses on the response of the entire intracellular biopolymer network, which is a substantially more difficult undertaking than studying individual, isolated stress fibres. The new finding, when working with a plane tensegrity CSK, is the governing role of the shape–geometry of the frame. The properties and general behaviour of the two different tensegrity frame geometries have been thoroughly analysed and discussed in the text.

Cellular orientation is a mechanochemical process involving the transduction of a mechanical stretching signal to changes in intracellular biochemistry (and vice versa), while the CSK exhibits dynamic, viscoelastic behaviour. Furthermore, it is certain that cellular architecture is far more complicated than any of its existing mechanical descriptions, and that tensegrity modelling is, rather, a simplification. For these reasons, the good agreement between experimental data and predictions, based on elastic stability considerations of the two, purely mechanical, plane tensegrity models, is quite remarkable. However, the models employed here are simple, physiologically compatible, and the analysis is based on fundamental principles; moreover, no far–fetched assumptions that could bias the results have been introduced. Taking all these into account, it is revealed that mechanical stability is a major determinant of cytoskeletal rearrangement, and that cellular orientation can be successfully treated as a problem of elastic stability. This conclusion does not–in any way–exclude other (chemical) agents that could influence the determination of the orientation direction. Albeit, the consistency of theoretical predictions to the experimental data suggests that the extent of the other agents effect is rather limited, or that their contribution is already integrated to the analysis through their mechanical expressions (e.g., prestrain).

REFERENCES

[1] Suresh, S. (2007) Biomechanics and biophysics of cancer cells. *Acta Biomaterialia*, **3**, 413-438.

[2] Dartsch, P.C. and Haemmerle, H. (1986) Orientation response of arterial smooth muscle cells to mechanical stimulation. *European Journal of Cell Biology*, **41**, 339-346.

[3] Takemasa, T., Sugimoto, K. and Yamashita, K. (1997) Amplitude - dependent stress–fiber reorientation in early response to cyclic strain. *Experimental Cell Research*, **230**, 407-410.

[4] Neidlinger-Wilke, C., Grood, E.S., Wang, J.H.–C., Brand, R.A. and Claes, L. (2001) Cell alignment is induced by cyclic changes in cell length: studies of cells grown in cyclically stretched substrates. *Journal of Orthopaedic Research*, **19**, 286-293.

[5] Wang, J.H.-C., Goldschmidt-Clermont, P., Wille, J. and Yin, F.C.-P. (2001) Specificity of endothelial cell reorientation in response to cyclic mechanical stretching. *Journal of Biomechanics*, **34**, 1563-1572.

[6] Takakuda, K. and Miyairi, H. (1996) Tensile behavior of fibroblasts cultured in collagen gel. *Biomaterials*, **17**, 1393-1397.

[7] Eastwood, M., Mudera, V.C., Mcgrouther, D.A. and Brown, R.A. (1998) Effect of precise mechanical loading on fibroblast populated collagen lattices: morphological changes. *Cell Motility and the Cytoskeleton*, **40**, 13-21.

[8] Collinsworth, A.M., Torgan, C.E., Nagada, S.N., Rajalingam, R.J., Kraus, W.E. and Truskey, G.A. (2000) Orientation and length of mammalian skeletal myocytes in response to unidirectional stretch. *Cell and Tissue Research*, **302**, 243-251.

[9] Ignatius, A., Blessing, H., Liedert, A., Kaspar, D., Kreja, L., Friemert, B. and Claes, L. (2004) Effects of mechanical strain on human osteoblastic precursor cells in type I collagen matrices. *Orthopade*, **33**, 1386-1393.

[10] Iba, I. and Sumpio, B.E. (1991) Morphological response of human endothelial cells subjected to cyclic strain in vitro. *Microvascular Research*, **42**, 245-254.

[11] Wang, J.H.-C., Goldschmidt-Clermont, P. and Yin, F.C.-P. (2000) Contractility affects stress fiber remodelling and reorientation of endothelial cells subjected to cyclic mechanical stretching. *Annals of Biomedical Engineering*, **28**, 1165-1171.

[12] Sipkema, P., van der Linden, J.W., Westerhof, N. and Yin, F.C.-P. (2003) Effect of cyclic axial stretch or rat arteries on endothelial cytoskeletal morphology and vascular reactivity. *Journal of Biomechanics*, **36**, 653-659.

[13] Wille, J.J., Ambrosi, C.A. and Yin, F.C.-P. (2004) Comparison of the effects of cyclic stretching and compression on endothelial cell morphological responses. *ASME Journal of Biomechanical Engineering*, **126**, 545-551.

[14] Kaunas, R., Nguyen, P., Usami, S. and Chien, S. (2005) Cooperative effects of Rho and mechanical stretch on stress fiber organization. *Proceedings of the National Academy of Sciences of the USA*, **102**, 15895-15900.

[15] Kurpinski, K., Chu, J., Hashi, C. and Li, S. (2006) Anisotropic mechanosensing by mesenchimal stemm cells. *Proceedings of National Academy Sciences*, USA, **103**, 16095-16100.

[16] Roth, B. and Whiteley, W. (1981) Tensegrity frameworks. *Transactions of the American Mathematical Society*, **265**, 419-446.

[17] Motro, R. (1992) Tensegrity systems: the state of art. *Int. Journal of Space Structure*, **7(2)**, 75-83.

[18] Connelly R. and Back, A. (1998) Mathematics and tensegrity, *American Scientist*, **86**, 142-151.

[19] Skelton, R.E., Helton, J., Adhikari, R., Pinaud, J. and Chan, W. (2002) An introduction to the mechanics of tensegrity structures (chapter 17), CRC Press.

[20] Williams, W.O. (2007) A primer on the mechanics of tensegrity structures. http://www.math.cmu.edu/users/wow/papers/newprimer.pdf

[21] Stamenović, D. (2006) Models of cytoskeletal mechanics based on tensegrity. In Mofrad, M.R.K., Kamm, R.D. (Eds.), Cytoskeletal mechanics: models and measurements, Cambridge University Press, Manhattan, 103-128.

[22] Ingber, D.E. (1993) Cellular tensegrity: defining new rules of biological design that govern the cytoskeleton. *Journal of Cell Science*, **104**, 613-627.

[23] Ingber, D.E. (1998) The architecture of life. *American Science*, **48(1)**, 75-83.

[24] Ingber, D.E. (2008) Tensegrity-based mechanosensing from macro to micro. *Progress in Biophysics and Molecular Biology*, **97(2-3)**, 163-179.

[25] Gilmore, R. (1981) Catastrophe theory for scientists and engineers. Wiley and Sons, New York.

[26] Thompson, J.M.T. and Hunt, G.W. (1984) Elastic instability phenomena. Wiley and Sons, Chichester.

[27] Lazopoulos, K.A. and Pirentis, A. (2007) Substrate stretching and reorganization of stress fibers as a finite elasticity problem. *International Journal of Solids and Structures*, **44**, 8285-8296.

[28] Pirentis, A.P. and Lazopoulos, K.A. (2009) On stress fibre reorientation under plane substrate stretching. *Archives of Applied Mechanics*, **79**, 263-277.

[29] Stamenović, D., Lazopoulos, K.A., Pirentis, A. and Suki, B. (2009) Mechanical stability determines stress fiber and focal adhesion orientation: a mathematical model. *Cellular and Molecular Bioengineering*, **2(4)**, 475-485.

[30] Lazopoulos, K.A. and Stamenovic, D. (2006) A mathematical model of cell reorientation in response to substrate stretching. *Molecular Cellular and Biomechanics*, **3**, 43-48.

[31] Kamm, R.D. and Mofrad, M.R.K. (2006) Introduction, with the biological basis for cell mechanics. In: Mofrad, M.R.K., Kamm, R.D. (Eds.), Cytoskeletal mechanics: models and measurements. Cambridge University Press, Manhattan, 1-17.

[32] Stamenović, D., Fredberg, J.J., Wang, N., Butler, J.P. and Ingber, D.E. (1996) A microstructural approach to cytoskeletal mechanics based on tensegrity. *Journal of Theoretical Biology*, **181**, 125-136.

[33] Ogden, R.W. (1997) Non–linear elastic deformations.

Dover, New York.

[34] Holzapfel, G.A. (2000) Nonlinear solid mechanics: a continuum approach for engineering. Wiley and Sons, Chichester.

[35] Ericksen, J.L. (1991) Introduction to the thermodynamics of solids. In: Knops, R.J., Morton, K.W. (Eds.). Chapman & Hall, London, 39-61.

[36] Pitteri, M. and Zanzotto, G. (2003) Continuum models for phase transitions and twinning in crystals. Chapman, *et al*., Boca Raton, etc.

[37] Hayakawa, K., Sato, N. and Obinata, T. (2001) Dynamic reorientation of cultured cells and stress fibers under mechanical stress from periodic stretching. *Experimental Cell Research*, **268**, 104-114.

[38] Deguchi, S., Ohashi, S. and Sato, M. (2006) Tensile properties of single stress fibers isolated from cultured vascular smooth muscle cells. *Journal of Biomechanics*, **39**, 2603-2610.

Advances in Bioscience and Biotechnology, 2010, 1, 26-29 **ABB**
doi:10.4236/abb.2010.11004 Published Online April 2010 (http://www.SciRP.org/journal/abb/).

Effect of intraperitoneal and intramuscular injection of killed aeromonas hydrophila on lymphocytes and serum proteins of common carp, cyprinus carpio

Rahim Peyghan*, Gholamhosain H. Khadjeh, Naghmeh Mozarmnia, Maryam Dadar

Veterinary Faculty, Shahid Chamran University, Ahvaz, Iran.
Email: peyghan_r@cua.ac.ir; rpeyghan@yahoo.com

Received 13 January 2010; revised 20 January 2010; accepted 25 January 2010.

ABSTRACT

The effects of injectable killed *Aeromonas hydrophila* on lymphocyte populations and on serum proteins of juvenile common carp, *Cyprinus carpio*, were examined. The fishes were injected either intraperitoneally or intramuscularly with killed *A. hydrophila* bacterin isolated from a diseased fish. 15 days after injection the lymphocyte count was significantly higher in the kidney of intraperitoneally bacteria injected fishes than in the normal saline injected fishes ($p < 0.05$), but in the blood smears the lymphocyte count difference was not significant ($p > 0.05$). In the intramuscular bacteria injected fishes in comparison with the normal saline group, the lymphocyte count was significantly higher only in the blood ($p < 0.05$) but in the kidney the difference was not significant ($p > 0.05$). In comparison between the serum protein parameters in different groups, in intraperitoneal injection of killed-bacteria, total albumin as well as the ratio of albumin/globulin was greater than the control group ($p < 0.05$). The other fractions had not showed any significant difference ($p > 0.05$). In intramuscular injection, the normal saline-injected group, amount of α_1-globulin was significantly higher than bacteria-injected group ($p < 0.05$). For the other fractions there was no significant difference between two groups ($p > 0.05$).

Keywords: Aeromonas hydrophila; Globulins; Albumin, Lymphocytes; Vaccination

1. INTRODUCTION

Aeromonas hydrophila has been recovered from a wide range of freshwater aquarium and cultured fish species worldwide [1,2]. These bacteria have been associated with tail and fin rot, hemorrhagic septicemia and epizootic ulcerative syndrome in many fish species [1,3]. *A. hydrophila* has also been described as the dominant infectious agent of 'fish-bacterial-septicemia' in freshwater cultured cyprinid fishes, mainly common carp.

At present, the chief means of controlling the diseases caused by *A. hydrophila* is by antibiotic treatment and improvement of management practices. However, the extensive use of antibiotics has led to an increase in antibiotic resistance in *A. hydrophila* [4]. An alternative to prophylactic antibiotics treatment is the use of vaccine to prevent the disease. At present no vaccine against *A. hydrophila* is commercially available [5]. Most investigations on fish vaccines development have been carried out mainly on salmonids. These experiments have mostly been based on antibody production and antibodies have been detected in experiments carried out on fish immunized with *A. hydrophila* antigens [6]. However, antibodies have not been detected in some experiments carried out with carp immunized with *A. hydrophila* antigen and several reports have stressed that *A. hydrophila* antigens stimulate non-specific immune mechanisms in fish resulting in cross-immunity against various strains belonging to the genus Aeromonas [7,8].

There have been only a few investigations on vaccination of carp with *A. hydrophila* [9] and no report observed on effect of vaccination with Aeromonas on lymphocyte proliferation and serum proteins in common carp. Lymphocytes through cell-mediated immunity also play an important role in teleost fish immunity against the bacterial pathogens. In blue gourami, Trichogaster trichopterus the proliferative response of head kidney leucocytes were observed after injection of killed *A. hydrophila* [5]. In this study the effects of injectable killed *Aeromonas hydrophila* on blood and kidney lymphocytes proliferation of common carp, have been determined and the changes in serum proteins have also been studied.

2. MATERIAL AND METHODS

2.1. Source of Experimental Fish

120 common carp weighed 30-70 g, were purchased

from a commercial fish farm, and placed into 12 large, 100 l aquaria in de-chlorinated tap water (water temperature, 22-24ºC; hardness, 368 mg/l as $CaCO_3$; pH, 7.6). The fish were fed once daily and mortality or disease sign was seen during the experiments period in the fish.

2.2. Bacterin Preparation

The *Aeromonas hydrophila* bacterin was prepared as follows in our laboratory. The bacterium was isolated and had been identified previously from a diseased common carp. The bacterin was prepared from an isolate grown for 24 h at 25ºC in nutrient agar and by washing with phosphate buffered saline (PBS). Cells were then suspended in PBS containing 0.3% formalin to a final concentration of 900×10^6cells ml^{-1}. To test for sterility, 0.1 ml of the each suspension were streaked on blood agar and incubated for 48 hour at 25ºC.

2.3. Vaccination

The fishes were randomly selected and separated to 4 groups. Two groups of 30 fish each were immunized by intramuscular (I.M.) and intraperitoneal (I.P.) injection, with formalin-killed whole culture cells of *Aeromonas hydrophila* (0.5 ml of bacterin solution in each fish). 40 other fish were separated into 2 groups. 20 fish were injected with 0.5 ml normal saline solution intraperitoneally and 20 fish intramuscularly (controls).

2.4. Sampling and Lymphocyte Counting

Blood samples were taken from the caudal vein without anticoagulant. From each blood sample, one drop was quickly smeared on to a glass slide for counting of lymphocytes. Blood smears were fixed with methanol immediately after drying. After euthanasia of fish by severance of the spinal cord just behind the opercula, the uppermost abdominal body wall was removed and a thin smear from the head kidney was also prepared. All smears were stained by Giemsa method and lymphocytes were counted in relation with counting 1000 RBC, in blood and hematopoietic tissue of anterior kidney of all groups 15 days post-injection by light microscopy.

2.5. Serum Electrophoresis

15 days after injection the serum protein fractions of blood were studied by gel electrophoresis method. Serum was separated by storing the blood in 4ºC for 30-60 min and centrifugation at 2000 rpm for 30 min. Total serum protein was determined by Biuret reaction using an automated biochemical analyzer (Elan, Eppendorf, Germany). Protein fractions were separated electrophoretically by agarose gel [Sebia Hydragel Protein (E) K20], using manufacturer's suggested procedure. Briefly, 10 µl of the serum sample was applied to the agarose gel plate and the plate was placed into an electrophoresis chamber (Sebia K20) with buffer solution (pH 8.5 ± 0.3) and was processed for 22 min at 90 v. Immediately after the electrophoresis, the fractionated proteins were fixed (fixative solution: 60% ethanol, 10% acetic acid and 30% deionized water) and stained in amidoblack solution for 4 min. After staining, the gel was decolorized, dried, and scanned by use of a densitometer (Sebia K20) and the calculation of various protein fractions was made from the resultant electrophoregram.

2.6. Statistical Analysis

For statistical analysis, means and standard deviations for all test values were calculated and one-way ANOVA test (Analysis of Variance) was used to determine whether differences existed between the means were significant or not.

3. RESULTS

The lymphocyte count in all experimental groups was higher than the control groups. The statistical analysis of data (**Table 1**) showed that, the lymphocyte counts were significantly higher in the kidney of intraperitoneal bacterin injected fishes than the normal saline injected fishes ($p < 0.05$), but in the blood the difference was not significant ($p > 0.05$). In the intramuscular bacteria injected fishes in comparison with the normal saline group, the lymphocytes count were significantly higher only in the blood ($p < 0.05$) and in the kidney the difference was not significant ($p > 0.05$). In both blood and kidney, the relative lymphocytes count were in I.M. injected group were significantly higher than I.P. injected group ($p < 0.05$).

Electrophoretogram of experimental and control groups indicated a pattern consisting of 6 peaks. According to other vertebrates' electrophoretogram pattern, from anode to cathode, the picks were named as prealbumin, albumin, α_1-globulin, α_2-globulin, β-globulin, γ-globulin and in some cases γ_2-globulin.

The results showed that in intraperitoneal injection of killed bacteria, total albumin as well as the ratio of albumin/globulins (A/G) was significantly greater than the control group. The other fractions had not showed any significant difference.

In intramuscular injection, normal saline injected group amount of α_1-globulin, was significantly higher than bacteria injected group ($p < 0.05$). For other fractions there was no significant difference between two groups (**Table 2**).

4. DISCUSSION

Despite the extensive reported works on teleost immunology there are a little reports on serum component and cellular antibacterial defense mechanisms in common carp, maybe due to the lack of investigation in this field.

Table 1. Lymphocyte count in blood and kidney of common carp after bacterin and normal saline injection.

Group	Blood lymphocytes[1]		Kidney lymphocytes[2]	
	Bacterin (n = 30)	Normal saline (n = 20)	Bacterin (n = 30)	Normal salin (n = 20)
I.M. injection	56.27 ± 24.51[an]	26.5 ± 9.79[a]	38.48 ± 12.05[n]	33.7 ± 11.05
I.P. injection	36.97 ± 22.11[n]	35.2 ± 22.49	33.05 ± 14.71[an]	23.8 ± 10.99[a]

[a]- The difference between experimental and control group was significant ($p < 0.05$)
[n]- The difference between two experimental group was significant ($p < 0.05$)
[1]- Number of lymphocyte in relation with counting 1000 RBC
[2]- Number of lymphocyte in relation with counting 1000 RBC

Table 2. Different fractions of serum proteins in experimental and control groups (Mean ± SD).

Groups Parameters	I.P. injection		I.M. injection	
	Bacterin (n = 30)	Normal saline (n = 20)	Bacterin (n = 30)	Normal saline (n = 20)
Total protein (g/dl)	3.76 ± 0.49	3.63 ± 0.36	3.57 ± 0.35	3.88 ± 0.75
Pre-albumin (g/dl)	0.23 ± 0.12	0.19 ± 0.09	0.21 ± 0.07	0.28 ± 0.12
Albumin (g/dl)*	1.97 ± 0.37*	1.81 ± 0.32*	1.92 ± 0.31	1.98 ± 0.48
α ı- globulin* (g/dl)	0.5 ± 0.2	0.48 ± 0.15	0.47 ± 0.09*	0.59 ± 0.17*
α 2- globulin (g/dl)	0.67 ± 0.16	0.55 ± 0.3	0.6 ± 0.1	0.6 ± 0.13
β- globulin (g/dl)	0.21 ± 0.17	0.27 ± 0.31	0.27 ± 0.11	0.22 ± 0.1
γ- globulin (g/dl)	0.21 ± 0.2	0.34 ± 0.25	0.11 ± 0.06	0.15 ± 0.1
Total globulin (g/dl)	1.6 ± 0.33	1.69 ± 0.36	1.44 ± 0.23	1.62 ± 0.35
Albumin/globulin ratio*	1.49 ± 0.53*	1.15 ± 0.49*	1.51 ± 0.35	1.41 ± 0.33

*- The difference between groups was significant ($p<0.05$)

In immune parameter studies in many investigations, it has been appeared that production of specific antibodies and lymphocytes, responded well to the bacterial vaccines [1]. Enhancement of protective specific immunity maybe reflected as a result of changing in serum protein composition. Our results showed that in intra-peritoneal injection of killed bacteria, total albumin as well as the ratio of albumin/globulins was significantly greater than the control group. Because of the high osmotic pressure produced by albumin relatively low molecular weight and rather high concentration in the blood stream, the albumin fraction exerts more influence on plasma volume than any other plasma protein. Hence, condition of hyperalbuminemia is rarely seen except in the presence of acute dehydration and shock. Although certain pathological conditions that may lead to hypoalbuminemia in control are: deficient intake of protein, deficient synthesis of albumin by liver and or excessive breakdown or loss of albumin. In intramuscular bacterin injected group the amount of 1-globulin, was significantly lower than the control group. In the 1-globulin fraction are some of the small lipoproteins, some enzymes, mucoproteins and factor V. Further works need to be carried out to determine in more detail, which protein of α-globulin group has been decreased in response to the bacterin injection. In our experiments the γ-globulin fraction didn't change significantly. The γ-globulin fraction contains the anti bodies. In fish, antibody production in the presence of antigen depends greatly on water temperature and in lower temperature it need more time to rise to significant level. So in our experiment if the experiment continued to 1 month the γ-globulin change might raise significantly. Some studies on serum composition in Atlantic salmon infected with A. salmonicida have shown that, some of indices such as total protein and γ-globulin fraction increased significantly [10,11]. On the other hand, Evenberg and his co-workers [12] found that the total serum protein and γ-globulin level was greatly reduced in carp experimentally infected with *A. salmonicida*.

According to our results, method of injection technique may influence the immune response of the fish to vaccination. Many researchers have found that injection is a more reliable method of vaccination compared with the oral or topical application of vaccines against Aeromonas infections. Indian carps and tilapia immunized either intramuscularly or intraperitoneally with Aeromonas vaccine, showed protection against challenge and the agglutinating antibody titre increased in the serum of immunized fish [13,14]. Catfish immunized intraperitoneally by injection with the acid extract of the S-layer protein of *A. hydrophila* were protected from the homologous, virulent strain [15]. In the study of the effects of inject able vaccines against *Aeromonas salmonicida* in rainbow trout, the greatest and broadest ranges of responses were caused by the microencapsulated bacterin with *V. anguillarum* LPS [16].

The experiment with juvenile common carp presented in this paper showed that in comparison with the control,

lymphocytes count has been altered significantly after vaccination. The increase in the number of peripheral blood and kidney lymphocytes that observed in our experimental groups expectedly may be correlated with development of anti-Aeromonas cell mediated immunity in the vaccinated fish. However, for confirmation of effectiveness of the method, changing in other immune parameter such as production of specific antibodies and challenging the fish with a virulent Aeromonas strains must be examined. Further more for the better results, many other factors such as, using immune-stimulators, the choice of the bacterial strains, fish age and water temperature also must be taken into consideration.

REFERENCES

[1] Austin, B. and Adams, C. (1996) Fish pathogens. In: Austin, B., Altwegg, M., Gosling, P.J. and Joseph, S. (Eds) *The Genus Aeromonas*, John Wiley and Sons, Chichester, pp. 197-243.

[2] Nielsen, M.E. Schmidt, A. Qian, D. Shimada, T. Shen, J.Y. and Larsen, J.L. (2001) Is *Aeromonas hydrophila* the dominant motile *Aeromonas* species that causes disease outbreaks in aquaculture production in the Zhejiang province of China. *Disease of Aquatic Organisms*, **46**, 23-29.

[3] Roberts, R.J. (1997) Epizootic ulcerative syndrome (EUS): progress since 1985. In: Flegel T.W. and MacRae I.H. (Eds) Diseases in Asian aquaculture III. *Asian Fisheries Society*, Manila, pp. 125-128

[4] Ansary, A., Haneef, R.M., Torres, J.L. and Yadav, M. (1992) Plasmids and antibiotic resistance in *Aeromonas hydrophila*, isolated in Malaysia from healthy and diseased fish. *Journal of Fish Diseases*, **15**, 191-196.

[5] Fang, H.M., Ling, K.C., Ge, R. and Sin. Y.M. (2000) Enhanchment of productive immunity in blue gourami, *Trichogaster trichopterus* (Pallas), against *Aeromonas hydrophila* and V*ibrio anguillarum* by *A. hydrophila* major adhesion. *Journal of Fish Diseases*. **23**, pp. 137-145.

[6] Loghothetis, P.N. and Austin, B. (1994) Immune response of rainbow trout (*Oncorhynchus mykiss*, Walbaum) to *Aeromonas hydrophila*. *Fish and Shell Fish Immunology*, **4(23)**, 254.

[7] Baba, T., Imamura, J. and Izawa, K. (1988) Immune protection in carp, *Cyprinus carpio* L., after immunization with *Aermonas hydrophila* crude lipopolysaccharide. *Journal of Fish Diseases*, **11**, 237-244.

[8] Stevenson, R.M.W. (1988) Vaccination against *Aeromonas hydrophila*. In: Ellis, A.E. (Ed.), *Fish Vaccination*, Academic Press, London, pp. 112-123.

[9] Kozinska, A. and Guz, L. (2004) The effect of various *Aeromonas bestiarum* vaccines on non-specific immune parameters and protection of carp (*Cyprinus carpio* L.). *Fish and Shellfish Immunology*, **16**, 437-445.

[10] Magnadottir, B. and Gudmundsdottir, B.K. (1992) A composition of total and specific immunoglobulin levels in healthy Atlantic salmon (*Salmo salar*, L.) and in salmon naturally infected with *Aeromonas salmonicida* sub sp. *Veterinary Immunology and Immunopathology*, **32**, 179-189.

[11] Moyner, K. (1993) Changes in serum protein composition occur in Atlantic salmon, *Salmo salar* L. during *Aeromonas salmonicida* infection. Journal of Fish Diseases. **16**: 6. 601-604.

[12] Evenberg, D., de Graaff, P., Fleuren, W. and van Muiswinkel, W.B. (1986) Blood changes in carp (*Cyprinus carpio*) induced by ulcerative *Aeromonas salmonicida* infections. *Veterinary Immunology and Immunopathology*, **12**, 321-330.

[13] Ruangapan, L., Kitao, T. and Yoshida, T. (1986) Protective efficacy of *Aeromonas hydrophila* vaccine in Nile tilapia. *Veterinary Immunology and Immunopathology*, **12**, 345-350.

[14] Karunasagar, I., Rosalind, G. and Karunasagar, I. (1991) Immunological response of the Indian major carps to *Aeromonas hydrophila* vaccine. *Journal of Fish Diseases*, **14**, 413-417.

[15] Ford, L.A. and Thune, R.L. (1992) Immunization of channel catfish with a crude, acid extracted preparation of motile aeromonad S-layer protein. *Biochemical Letters*, **47**, 335-362.

[16] Ackerman, P.A., Iwama, G.K. and Thornton, J.C. (2000) Physiological and immunological effect of adjuvanted *Aeromonas salmonicida* vaccines on juvenile rainbow trout. *Journal of Aquatic Animal Health*, **12(2)**, 157-164.

Advances in Bioscience and Biotechnology, 2010, 1, 30-38 **ABB**
doi:10.4236/abb.2010.11005 Published Online April 2010 (http://www.SciRP.org/journal/abb/).

Biomass and productivity in sal and miscellaneous forests of Satpura plateau (Madhya Pradesh) India

Pramod Kumar Pande[1], A. K. Patra[2]

[1]Wood Anatomy Discipline, Botany Division, Forest Research Institute, Dehradun, India;
[2]Conservator of Forest, Bokaro (Jharkhand), India.
Email: Pandep123@rediffmail.com

Received 18 January 2010; revised 25 January 2010; accepted 28 January 2010.

ABSTRACT

The paper deals with the biomass and productivity of sal (SF) and miscellaneous forests (MF) of Satpura plateau (Madhya Pradesh) India. These forest types were divided into four sites namely open miscellaneous (OMF, site-I), closed miscellaneous (CMF, site-II), open sal (OSF, site-III) and closed sal (CSF, site-IV). The degree of disturbance followed the order: III (0.70) < I (0.12) < II (0.054) < IV (0.018) while considering total trees as measure. OSF (III) and CSF (IV) were most and least disturbed sites among the four. The percent allocation of above ground tree biomass followed the order: 85.08 (II) < 85.51 (I) < 81.31 (III) < 78.09 (IV). The higher above ground tree biomass was produced by MF than of SF. Closed canopy forests produced higher above ground tree biomass than of the open forests. OMF produced 9.5% less biomass than of the CMF whereas, OSF has 39.91% less biomass than of the CSF. The contribution of above ground biomass of shrubs (%) are as follows: 8.3 (IV)< 32.72 (I) <33.77 (III) <52.63 (II). The percent contribution of root biomass was higher for closed sites as compared with open and sites. The root: shoot ratio was ranged between 0.169-0.249. NPP_{tree} (kg $ha^{-1}yr^{-1}$) was highest for site –IV (38094.79), followed by III (33384.29), II (12374.89 and I (9736.52). NPP_{shrub} followed the order: 204 (IV) > 109 (III) > 79.80 (I) > 52.69 (II), while for NPP_{herb}, the order of importance was, 109.50 (IV) > 73.27 (I) > (II), 71.75 (III) > 55.71 (II). NPP_{total} was highest for closed forest stands than of the open ones. NPP_{teak} was lower for high-disturbed site than of the less disturbed site. Photosynthetic/ non - photosynthetic ratio follows the order: 0.067 (II) > 0.030 (III) > 0.026 (IV) > 0.018 (I). Open forests showed lower values for this ratio. NEP was higher for SF than of the MF. Further closed forests showed higher values of NEP. OSF showed lower values of NEP_{sal} than of the CSF. Disturbances in open forests not only reduced stand biomass of tree species, dominant species in particular, but also declined the tree productivity. So, gap filling plantation in side the forest is suggested to improve the productivity of open forests.

Keywords: Biomass; Net Ecosystem Productivity; Net Primary Productivity; Litter Production

1. INTRODUCTION

Satpura plateau is a wide table land stretching from Maikal range in the east to Nimar in the west. It covers Chhindwara, Betul, Seoni, Hosngabad and Balaghat district of Madhya Pradesh (India). The total geographical area of these districts is 49882 km^2. Total dense and open canopy forests were 14291 km^2 (28.65% of the total area) and 5128 km^2 (10.29% of the total area) respectively. The loss in forest area was 83 km^2 as compared to 1997 assessment [1]. The villages of the Satpura are mainly inhabited by tribals. The tribals are mostly Jharias and Gond. They mostly depend on these forest for their livelihood. This creates the pressure on these forests. As a result, closed canopy forests are converting into open canopy forests, and open canopy forests into shrub-lands, savanna and finally to barren lands.

Most of the studies have been carried out on biomass estimation and productivity in different types of forest ecosystems [2-8]. The information on the tropical dry disturbed forests is sparse. In view of the above, the paper deals with: 1) the allocation of biomass in different life forms and their components at different sites and 2) comparison of the standing biomass and productivity of the selected sites. An attempt has also been made to compare the biomass and current productivity of the study sites with other forests of India.

2. MATERIAL AND METHODS

2.1. Study area

The study area is located in Chhindwara district of Madhya Pradesh (India). The forest area comes under Delakhari and Tamia Range of Chhindwara West Forest

Table 1. Physico-chemical properties of soil at different sites.

Site	Soil depth (cm)	PH	N kg ha^{-1}	K Kg ha^{-1}	Carbon (%)	Organic mater (%)
Open Miscellaneous Forest (site - I)	0-20	5.85	156.80	1012.5	1.44	3.26
Closed Miscellaneous Forest (site – II)	0-20	5.95	188.16	500.0	0.75	1.71
Open Sal Forest (site - III)	0-20	6.86	125.44	462.5	0.31	0.70
Closed Sal Forest (site – VI)	0-20	5.95	156.80	375.0	0.29	0.67

Table 2. Density (Plant $100m^{-2}$), species richness (SR)*, Shannon – Wiener diversity index (H) and dominance index (cd)**.

Site/Parameter		OMF	CMF	OSF	CSF
Tree	Density	16.5	23.7	23.7	30.30
	S.R.	28	24	15	17
	TBA	7883	1658	12847	16382
	H	2.995	2.79	2.189	2.048
	cd	0.0685	0.096	0.153	0.216
Shrub	Density	49.6023	64	95.5	108.4
	S.R.	23	21	14	19
	TBA	54.28	136.81	125.05	161
	H	2.62	2.397	1.955	2.054
	cd	0.101	0.128	0.2335	0.246
Herbs	Density	3180	3380	1890	1880
	S.R.	30	35	21	11
	TBA	147.78	547.04	112.80	214.88
	H	3.173	3.01	2.57	1.822
	cd	0.0503	0.084	0.113	0.251

*Speices richness = Number of species, ** Dominance index (cd)= Simpson index, TBA = Total basal area (cm^2 100^{-2})

Division. The area lies between 78°.17' to 79° 10' E longitude and 20°.52¹ to 20°-43'N latitude. The attitude ranges from 387 to 1242 m asl. The study pertains to southern tropical dry peninsular Sal (*Shorea robusta* Gaertn.) forest (5B/C-1c) and southern tropical dry deciduous mixed forest (51/ c-3) [9]. Sal (*Shorea robusta* Gaertn.) was dominating in moist Sal type while teak (*Tectona grandis* Linn.) was in dry mixed forest. These forest types were divided into four sites as open and closed forests on the basis of records of Forest Department and further confirmed by tree density and other parameters of vegetation (**Table 1**). These sites were open miscellaneous (OMF, site-I), closed miscellaneous (CMF, site-II), open sal (OSF, site-III) and closed sal (CSF, site-IV) of tropical dry deciduous mixed (MF) and tropical dry sal forests (SF).

The degree of past disturbances was estimated by calculating coefficient of determiners (R^2) between density and diameter relationship [10]. The magnitude of coefficient indicates the degree to which a stand approximates a balanced structure. The values of 'R^2 ' closer to 'one' means the system is more balanced. The lower values of 'R^2' for these stands are due to unbalanced distribution of many species as a result of disturbances [10]. Examination of R^2 values, the degree of disturbance followed the order: OSF (0.70) < OMF (0.12) < CMF (0.054) < CSF (0.018) while considering total trees as measure. OSF and CSF were most and least disturbed sites far as past disturbances are concerned. While considering main species as measure, the degree of disturbances followed the order: OMF (0.85) < CMF (0.63) < CSF (0.38) < OSF (0.24).

The geology of the ares is extremely complex. Principal geological formations are oldest Archeans, upper and lower Gondwans, Lametas and Deccan trap with patches of recent Alluvium, Talchirs, Barakar, Mootur and Bijories. The soil type was sandy loam to black cotton. Other characteristics of the site are given in **Table 2**.

2.2. Climate

Climate of the area is monsoonal with seasonal rainfall. Average annual rainfall in recent years has been 1100 mm. Approximately 90% of annual precipitation occurs during the wet period (June to September) and distributed over about 120 rainy days. Relative humidity is 22% to 89%. Mean minimum to maximum temperature ranges from 15°C to 40°C. January and May are the coldest and hottest months respectively.

2.3. Biomass Studies

Biomass studies were conducted during 2004 using Harvest method of stratified tree technique, following Peterken and Newbould [11]. In the study, 'multiple random quadrat method' was used. The advantages of multiple random quadrat method over single plot method are;

firstly, it samples optimum area and secondly, it avoid homogeneity of the samples. Twenty quadrats (size, 10 × 10 m for trees, 3 × 3 m for shrubs and 1 × 1 m for herbs) were laid randomly along the transect on each site to sample the maximum representative area. The size of quadrat was determined by plotting species area curve and number of quadrats was determined by plotting increasing number of quadrats against the number of species [12]. The girth (gbh) and height of each tree was measured, individually. In order to have better distribution of sample trees over the population, the whole number of trees was divided into different girth classes. Sample trees for each girth class were selected as being nearest to the average of each class [13]. These sample trees were felled and roots were excavated for underground biomass. The whole tree biomass was recorded for different components viz. leaves, twigs, branches, bole and roots and presented on oven dry weight basis. The tree biomass was calculated as total biomass of standing crop minus leaf biomass plus litter stock. Shrub biomass was estimated using mean tree technique [13]. The mean girth was also calculated for estimating shrub biomass for each species. One plant of near to mean girth of each species was selected for felling. In all, 10 plants of different shrub species were felled and roots were excavated. The 'harvest method' was also used for estimating herb biomass. Five quadrats (1 m × 1 m) were laid randomly at each site for estimating herb biomass. Biomass was harvested and separated into different species as far as possible. Unidentified material is grouped as 'miscellaneous'. The herb biomass was divided into shoot and root and weighed and presented on oven dry weight basis. The biomass of all herbs pooled to get total herb biomass.

The calculated biomass of each sample tree leaving leaf biomass of each girth class was divided by age. Age was determined by volume tables and further confirmed by counting growth rings. The growth rings were counted manually after the smoothing the cross surfaces mechanically and applying glycerin on the smooth surface of the basal disc of each sample [14]. The density of that diameter class was multiplied by this value. This exercise was done for each species. Finally, all the values were summed and value of litter production was added to get 'net primary productivity' (NPP). NEP (Net Ecosystem Productivity) was calculated as bole production of trees [15]. NPP_{tree} is derived from bole, bark, twigs, roots and litter production, while NEP is bole production of trees.

2.4. Litter Studies

Three permanent quadrats of 5 × 5 m size were randomly placed in each site. All the quadrat were initially cleared and swept of any deposited debris. A total of 9 × 12 samples in each site were considered for the estimation of annual litter production. Collecting the litter from these quadrates made monthly estimation of litter fall and then sorting it into leaves and twigs. The miscellaneous litter, which consists of leaf litter of other than of the main species and other unidentified organic matter, was included in leaf litter. Triplicate samples of leaf and twig litter fractions were collected and brought to the laboratory for determining oven dry weight (80°C) from each quadrat. All results are expressed on oven dry weight basis.

3. RESULTS AND DISCUSSION

All the results of biomass and productivity are set in **Tables 3-9**.

3.1. Allocation of Biomass in above Ground and below Ground Components

In general higher value of biomass was observed in bole followed by root, bark, twig and leaves irrespective of species and sites. Further, higher girth classes showed higher biomass in all the sites. It is the reflection of both the age and stature.

The percent allocation of above ground tree biomass followed the order: 85.08 (II) < 85.51 (I) < 81.31 (III) < 78.09 (IV). The higher above ground tree biomass was produced by MF than of SF. Further, closed canopy forests produced higher above ground tree biomass than of the open forests. The contribution of above ground biomass of shrubs (%) were as follows: 8.3 (IV) < 32.72 (I) < 33.77 (III) < 52.63 (II). The MF showed higher biomass than of the SF. It simply reflects the more number of tree species and density of the stand (**Table 3**).

The percent contribution of root biomass was higher for closed sites as compared with open and disturbed sites. Moreover, this was also more for dominant tree species like sal and teak in their respective stands as indicated by below ground and above ground biomass ratio. It indicated that teak and sal allocated more resources to root system at the early stages of tree growth to optimize the nutrient uptake.

The root: shoot biomass ratio was ranged between 0.169-0.249. The mean root: shoot biomass ratio was reported as 0.24±0.14 for tropical forests [16]. The values of root: shoot ratio for present are well within the reported range for tropical forests [16]. Further this ratio was higher for closed and undisturbed sites.

The allocation of biomass in different components in tropical and subtropical forest is given in **Table 4**. The total above ground biomass ranged between 27.5-205.50 t ha^{-1}. The range for the below ground biomass is in between 7.6-34.3 t ha^{-1}. Total biomass ranged between 37.12-239.80 t ha^{-1}. The ranges for the present study for above ground, below ground and total biomass (t ha^{-1}) were 154.9-345.6; 35.60-62.16 and 190.53-406.27 respectively. The results on biomass of present study are on the higher side than the reported range for tropical/subtropical forests published elsewhere in literature

Table 3. Above ground biomass (AGB) and below ground biomass (BGB) at different sites (kg ha^{-1}).

Component	AGB	BGB	BGB/AGB	Total
OMF (Site-I)				
T. grandis	42958.59	8201.54	0.191	51160.13
Miscellaneous	272783	45293.93	0.166	318077
Total	315741.6	53495.47	0.169	369237.1
CMF (Site-II)				
T. grandis	78775.13	15298.6	0.194	94073.73
Miscellaneous	266889.5	45303.01	0.170	312192.5
Total	345664.6	60601.61	0.175	406266.2
SOF (Site-III)				
S. robusta	48845.7	14939.7	0.306	63785.4
T. grandis	34627.51	6596.69	0.191	41224.2
Miscellaneous	71462.16	14060.25	0.197	85522.41
Total	154935.4	35596.64	0.230	190532
SCF (Site-IV)				
S. robusta	139560.3	40606.5	0.291	180166.8
T. grandis	88073.29	14154.89	0.161	102228.2
Miscellaneous	29683.51	7402.55	0.249	37086.06
Total	257317.1	62163.94	0.242	319481.1

Table 4. Dry Phytomass (tha^{-1}) of tropical dry forests.

Locality	Phytomass				Authority
	AGB*	BGB**	Total	BLG/ABG	
Varanasi	-	7.6	-	-	Bandhu, 1970 [17]
Varanasi	205.5	34.3	239.8	0.17	Singh, 1975 [2]
Varanasi	64.3	9.5	73.8	0.15	Singh and Singh, 1981 [4]
Chandraprabha	95.0	-	-	-	Singh, 1989
Udipur	28.2	-	-	-	Ranawat and Vyas, 1975 [3]
Haldwani	74.6-164	15.4-17.9	90-192	0.21-0.11	Negi, *et al.*, 1995 [7]
Tripura	113.97	24.39	138.37	0.21	Negi *et al.*, 1990 [6]
Coimbatore	27.55	11.08	38.63	0.40	George *et al.*, 1990 [5]
Dehra Dun	129.58	-	-	-	Kaul *et al.*, 1979 [18]
Chhindwara (MP)	28.11-85.26	9.08-15.63	37.12-100.89	0.32-0.18	Pande, 2002 [8]

* AGB- Above ground biomass, * BGB- Below ground biomass

(**Table 4**). It may be accounted for the higher tree density of the preset study sites.

Table 5 shows allocation of biomass (kg ha^{-1}) in different tree species at different sites. *Tectona grandis* (51160.13) and miscellaneous species (318076.59) like *Butea monosperma, Lagerstroemia parviflora, Anogeissus latifolia, Lannea grandis* were the major contributors towards total tree biomass (kg ha^{-1}) at site-I, whereas *T. grandis* (94073.7) and miscellaneous tree species like *Butea monosperma*, *Diospyros melanoxylon*, *Buchanania lanzen*, *Butea monosperma* and others have contributed 312192.46 towards total biomass at site- II. In site-III, *Shorea robusta* (63785.4) *Tectona grandis* (41224.2), and species like *Buchanania lanzen*, *Terminalia tomentosa* and others forms of the miscellaneous contributed major part (85522.41 kg ha^{-1}) towards the total tree biomass. The site-IV, *Shorea robusta* (180166.84), *Tectona grandis* (102228.18) and other species like *Buchanania lanzen*, *Madhuca latifolia*, *Diospyros melanoxylon*, *Lagerstroemia parviflora*, *Emblica officinalis*, etc. forms miscellaneous and contributed (37086.06) towards total biomass. Invariably, higher age groups accounted for higher biomass for their higher total basal area.

The higher biomass values were obtained for closed forests than of the open forests. It is the reflection of higher tree density and total basal area of those stands which realized higher biomass at those sites. More herb and shrub biomass produced by OMF than CMF and is indicative of the space/resource created by disturbances are efficiently utilized by herbs and shrubs due to their relative smaller niche-size. The higher shrub biomass in CSF than of the OSF may be due to the higher regeneration potential of different tree species at that site.

Table 6 shows biomass stocks (kg ha^{-1}) at different sites. MF showed higher biomass than of the SF. It may be due to more tree density, species richness and mean basal area. OMF produced 9.5% less biomass than of the CMF whereas, OSF have 39.91% less biomass than of the

Table 5. Biomass (kg ha^{-1}) in different components at different sites.

Component/Sites	Age	Leaf	Bole	Twig	*Bark*	Root	Total
OMF (Site-I)							
T. grandis	10	21	60	10.8	12	42	145.8
	15	52.64	341.84	38.72	104	217.04	754.24
	18	243	1644.3	300.6	414	567	3168.9
	22	253.4	1915.34	304.29	478.8	661.5	3613.33
	30	390	4633.8	874.5	948	2028	8874.3
	90	388.2	26797.2	1388.16	1344	4686	34603.56
Total (A)		1348.24	35392.48	2917.07	3300.8	8201.54	51160.13
Miscellaneous	10	70	200	36	40	140	486
	15	72.38	470.03	53.24	143	298.43	1037.08
	18	513	3471.3	634.6	874	1197	6689.9
	22	470.6	3557.06	565.11	889.2	1228.5	6710.47
	30	650	7723	1457.5	1580	3380	14790.5
	90	3235	223310	11568	11200	39050	288363
Total (B)		5010.98	238731.4	14314.45	14726.2	45293.93	318076.95
Total (A+B)		6359.22	274123.9	17231.52	18027	53495.47	369237.08
					Shoot	Root	
Shrub					104.448	214.768	319.21
Herb							73.27
Litter accumulation							3390
Leaf biomass (-)							6359.22
Grand Total							366660.34
CMF (Site-II)							
T. grandis	10	66.5	190	34.2	38	133	461.7
	15	131.6	854.6	96.8	260	542.6	1885.6
	18	378	2557.8	467.6	644	882	4929.4
	22	289.6	2188.96	347.76	547.2	756	4129.52
	30	845	10039.9	1894.75	2054	4394	19227.65
	90	711.7	49128.2	2544.96	2464	8591	63439.86
Total (A)		2422.4	64959.46	5386.07	6007.2	15298.6	94073.73
Miscellaneous	10	108.5	310	55.8	62	217	753.3
	15	177.66	1153.71	130.68	351	732.51	2545.56
	18	243	1644.3	300.6	414	567	3168.9
	22	470.6	3557.06	565.11	889.2	1228.5	6710.47
	30	975	11584.5	2186.25	2370	5070	22185.75
	90	3105.6	214377.6	11105.28	10752	37488	276828.48
Total (B)		5080.36	232627.2	14343.72	14838.2	45303.01	312192.46
Total (A+B)		7502.76	297586.6	19729.79	20845.4	60601.61	406266.19
					Shoot	Root	
Shrub					110.92	99.82	210.74
Herb							55.71
Litter accumulation							3514.6
Leaf biomass (-)							5080.36
Grand Total							404966.88
SOF (Site-III)							
S. robusta	10	126.4	89.6	30.4	44.8	131.2	422.4
	15	176.4	1992.9	409.5	1113	1272.6	4964.4
	18	241.05	3367.5	648	1485	1896	7637.55
	22	472.6	7923.7	1443.3	2857.7	4005.2	16702.5

	30	138.75	2742.6	475.2	822	1257.3	5435.85
	80	651.6	15221.7	2520	3852	6377.4	28622.7
Total (A)		1806.8	31338	5526.4	10174.5	14939.7	63785.4
T. grandis	10	52.5	150	27	30	105	364.5
	15	85.54	555.49	62.92	169	352.69	1225.64
	18	216	1461.6	267.2	368	504	2816.8
	22	144.8	1094.48	173.88	273.6	378	2064.76
	30	260	3089.2	583	632	1352	5916.2
	90	323.5	22331	1156.8	1120	3905	28836.3
Total (B)		1082.34	28681.77	2270.8	2592.6	6596.69	41224.2
Miscellaneous	10	80.5	230	41.4	46	161	558.9
	15	164.5	1068.25	121	325	678.25	2357
	18	621	4202.1	768.2	1058	1449	8098.3
	22	651.6	4925.16	782.46	1231.2	1701	9291.42
	30	585	6950.7	1311.75	1422	3042	13311.45
	90	582.3	40195.8	2082.24	2016	7029	51905.34
Total (C)		2684.9	57572.01	5107.05	6098.2	14060.25	85522.41
Total (A+B+C)		5574.04	117591.8	12904.25	18865.3	35596.64	190532.01
					Shoot	Root	
Shrub					74.256	145.581	219.83
Herb							71.75
Litter accumulation							4368.8
Leaf biomass (-)							2684.9
Grand Total							192507.49
SCF (Site-IV)							
S. robusta	10	197.5	140	47.5	70	205	660
	15	394.8	4460.3	916.5	2491	2848.2	11110.8
	18	594.59	8306.5	1598.4	3663	4676.8	18839.29
	22	695	11652.5	2122.5	4202.5	5890	24562.5
	30	693.75	13713	2376	4110	6286.5	27179.25
	90	1956	55417.5	8392.5	11349	20700	97815
Total (A)		4531.64	93689.8	15453.4	25885.5	40606.5	180166.84
T. grandis	10	24.5	70	12.6	14	49	170.1
	15	19.74	128.19	14.52	39	81.39	282.84
	18	54	365.4	66.8	92	126	704.2
	22	108.6	820.86	130.41	205.2	283.5	1548.57
	30	65	772.3	145.75	158	338	1479.05
	90	1099.9	75925.4	3933.12	3808	13277	98043.42
Total (B)		1371.74	78082.15	4303.2	4316.2	14154.89	102228.18
Miscellaneous	10	66.5	190	34.2	38	133	461.7
	15	230.3	1495.55	169.4	455	949.55	3299.8
	18	810	5481	1002	1380	1890	10563
	22	362	2736.2	434.7	684	945	5161.9
	30	520	6178.4	1166	1264	2704	11832.4
	90	64.7	4466.2	231.36	224	781	5767.26
Total (C)		2053.5	20547.35	3037.66	4045	7402.55	37086.06
Total (A+B+C)		7956.88	192319.3	22794.26	34246.7	62163.94	319481.08
					Shoot	Root	
Shrub					67.634	750.936	818.57
Herb							109.5
Litter accumulation							7815
Leaf biomass (-)							2053.5
Grand Total							320409.5

Table 6. Biomass stocks (kg ha^{-1}) at different sites.

Life forms/Site	Tree		Shrub	Herb	Litter Accumulation	Leaf biomass (-)	Total
	Bole	Total					
I	274123.9	369237.1	319.21	73.27	3390	6359.22	366660.34
II	297586.6	406266.2	210.74	55.71	3514.6	5080.36	404966.88
Average	285855.3	387751.7	264.98	64.49	3452.3	5558.79	385813.61
III	117591.8	190532.01	219.83	71.75	4368.8	2684.9	192507.49
IV	192319.3	319481.1	818.57	109.5	7815	2053.5	320409.5
Average	154955.5	255006.6	519.18	90.63	6091.9	2369.2	256458.25

Table 7. Biomass stocks (kg ha^{-1}) at per tree basis at different sites

Life forms/Site	Tree		Shrub	Herb	Litter Accum-ulation	Leaf biomass (-)	Total
	Bole	Total					
I	166.14	223.78	0.19	0.04	2.05	3.85	222.22
II	130.52	178.19	0.09	0.02	1.54	2.23	177.62
Average	148.33	200.98	0.14	0.03	1.80	3.04	199.92
III	49.62	83.57	0.10	0.03	1.92	1.18	84.43
IV	641.06	140.12	0.36	0.05	3.43	0.90	140.53
Average	345.34	111.84	0.23	0.04	2.67	1.04	112.48

Table 8. Photosynthetic (P) and non-photosynthetic (NP) biomass (kg ha^{-1}).

OMF (Site-I)	P	NP	P/NP	Total
T. grandis	1348.24	49811.89	0.027	51160.13
Miscellaneous	5010.98	313065.97	0.016	318076.95
Total	6359.22	362877.86	0.018	369237.08
CMF (Site-II)				
T. grandis	12718.44	81355.29	0.156	94073.73
Miscellaneous	25436.88	286755.58	0.089	312192.46
Total	25436.88	380829.31	0.067	406266.19
SOF (Site-III)				
S. robusta	1806.80	61978.60	0.029	63785.40
T. grandis	1082.34	40141.86	0.027	41224.20
Miscellaneous	2684.90	82837.51	0.032	85522.41
Total	5574.04	184957.97	0.030	190532.01
SCF (Site-IV)				
S. robusta	4531.64	175635.20	0.026	180166.84
T. grandis	1371.74	100856.44	0.014	102228.18
Miscellaneous	2053.50	35032.56	0.059	37086.06
Total	7956.88	311524.20	0.026	319481.08

CSF. OMF produced 9.1% less bole biomass than of the CMF while OSF produced 40.36% les biomass than of the CSF.

Biomass stocks on tree^{-1} basis (kg ha^{-1}) and plant^{-1} are given in **Table 7**. The average values for total tree^{-1}/ plant^{-1} and total biomass in all life forms was more in case of MF than of the SF. But the situation was reverse in case of bole biomass. While comparing the open and closed forests, it was higher for closed forests in both the cases.

3.2. Photosynthetic and Non-Photosynthetic Biomass

Allocation of biomass in photosynthetic and non-photosynthetic components at different sites is tabulated in **Table 8**. Photosynthetic/non-photosynthetic ratio follows the order: 0.067 (II) > 0.030 (III) > 0.026 (IV) > 0.018 (I). Open forests showed lower values for this ratio. It may be explained as; firstly, the photosynthetic demand is higher at early developmental stages of stand growth thus form higher foliage in closed forests and, secondly, the less disturbances protect the foliage from the lopping and grazing at closed forest sites.

3.3. Biomass: Total vs. Main Species

The contribution of biomass of *Tectona grandis* (teak) and Shorea *robusta* towards total biomass is given in

Table 9. NPP and NEP (kg ha^{-1} yr^{-1}) at different sites.

	NPP leaf	NPP	NEP		NPP leaf	NPP	NEP
					SOF (Site-III)		
	OMF (Site-I)				Tree		
	Tree			*S. robusta*	72.04	2095.69	970.76
T. grandis	47.94	1085.45	659.41	*T. grandis*	41.80	886.11	534.08
Miscellaneous	119.33	4491.47	3144.53	Miscellaneous	109.10	2105.71	1229.85
Total	167.27	5576.92	3803.93	Total	222.94	5087.51	2734.69
Shrub		79.80		Shrub		109.92	
Herb		73.27		Herb		71.75	
LP		4173.80		LP		33089.60	
NPP leaf (-)		167.27		NPP leaf (-)		222.94	
Grand Total		9736.52		Grand Total		33384.29	
	CMF (Site-II)				SCF (Site-IV)		
	Tree				Tree		
				S. robusta	155.55	4962.63	2375.33
T. grandis	85.66	1979.25	1198.10	*T. grandis*	26.09	1284.05	942.52
Miscellaneous	124.59	4541.50	3129.07	Miscellaneous	101.51	1546.12	803.15
Total	210.25	6520.75	4327.18	Total	283.15	7792.80	4121.00
Shrub		52.69		Shrub		204.64	
Herb		55.71		Herb		109.50	
LP		5956.00		LP		30271.60	
NPP leaf (-)		210.25		NPP leaf (-)		283.15	
Grand Total		12374.89		Grand Total		38094.79	

Table 3. The highest percent contribution of teak towards total biomass is shown by site-IV (31.19) and followed by-II (23.15), -III (21.16), and -I (13.85). It clearly indicated negative impact of disturbance on dominant tree species (teak) at open forest sites. The highly disturbed site-I contributed only 13.85% biomass towards total, whereas site-III - the least disturbed, contributed 23.85% towards total biomass. The contribution of biomass of sal at open and closed forests was 33.47% and 56.37% respectively. The lower contribution of main species at open forest may be due to higher contribution of miscellaneous tree biomass. The open forest sites of the present study (I) and (III)undergone various anthropogenic disturbances like lopping, felling, grazing, etc. during the remote and recent past. It created large gaps inside the forest. These gaps provided space/resource for invading species. Thus, create opportunity to acclimatize and establish them in the prevailing climate. These species became second and even first canopy species at present and their contribution in total biomass is 86% and 44.88% respectively for OMF and OSF.

3.4. Net Primary Productivity

A perusal of **Table 9** shows that NPP_{tree} ($kgha^{-1}yr^{-1}$) is highest for site -IV followed by (38094.79), III (33384.29), II (12374.89 and I (9736.52). NPP_{shrub} followed the order: 204 (IV) > 109 (III) > 79.80 (I) > 52.69 (II), while for $NPP_{herb,}$ the order of importance was, 109.50 (IV) > 73.27 (I)> (II), 71.75 (III) > 55.71 (II). NPP_{total} was highest for closed forest stands than of the open ones. NPP_{teak} was lower for high-disturbed site than of the less disturbed site. It indicated that disturbances decreased productivity of teak in the both miscellaneous and sal forests of Satpura forests. This is also true for NPP_{shrub}. In contrary, NPP_{herb} is almost accounting more or similar values for the sites.

Net primary productivity (kg ha^{-1} yr^{-1}) of *Tectona grandis* is highest for site-II and followed by IV, I, III. NPP teak was higher for closed forest sites. George et al. [5] reported NPP in some southern tropical forests of Coimbatore as 2476 kg ha^{-1} yr^{-1}. Karmacharya and Singh [19] reported NPP between 12933-25588 kg ha^{-1} yr^{-1} in some tropical teak plantations. Negi *et al.* [7] reported NPP in between 6421-11289 kg ha^{-1} yr^{-1} in some tropical teak plantations of Haldwani (UP). The values of NPP_{tree} in present study are well with in the reported range for tropical forests. However, the values are higher than of George *et al.* [5] and Kaul *et al.* [18]. This is the reflection of good regeneration and - fertility of the forests. This view is also supported by George *et al.* [5]. The same is also true for NPP on per tree basis.

3.5. Net Ecosystem Productivity

NEP is calculated from bole biomass. NEP was higher for sal forests than of the miscellaneous forests. Further closed forests showed higher values of NEP. Net eco-

system productivity for *Tectona grandis* was also higher for sal ecotone forest. Open sal forest showed lower values of NEP_{sal} than of the closed sal forest (**Table 9**).

3.6. Comparison with Other Forests

Murphy and Lugo [20] reported that stem wood biomass production ranged between 4 – 18 t ha^{-1} yr^{-1} in tropical dry regions compared with 10-30 t ha^{-1} yr^{-1} in tropical moist and wet region. The bole production (0.85-1.354 t ha^{-1} yr^{-1}) in teak forests at Chhindwara towards the lower end of the dry tropical forests This is due to lower soil depth and nutrient poor soil of the investigation sites [8]. The bole production in the present study was in the range of 2.734-4.327 t ha^{-1}. It is well with in reported range of tropical dry deciduous forests.

3.7. Management

It is clear from the preceding discussion that disturbances in open forests not only reduce stand biomass of tree species (dominant species in particular) but also decline the tree productivity. In another study, Pande (2002) reported that the NPP_{teak} was 63% higher in the plantation inside the forest, than of the actual site. It clearly indicated that productivity of open forest sites increased substantially, for target species by gap filling plantation. Therefore, it is suggested to forest managers to fill the blanks in side the forest by target species so that tree productivity would be maintained. This will also helpful to maintain the tree composition of the forest.

REFERENCES

[1] F.S.I. (2000) State of Forest Report (1999) Forest Survey of India (Ministry of Environment & Forest, India), Dehradun, p. 113.

[2] Singh, R.P. (1975) Biomass, nutrient and productivity structure of a stand of dry deciduous forest of Varanasi. *Tropical Ecology*, **22**, 97-105.

[3] Ranawat, M.P.S. and Vyas, L.N. (1975) Litter production in deciduous forests of Koriyat, Udaipur (South Rajesthan) India. *Biologia*, **30**, 41-47.

[4] Singh, K.P. and Singh, R.P. (1981) Seasonal variation in biomass, nutrient and productivity structure of a stand of dry deciduous forest of Varanasi. *Tropical Ecology*, **16**, 104-109.

[5] George, M., Varghees, G. and Manivachakam, P. (1990) Nutrient cycling in Indian tropical dry deciduous forest ecosystem. Proceeding of the Seminar on Forest Productivity Held at F.R.I. Dehradun, 23-24 April 1990, pp. 289-297.

[6] Negi, J.D.S., Bahuguna, V.K. and Sharma, D.C. (1990) Biomass production and distribution of nutrients in 20 years old teak (*Tectona grandis*) and gamar (*Gmelina arborea*) plantation in Tripper. *Indian Forester*, **116**, 681-686.

[7] Negi, M.S., Tandon, V.N. and Rawat, H.S. (1995) Biomass and nutrient distribution in young teak (*Tectona grandis* Linn f) plantations in Tarai region of Uttar Pradesh. *Indian Forester*, **121**, 455-464.

[8] Pande, P.K. (2002) Structure and function of tropical dry deciduous teak forest as per their disturbance magnitude with emphasis on regeneration and management. *Final Technical Report* (CFRHRD/2; TFRI/18), ICFRE, Dehradun, India, 65.

[9] Champion, H.G. and Seth, S.K. (1968) A revised survey of forest types of india. Government, India Printers, New Delhi.

[10] Robertson, P.A., Weaver, G.T and Cavanaugh (1978) Vegetation and tree species patterns near the northern terminus of the southern flood plain forests. *Ecological Monograph*, **48**, 249-269.

[11] Peterken C.F. and Newbould, P.S. (1966) Dry matter production *Xlex aquifolium* in New Forest. *Journal of Ecology*, **54**, 143-150.

[12] Misra, R. (1968) Ecology work book. Oxford and IBP Publishing Co., Calcutta.

[13] Ovington, J.D., Forest, W.G. and Armstrong, J.S. (1967) Tree biomass estimation. Symposium primary productivity & mineral cycling in natural ecosystems. *AAAS Ecological Society of America*, 4-31.

[14] Ramesh Rao, K. (1966) Studies of density and fibre characteristics of Indian timbers. PL 480 Project, Final Technical Report Forest Research Institute, Dehradun.

[15] Turner, D.P., Koerper, G., Horman, M.E. and Lee, J.J. (1995) A carbon budget for the conterminous United States. *Ecological Applications*, **5**, 421-436.

[16] Cairns, C.A., Brown, S., Heeler, E.H. and Baumgardner, G. A. (1997) Root biomass allocation in the world's upland forests. *Oecologia*, **111**, 1-11.

[17] Bandhu, D. (1970) A study of productive structure of northern tropical dry deciduous forest near Varanasi. I. Stand structure and non-photosynthetic biomass. *Tropical Ecology*, **11**, 90-104.

[18] Murphy P.G. and Lugo, A.E. (1986) Ecology of tropical dry forest. *Annual Review of Ecology & Systematics*, **17**, 67-88.

[19] Karmacharya, S.B. and Singh, K.P. (1992) Biomass and net production of teak plantation in a dry tropical region in India. *Forest Ecology & Management*, **55**, 233-247.

[20] Kaul, O.N., Sharma, D.C., Tandon, V.N. and Srivatava, P.B.L. (1979) Organic matter and plant nutrients in a teak (*Tectona grandis*) plantation. *Indian Forester*, **105**, 573-582.

Advances in Bioscience and Biotechnology, 2010, 1, 39-46 **ABB**
doi:10.4236/abb.2010.11006 Published Online April 2010 (http://www.SciRP.org/journal/abb/)

Osmolyte modulated enhanced rice leaf catalase activity under salt-stress

Sushmita Sahu, Priyanka Das, Mamata Ray, Surendra Chandra Sabat*

Gene Function and Regulation Group, Stress Biology Laboratory, Institute of Life Sciences, Orissa, India.
Email: surendrachandra@gmail.com

Received 27 January 2010; revised 26 February 2010; accepted 8 March 2010.

ABSTRACT

Change in catalase activity was examined in leaves of rice plant exposed to salinity. Depending on the method of preparation of crude protein extract from leaf and the constituents of the assay medium, a significant difference in enzyme activity was recorded. Inclusion of sorbitol or mannitol or sucrose in the extraction and enzyme assay medium enhanced the enzyme activity in salt-stressed samples by nearly 1.5-1.8 fold, compared to the activity found in unstressed plants, which otherwise showed a 50% declined activity in leaf extract prepared in buffer solution and assayed in a medium depleted of these sugars. In view of the accumulation of osmolytes under saline condition, these observations suggest that the catalase activity is modulated by the osmolytes and maintains a high rate of hydrogen peroxide scavenging property *in vivo* and serves as the major antioxidant enzyme to scavenge the salt-induced formation of peroxide. Therefore, the salt-stress induced appearance of low activity of the enzyme under normal buffer extraction and assay conditions, as reported in literature may represent an apparent than for its real *in vivo* activity.

Keywords: Catalase Activity; Hydrogen Peroxide; Osmolyte; Rice; Salt-Stress

1. INTRODUCTION

Salinity, comprising both osmotic and ionic effects is known to induce secondarily an oxidative stress in plants forming reactive oxygen species of various natures [1-3]. The reactive oxygen species (ROS) are highly cytotoxic and if remain un-scavenged, can react with vital biomolecules like protein, nucleic acid, lipids etc. causing an array of deformity to cell constituents [4]. Both non-enzymatic (tocopherol, ascorbic acid, glutathione etc.) and enzymatic (superoxide dismutase, ascorbate peroxidase, peroxidases, catalase etc.) antioxidant systems operate through a complex networking machinery to avoid damage caused by these ROS [5]. Among the enzymatic antioxidants, superoxide dismutase (SOD) is the primary scavenger of ROS that dismutates superoxide anion (O_2^-) to hydrogen peroxide (H_2O_2) and water. A multiple enzyme systems like ascorbate peroxidase (APOX), peroxidases (POX) and catalase (CAT) further decomposes the H_2O_2. The CAT, as compared to APOX and POX, with low affinity towards H_2O_2 but with a high processing rate [6], may become the principal enzymatic H_2O_2 scavenger in plants under salt-stressed conditions, where the cellular H_2O_2 level become several fold higher than found in plants grown under normal conditions [1,7]. This is essentially because, unlike other H_2O_2 scavenging enzymes (POX and APOX), CAT enzymatic reaction is not saturated with increasing concentrations of the peroxide and is independent of other cellular reductants for instituting its activity [6]. However, a large body of literature reports suggest that as compared to un-stressed plants the CAT activity is significantly down regulated in salt-stressed plants [8-14], suggesting that the enzyme may not serve as the major scavenger of H_2O_2 under salt offence to plants [13]. However, it is also suggested that maintenance of CAT activity could be a key factor for determining the stress tolerance in plants [12]. This bears importance particularly for C_3 categories of plants like rice, where the photorespiratory activity is elevated under salt-stress [15]. The peroxisomal instituted elevation of photorespiratory activity may lead for higher accumulation of H_2O_2 as a result of conversion of glycolate to glyoxyate. Further, the peroxisome has been shown to be rapidly proliferated under oxidative stress [16]. Thus the CAT, principally a peroxisomal localized enzyme needs to operate effectively to eliminate the photorespiratory produced H_2O_2 [17].

Salt-stress also brings numerous metabolic changes in plant, the principal being the synthesis and accumulation of organic osmolytes [18-19]. Salt-induced accumulation of sugar alcohols like sorbitol, mannitol, inositol etc., or carbohydrates (sucrose, fructans etc.), and organic and

amino acids like malate and proline, and many redox-regulating compounds such as glutathione, cystein and ascorbate and synthesis of LEA group of proteins have been documented in various plant species [20-21]. Metabolically engineered transgenics, leading for increase synthesis and accumulation of osmolytes of various natures have been shown to protect the plant against salinity stress [22-24]. It is presumed that while maintaining the cell turgor pressure in salt-stressed plants, the osmolytes also behave as osmo-protectants towards membrane-protein complexes and enzyme-proteins, and protect them from salt-induced impairments [25].

In the present investigation we found that supplementation of sugars or sugar alcohols like sucrose, sorbitol and mannitol in extraction and enzyme assay medium can sustain a significant high activity of CAT in rice plant, which otherwise showed a declined activity when exposed to saline environment. We put evidence that CAT in salt-stressed rice plant, as compared to the un-stressed one, is modulated by osmolytes *in vivo*, achieving a substantially high catalatic activity so as to serve as the major scavenger of H_2O_2.

2. MATERIALS AND METHODS

2.1. Plant Material and Salt Treatment

Seeds of *Oryza sativa* (Indica cultivar var. Ratna) were germinated on water soaked cotton pads for 72-h in dark at 25℃. Seedlings were subsequently transferred for sand culture at 25℃ under 12-h photoperiod (light intensity 80 $\mu Em^{-2}\ s^{-1}$) and routinely irrigated with rice culture medium [26]. Ten days grown plants were further irrigated with rice culture medium containing 300 mM NaCl for 4-d to develop salt-stress. The control set of plants were kept irrigated with normal rice culture medium.

2.2. Spectrophotometric and In-Gel Assay of Catalase Activity

The fully expanded secondary leaves (nearly 100 mg fresh mass) were homogenized in 2 ml ice cold 50 mM K-PO_4 buffer (pH 7.5) containing 0.1 mM PMSF. The homogenate was centrifuged at 12,000 xg for 10 min at 4℃ and the supernatant was used for CAT activity assay. As when required, the leaf extract was prepared using the same extraction buffer containing required concentration of either mannitol or sorbitol or sucrose (see results).

Catalatic activity of the enzyme was monitored spectrophotometrically [27] by recording the decline of absorbance at 240 nm due to decomposition of H_2O_2 (€= 40 $M^{-1}\ cm^{-1}$). For in-gel activity assay, the crude protein extract was first separated in 10% native PAGE at 4℃ under constant current of 30 mA and the catalase activity in the gel was visualized through enzyme specific staining [28]. The protein concentration was measured following Bradford [29].

2.3. Western Blot Analysis

Catalase protein concentration in both control and salts-stressed leaf tissues were visualized through western blot analysis using rice catalase antibody, developed in rabbit (primary antibody). The Goat anti rabbit IgG horseradish peroxidase conjugate was used as secondary antibody. The PVDF membrane with transferred protein was treated with H_2O_2 and the protein bands were developed with DAB coloured reaction.

2.4. Measurement of Glycolate Oxidase Activity

Activity of glycolate oxidase (GO), an exclusively peroxisomal localized enzyme was measured following [30]. The leaf extract was prepared in 50 mM K-PO_4 buffer (pH 7.5) containing 1 mM PMSF. The assay involves the measurement of the rate of formation of glyoxylate from glycolate in form of glyoxylate-phenylhydrazone. The reaction mixture in 1 ml included 100 mM K-PO_4 buffer (pH 7.8), 6.5 mM glycolic acid, 3.22 mM cysteine, 3.22 mM phenylhydrazine, 0.03 mM flavin-mononucleotide and 18 µg protein equivalent leaf extracts as enzyme source. The quantification was made using € of 17 $mM^{-1}\ cm^{-1}$ for glyoxylate-phenylhydrazone at 324 nm.

Effect of sucrose in the enzymatic reaction GO was also determined as done for CAT.

2.5. Estimation of Steady State H_2O_2 Level and NADH-Oxidase Activity

Steady state level of H_2O_2 in leaves of control and salt-stressed plants were determined using FOX-1 method [31]. Leaves (100 mg fresh weight) were ground with 10% trichloro aceticacid and centrifuged at 12,000 xg for 5 min. The supernatant was passed through a bed of activated charcoal and a measured volume of filtrate was incubated with FOX-1 reagent (Ferrous oxidation with xylenol orange; 100 µM xylenol orange, 250 µM ammonium ferrous sulfate, 100 mM sorbitol, and 25 mM H_2SO_4) for 30 min (pre determined with standard H_2O_2) and absorbance was recorded at 560 nm. The concentration of H_2O_2 was determined from a standard chart, obtained using 0.2-1 µmol of H_2O_2.

NADPH-oxidase activity was monitored in tissue extract made with K-PO_4 buffer (pH 7.5) containing 0.5% (V/V) Triton X-100. The extract was centrifuged at 12,000 xg for 10 min at 4℃. The supernatant was used for enzyme assay in a reaction mixture containing 50 mM Tris-HCl (pH 7.5), 250 mM sucrose, 0.1 mM NBT, 0.02% Brij-58 and 30 µg protein equivalent leaf extract. The SOD activity was inhibited using 1 mM Na-azide and 10 mM KCN. The reaction was initiated by addition of NADH (0.1 mM final concentration).

The NADPH dependent O_2^- generation activity was monitored by following the rate of NBT reduction spectrophotometrically at 530 nm using € 12. 8 mM^{-1} cm^{-1} [32].

3. RESULTS

3.1. Catalase Activity and Protein Quantity

The H_2O_2 scavenging activity of CAT, when examined in the leaf extracts prepared in buffer solution, a significant decline in the activity was noticed with the salt-stressed samples as compared to un-stressed one. The average decline was found to be nearly 50 to 55% of the activity recorded in control plant leaf. Irrespective of the units used for the expression of enzyme activity, either in terms of tissue fresh weight (absolute activity) or on the basis of protein quantity (specific activity), the extent of decline was comparable (**Figure 1**). In assenting with spectrophotometric analysis (**Figure 1**), the in-gel activity assay also showed a significant low level of CAT activity in salt-treated samples (**Figure 2(a)**). The CAT protein quantity as visualized with western blot analysis (**Figure 2(b)**), suggested that under salt-stress condition although the CAT activity is significantly reduced, the CAT protein quantity per unit of leaf protein largely remained unaffected.

3.2. Cellular Level of H_2O_2 and NADPH-Oxidase Activity

In plants, the decline in catalase activity is accompanied with a significant increase in cellular level of H_2O_2 [1, 13]. However, our experimental results in rice plant showed a parallel relationship between catalase activity and the cellular H_2O_2 concentration. In salt-stressed leaves, concomitant with decline in enzyme activity there was also a decline in the level of H_2O_2 (**Figure 3**). Compared to control leaf, nearly 25-35 % low concentration of cellular H_2O_2 was evident in salt-stressed leaves.

The intrinsic H_2O_2 formation rate in the leaf tissues of salt-stressed and un-stressed plants were evaluated by measuring NADPH-oxidase activity as a representative of oxidase enzymes, responsible for generating O_2^- in the cell (**Figure 4**) that eventually is translated to H_2O_2. The enzyme was found to maintain nearly a 1.5 fold high activity in leaves of salt-stressed plants than the un-stressed one, suggesting that salt-stress induces a higher formation of H_2O_2 in the leaf tissue.

3.3. Effect of Osmolytes on the Catalatic Activity of CAT

We made an attempt to find out the effect of the osmolytes like sorbitol, mannitol and also sucrose on the H_2O_2 scavenging activity of the CAT in the extracts made from leaves of both control and salt-stressed rice plant.

To achieve this end, the extraction and enzyme assay

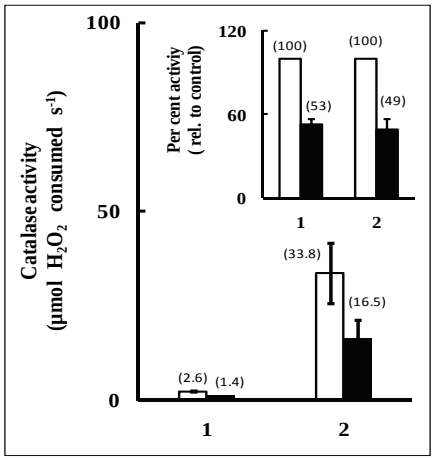

Figure 1. Hydrogen peroxide scavenging activity of catalase in crude leaf extracts of control (open bar) and 300 mM NaCl stressed (solid bar) rice plant. The enzyme activity was measured in 50 mM K-PO_4 buffer (pH 7.5) containing 24 mM H_2O_2 (final concentration) and the leaf extract 30 µg protein equivalent protein extracts. The rate of enzyme activity is expressed both in terms of unit protein (specific activity, 1), and leaf fresh mass (absolute activity, 2). The inset depicts the per cent loss in CAT activity in salt-stressed leaf relative to activity of control leaf taken as 100%. Vertical bars represent the ± SD (n=13). The respective values of enzyme activity have been shown in bracketed numbers.

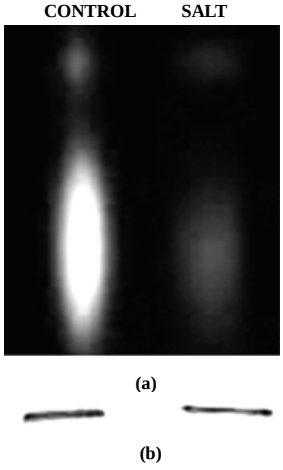

Figure 2. (a) In-gel catalase activity assay of crude protein extracts from the leaves of control (CONTROL) and salt treated (SALT) rice plant. The quantity of crude protein loaded from each of the respective preparations was 30 µg; (b) shows the rice CAT-antibody reactivity in the crude leaf protein extract separated in SDS-PAGE.

medium was supplemented with varied concentrations of the osmolytes. Inclusion of osmolytes in both extraction and assay medium significantly enhanced the activity (**Figure 5**). The stimulation was registered to be an os-

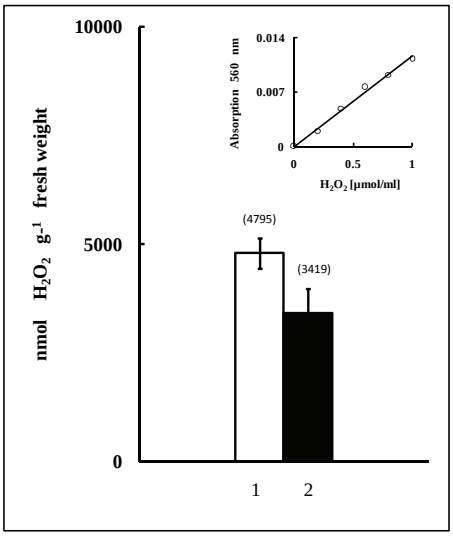

Figure 3. Comparison of steady state level of leaf tissue H_2O_2 in control (1) and salt-stressed (2) rice plant. The data points represent the mean of 7 independent experimental observations and the variation in the quantity from mean value has been depicted as ± SD in form of vertical bars. The inset depicts the sensitivity of the methodology in µmol range of H_2O_2.

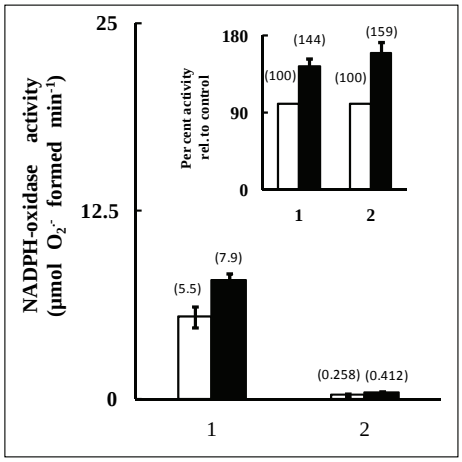

Figure 4. NADPH-oxidase activity in crude leaf extracts from control (open bar) and 300 mM NaCl stressed (solid bar) rice plant. The enzyme activity was expressed both in terms of unit leaf fresh weight (absolute activity, 1) and per unit protein quantity (specific activity, 2). The inset depicts the per cent increase in enzyme activity in salt-stressed leaf relative to activity of control leaf taken as 100%. The respective values of activity have been shown in bracketed numbers, averaged from 5 independent observations with ± SD shown as vertical bars.

molyte concentration dependent phenomenon. Maximum stimulation was visualized in the range of 300-500 mM with sugar alcohols and between 200-300 mM with sucrose. Excesses of sucrose beyond 300 mM induced a decline in activity. While a comparable stimulation in activity was discernible with sugar alcohols like sorbitol and mannitol, a significant higher stimulation was achieved by inclusion of sucrose in the medium.

3.4. *In Vitro* Susceptibility of Catalase Activity to NaCl

Susceptibility of catalase activity to exogenously added salt was examined by incubating the crude extracts prepared from control and salt-stressed rice plant leaves with 150 mM NaCl. The effect of osmoticum was also evaluated in this preparation. Incubation with NaCl diminished the CAT activity in a time dependent manner in control-extract made and assayed only in buffer solution (data not shown). Nearly 70-75% of original activity present in the extract made before the addition of salt was inhibited at the end of 2-h of salt incubation. However, in preparations and measurements made in presence of osmolytes, this decline was appreciably reduced. At 2-h of salt-incubation, the decline was noted to be 27, 37 and 18 percent with mannitol, sorbitol and sucrose respectively (**Figure 6**). Contrary to this observation, a marginal (3-4%) enhancement in CAT activity was marked in salt-stressed leaf extract prepared in presence of osmolytes (data not shown).

3.5. Glycolate Oxidase Activity

Glycolate oxidase showed nearly a 1.5 fold increased activity in extracts made from leaves of salt-stressed plant as compared control activity (un-stressed). The salt-induced stimulation in GO activity was fall back to the level of control activity on inclusion of sucrose in the extraction and assay medium (**Figure 7**).

4. DISCUSSION AND CONCLUSION

The response of CAT activity to salt-stress in salt sensitive plants has frequently been contradictory. Majority of reports suggest a salt-induced down regulation of its activity [13]. Although the rice plant used in the present investigation showed a declined enzyme activity under salt-stress as compared to control plant, the protein level was found to remain almost identical (**Figures 1**, **2(a)** and **2(b)**). The reduction in CAT activity was also accompanied with a low level of H_2O_2 in salt-treated plants than control (**Figure 3**). Diverse methodologies have been employed by different workers to quantify the H_2O_2 level in varieties of plant tissues [7,33]. The Fox-1 method having H_2O_2 detection sensitivity as low as 0.2 µmol has been employed in our investigation (**Figure 3** inset). Contradictory to reported results, instead of an inverse relation between H_2O_2 level and CAT activity, our results showed a direct relationship between them (**Figure 1** and **Figure 3**). Appearance of a direct relationship between the CAT activity and the steady state level of cellular peroxide content in rice plant used in this investigation may be explained by arguing that un-

der low activity of CAT, the plant uses other H_2O_2 scavenging enzymes like POX and APOX as the major scavenger of the peroxide. However, this is very unlike because of the limitation of the sensitivity of these enzymes to the substrate, H_2O_2. As compared to CAT, the activities of these enzymes are known to be saturated at substantially low concentration of H_2O_2 [17]. Further, the measurement of steady state level of H_2O_2 does not signify the actual quantity of the peroxide formed in the system, since the protocol involves the quantification of the residual peroxide following its removal by the antioxidant enzyme(s). Therefore, we evaluated the catalatic rate of one of the major enzyme engaged in formation of H_2O_2; the NADPH-oxidase. The enzyme showed nearly 1.5 fold enhanced activity in salt-stressed leaf compared to control (**Figure 4**). In addition to NADPH-oxidase, the high catalatic activity of glycolate oxidase in salt-stressed leaves also indicate a higher formation of H_2O_2 due to salt-induced enhanced photorespiratory activity of the plant (**Figure 7**). These results suggest that the salt-stress indeed induces a high level of H_2O_2 generation in control rice plant leaf but due an efficient scavenging system the cellular concentration of the peroxide is maintained at a lower level than the control.

Salt-stress induced synthesis of low molecular weight metabolites of varied chemical constituents having compatibility with cell cytoplasm is a wide spread response in diverse range of organisms [25]. These metabolites although have been implicated as osmo-regulators, they are also engaged as osmo-protectants in maintaining protein function by protecting them against salt-induced damages [25]. Hence, the *in vivo* milieu available for the enzyme catalysis in salt-stressed and un-stressed plants is different in terms of their osmo-molarity, salt concentration, and also the redox conditions; prevailing in the cell. Therefore, the observed decline in CAT activity (**Figure 1**) may have been an apparent reflection due to non-availability of *in vivo* milieu for achieving its maximal catalatic activity under cell free condition, when extracted and assayed using only buffer solution (**Figure 1**). This assumption was found to be true since inclusion of mannitol, sorbitol or sucrose in extraction and assay medium enhances the catalatic activity of the enzyme in salt-stressed plant that exceeded by nearly 1.5 to 1.8 fold higher than the activity obtained in unstressed plants. These results imply that under salt-stress environment the observed decline in CAT activity, measured without applying the probable *in vivo* conditions of osmotic milieu results in an apparent observation than in real. Thus our observation on low steady state level of H_2O_2 in salt-stressed rice plant (**Figure 3**) can now be explained on the basis that the *in vivo* activity of the CAT enzyme is much higher than the unstressed plant and thereby a greater extent of scavenging activity of the enzyme maintains a reduced level of the peroxide in the cell.

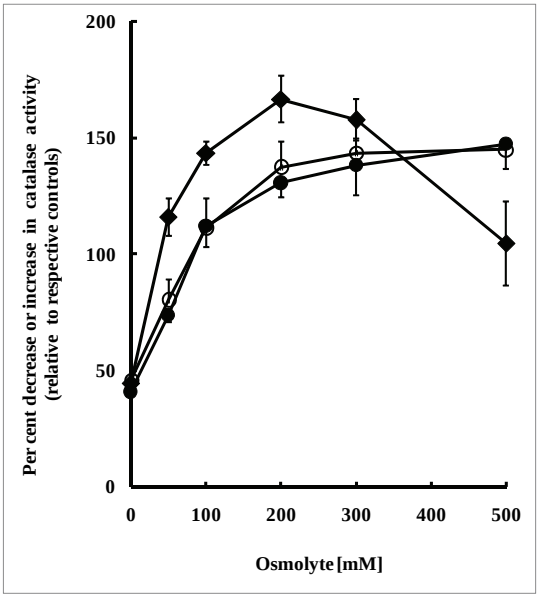

Figure 5. Osmolyte concentration dependent relative stimulation in CAT activity in leaf extract from salt-stressed rice plant. The relative activities were determined taking the control CAT activity as 100%, at each of the osmolyte concentration considered under identical extraction and assay protocol. The symbol denoting closed circle, open circle and closed triangle refers respectively to CAT activity in presence of mannitol, sorbitol and sucrose. The data points are the average of 5 independent experiments with ± SD shown as vertical bars.

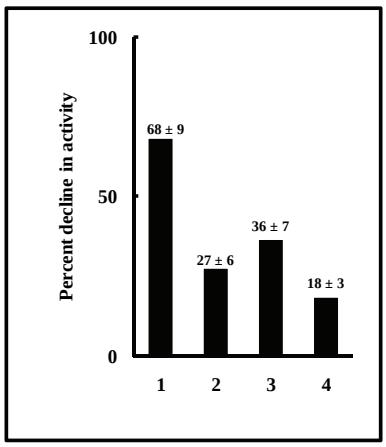

Figure 6. Decline in control plant leaf CAT activity in crude extract during 2-h *in vitro* incubation with 150 mM NaCl in absence (1) and presence of osmolytes like, 500 mM mannitol (2), 500 mM sorbitol (3) and 300 mM sucrose (4). The results have been shown as their respective inhibition percentage taking the respective control activities as 100%. The inhibition percentage are shown in bracketed numbers with the ± SD (n = 5).

The relative accumulation of various osmolytes belonging to different chemical categories like carbohy

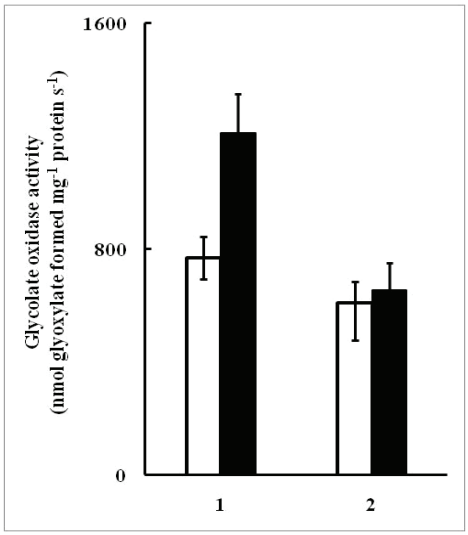

Figure 7. Histogram showing the glycolate oxidase activity of rice leaf extracts prepared and assayed from control (open bar) and 300 mM salt-treated (solid bar) either in absence (1) and presence (2) of 300 mM sucrose. The vertical bars represent the ± SD of six independent experiments.

drates, amino acids, organic acids and sugar alcohols in rice plant on imposition of NaCl-stress has been worked out [34]. Among the various osmolytes identified, the sucrose synthesis is significantly higher (600-700 µg 100 mg^{-1} fresh mass) compared to other simple carbohydrates and sugar alcohols like mannitol and sorbitol (0.20-160 µg 100 mg^{-1} fresh mass). Our investigation indicates that compared to mannitol or sorbitol, sucrose is superior in arresting salt-induced decline in CAT activity. This carbohydrate besides its osmo-regulatory role in tissue, has also been shown in vitrocally to render protection against unfolding of creatine kinase [35], thus maintaining the adequate rate of enzyme catalysis and stabilizing the secondary and tertiary confirmation of protein. Presently we have no experimental results to argue that NaCl per se can act as a denaturant in purified catalase plant protein and the effective role of sucrose in arresting the same. However, from our in vitro time kinetics results of salt-effect, it is suggested that NaCl per se can be a potent inhibitor of CAT activity in crude leaf extract prepared from unstressed but not in salt-stressed rice plant and the inhibition can maximally be retarded in presence of sucrose followed by sorbitol and mannitol respectively (**Figure 5**). Sodium chloride induced decline in CAT activity has also been reported in partially purified CAT from *Phaseolus vulgaris* and *Medicago sativa* [36].

Catalase activity in rice plant leaf, under salt-stress is found to be regulated by osmolytes (maximally with sucrose as shown here). The interaction of osmolytes induces a stimulatory characteristic to CAT, thus increasing its H_2O_2 scavenging efficiency more than the control plant enzyme. The underlying mechanism in osmolyte mediated elevation in CAT activity, specifically under salt-stress condition is further to be understood. In our investigation it is also clearly established that osmolyte acts preferably with the major H_2O_2 scavenging enzyme, the CAT with marginal stimulatory effects on other H_2O_2 liberating enzyme like GO. Further, the presence of low level of stimulation in CAT activity by the osmo-protectants in leaf extracts from control plants suggest that the osmolytes alone may not be the sole candidate in instituting this stimulatory effect in salt-stressed leaves. The stimulation by osmolytes may be a co-ordinated effect of participation of other cellular protein factor (s) synthesized in the salt-stressed plants. The exact nature of the compound and the under lying mechanism of co-ordinated action in bringing stimulatory effect of CAT activity remains to be deciphered. The basis for appearance of differential interaction of the osmolyte with different enzyme proteins is not known to us at present. However, our investigation also brings a major alert for choice of an appropriate protocol to measure the CAT activity in salt-stressed rice plant so as to obtain the real intrinsic catalatic efficiency of the enzyme.

5. ACKNOWLEDGEMENTS

Grateful acknowledgement is due to the financial help received from UGC in form of JRF to MR. Thanks are due to the Director, Institute of Life Sciences, Bhubaneswar.

REFERENCES

[1] Nor'aini, M.F., Robert, P.F. and Roy, H.B. (1997) Salinity, oxidative stress and antioxidant responses in shoot cultures of rice. *Journal of Experimental Botany*, **48**, 325-331.

[2] Hernánde, J.A., Ferrer, M.A., Jiménez, A., Barceló, A.R. and Sevilla, F. (2001) Antioxidant systems and $O_2^{\cdot-}$/ H_2O_2 production in the apoplast of pea leaves, its relation with salt-induced necrotic lesions in minor veins. *Plant Physiology*, **127**, 817-831.

[3] Foyer, C.H. and Noctor, G. (2003) Redox sensing and signalling associated with reactive oxygen in chloroplasts, peroxisomes and mitochondria. *Physiologia Plantarum*, **119**, 355-364.

[4] Mittler, R. (2002) Oxidative stress, antioxidants, and stress tolerance. *Trends in Plant Science*, **7**, 405-410.

[5] Arora, A., Sairam, R.K. and Srivastava, G.C. (2002) Oxidative stress and antioxidant system in plants. *Current Science*, **82**, 1227-1238.

[6] Scandalios, J.G. (2005) Oxidative stress: molecular perception and transduction of signal triggering antioxidant gene defenses. *Brazilian Journal of Medical and Bio-*

logical Research, **38**, 995-1014.

[7] Cheeseman, J.M. (2006) Hydrogen peroxide concentration in natural conditions. *Journal of Experimental Botany*, **67**, 2435-2444.

[8] Shim, I.S., Naruse, Y., Kim, Y.H., Kobayashi, K. and Usui, K. (1999) Scavenging activity of NaCl-induced activated oxygen in two rice (*Oryza sativa* L.) cultivars differing in salt tolerance. *Japanese Journal of Tropical Agriculture*, **43**, 32-41.

[9] Tanaka, Y., Hibino, T., Hayashi, Y., Tanaka, A., Kishitani, S., Takabe, T., Yokota, S. and Takabe, T. (1999) Salt tolerance of transgenic rice over expressing yeast mitochondrial Mn-SOD in chloroplasts. *Plant Science*, **148**, 131-138.

[10] Foyer, C.H. and Noctor, G. (2000) Oxygen processing in photosynthesis: regulation and signaling. *New Phytologist*, **146**, 359-388.

[11] Lee, D.H., Kim, Y.S. and Lee, C.B. (2001) The inductive responses of the antioxidant enzymes by salt stress in the rice (*Oryza sativa* L.). *Journal of Plant Physiology*, **158**, 735-745.

[12] Shim, I.S., Momose, Y., Yamamoto, A., Kim, D.W. and Usui, K. (2003) Inhibition of catalase activity by oxidative stress and its relationship to salicylic acid accumulation in plants. *Plant Growth Regulation*, **39**, 285-292.

[13] Cavlcanti, F.R., Oliveira, J.T.A., Martins-Miranda, A.S., Viegas, R.M. and Silveria, J.A.G. (2004) Superoxide dismutase, catalase and peroxidase activities do not confer protection against oxidative damage in salt-stress cowpea leaves. *New Phytologist*, **163**, 563-571.

[14] Demiral, T. and Türkan, I. (2004) Does exogenous glycinebetaine affect antioxidative system of rice seedlings under NaCl treatment? *Journal of Plant Physiol*, **161**, 1089-1100.

[15] Wingler, A., Lea, P.J., Quick, W.P. and Leegood, R.C. (2000) Photorespiration: metabolic pathways and their role in stress protection. *Philosophical Transactions of the Royal Society London*, **355**, 1517-1529.

[16] Lo´pez-Huertas, E., Charlton, W.L., Johnson, B., Graham, I.A. and Baker, A. (2000) Stress induces peroxisome biogenesis genes. *The EMBO Journal*, **19**, 6770-6777.

[17] Willekens, H., Chamnongpol, S., Davey, M., Schraudner, M., Langebartels, C., Van Montagu, M., Inze, D. and Van Camp, W. (1997) Catalase is a sink for H_2O_2 and is indispensable for stress defense in C_3 plants. *The EMBO Journal*, **16**, 4806-4816.

[18] Rathinasabapathi, B. (2000) Metabolic engineering for stress tolerance: installing osmo-protectant synthesis pathways. *Annals of Botany*, **86**, 709-716.

[19] Hussain T.M., Chandrasekhar, T., Hazara, M., Sultan, Z., Saleh B.K. and Gopal, G.R. (2008) Recent advances in salt stress biology – a review. *Biotechnology and Molecular Biology Review*, **3**, 8-13.

[20] Bajaj, S. and Mohanty, A. (2005) Recent advances in rice biotechnology—towards genetically superior transgenic rice. *Plant Biotechnology Journal*, **3**, 275-307.

[21] Kalefetoglu, T. and Ekmekci, Y. (2005) The effect of drought on plants tolerance mechanisms. *Journal of Science*, **18**, 723-740.

[22] Tarczynaki, M.C., Richard, G.J. and Bohnert, H.J. (1993) Stress protection of transgenic tobacco by production of osmolyte mannitol. *Science*, **259**, 508-510.

[23] Garg, A.K., Kim, J.-K., Owens, T.G., Ranwala, A.P., Choi, Y.D., Kochian, L.V. and Wu R.J. (2002) Trehalose accumulation in rice plants confers high tolerance levels to different abiotic stresses. *Proceedings of National Academy Science*, USA, **99**, 15898-15903.

[24] Dastidar, K.G., Maitra, S., Goswami, L., Roy, D., Das, K. P. and Lahiri Majumder, A. (2006) An insight into the molecular basis of salt tolerance of L-myo-inositol 1-P synthase (PcINO1) from *Porteresia coarctata* (Roxb.) Tateoka, a halophytic wild rice. *Plant Physiology*, **140**, 1279-1296.

[25] Burg, M.B. and Ferraris, J.D. (2008) Intracellular organic osmolytes: function and regulation. *Journal of Biological Chemistry*, **283**, 7309-7313.

[26] Yoshida, S., Forno, D.A., Cock, J.H. and Gomez, K. (1976) Laboratory manual for physiological studies of rice. 3rd Edition, the International Rice Research Institute, Los Banos.

[27] Aebi, H. (1984) Catalase *in Vitro*. In Packer, L., (Ed.), *Methods in Enzymology*, Academic Press, San Diego, **105**, 121-126.

[28] Woodbury, W., Spenser, A.K. and Stahmann, M.A. (1971) An improved procedure using ferricyanide for detecting catalase isoenzymes. *Analytical Biochemistry*, **44**, 301-305.

[29] Bradford, M.M. (1976) A rapid and sensitive method for the quantitation of microgram quantities of protein utilizing the principle of protein-dye binding. *Analitycal Biochemistry*, **72**, 248-254.

[30] Baker, A.L. and Tolbert, N.C. (1966) Glycolate oxidase (ferredoxin containing form). In Wood, W.A. (Ed.), *Methods in Enzymology*, Academic Press, New York-London, **9**, 339-340.

[31] Wolff, S.P. (1994) Ferrous ion oxidation in the presence of ferric ion indicator xylenol orange for measurement of hydroperoxidase. *Methods in Enzymology*, **233**, 182-189.

[32] Yang, Y., Xu, S., An, L. and Chen, N. (2007) NADPH oxidase-dependent hydrogen peroxide production, induced by salinity stress, may be involved in regulation of total calcium in root of wheat. *Journal of Plant Physiology*, **164**, 1429-1435.

[33] Queval, G., Hager, J., Gakie`re, B. and Noctor, G. (2008) Why are literature data for H_2O_2 contents so variable? A discussion of potential difficulties in the quantitative

assay of leaf extracts. *Journal of Experimental Botany*, **59**, 135-146.

[34] Garcia A.B., Engler, J.A., lyer, S., Cerats, T., Montagu, M.V. and Caplan, A.B. (1997) Effects of osmoprotectants upon NaCl stress in Rice. *Plant Physiology*, **115**, 159-169.

[35] Ou, W.B., Park,Y.D. and Zhou, H.M. (2001) Molecular mechanism for osmolyte protection of creatine kinase against guanidine denaturation. *Europian Journal of Biochemistry*, **268**, 5901-5911.

[36] Gracia, N.A.T., Iribarne, C., Palma, F. and Lluch, C. (2007) Inhibition of catalase activity from *Phaseolus vulgaris* and *medicao sativa* by sodium chloride. *Plant Physiology and Biochemistrty*, **45**, 535-541.

Advances in Bioscience and Biotechnology, 2010, 1, 47-50 **ABB**
doi:10.4236/abb.2010.11007 Published Online April 2010 (http://www.SciRP.org/journal/abb/).

Growth rate data fitting of *Yarrowia lipolytica* NCIM 3589 using logistic equation and artificial neural networks

Sarat Babu Imandi[1,*], Sita Kumari Karanam[2], Surekha Darsipudi[3], Hanumantha Rao Garapati[1,4]

[1]Department of Biotechnology, ANITS, Bheemunipatnam, India;
[2]M. R. College of Pharmacy, Phool Baugh, India;
[3]Koringa College of Pharmacy, Korangi, India;
[4]Department of Chemical Engineering, Andhra University, Andhra Pradesh, India.
Email: saratbabu_imandi@yahoo.com; saratbabuimandi@gmail.com; sita_karanam@yahoo.com; sitakaranam@gmail.com

Received 9 February 2010; revised 25 February 2010; accepted 5 March 2010.

ABSTRACT

Growth rate of *Yarrowia lipolytica* NCIM 3589 was observed in a fermentation medium consisting of peptone, yeast extract, sodium chloride. Logistic equation was fitted to the growth data (time vs. biomass concentration) and compared with the prediction given by Artificial Neural Networks (ANN). ANN was found to be superior in describing growth characteristics. A single MATLAB programme is developed to fit the growth data by logistic equation and ANN.

Keywords: *Yarrowia lipolytica*; Logistic Equation; Artificial Neural Networks

1. INTRODUCTION

Yarrowia lipolytica is one of the most extensively studied ‘‘non-conventional’’ yeasts which is currently used as a model for the study of protein secretion, peroxisome biogenesis, dimorphism, degradation of hydrophobic substrates, and several new fields. Recently, the entire sequence of the six *Y. lipolytica* chromosomes has been determined [1], allowing its admission into the ‘‘omic’’ disciplines such as genomics, transcriptomics and proteomics. Several reviews have already been published on its physiology and genetics [2-4], secretion [5-7], dimorphism [8], peroxisome biogenesis [9,10] and mitochondrial complex I [11].

Yarrowia lipolytica is ascomycetous yeast which has been assigned to the family *Dipodascaceae* [12]. This organism is non-pathogenic and oil degrading yeast. It is suitable for the aerobic biodegradation and detoxification of oil mill waste water. It is good for the waste water purification and reduction of pollution due to its ability to reduce chemical oxygen demand and biological oxygen demand. It is also suggested for a deliberate use in cheese ripening due to its extra cellular enzyme activities. It is therefore important to know the growth behavior of this microorganism. The growth capacity of the organism can be evaluated by using growth curves which can be plotted by taking log number of cells versus incubation time. Logistic equation is conveniently used to evaluate the growth capacity of the organism.

Recently, a number of new models have been introduced which involve the application of artificial neural networks to describe the complex growth of yeasts. ANN is highly interconnected network consisting of many simple processing elements capable of performing a massively parallel computation for data processing inspired by the elementary principles of the nervous system. ANN tends to correlate the input data with the output data. In this paper, the growth data were fitted by using both logistic equation and ANN.

2. MATERIALS AND METHODS

2.1. Microorganism

Y. lipolytica NCIM3589 obtained from National Chemical Laboratory, Pune, India, was used throughout the study.

2.2. Growth Conditions

The culture was maintained on MGYP slants having the composition (%): malt extract 0.3, glucose 1.0, yeast extract 0.3, peptone 0.5 and agar agar 2.0. The pH of the medium was adjusted to 6.4–6.8 and culture was incubated at 30^{o}C for 48 h. Sub-culturing was carried out once in every 2 weeks and the culture was stored at 4^{o}C.

2.3. Growth of *Y. lipolytica*

The yeast *Yarrowia* strain was cultivated in a medium containing peptone 5 g, yeast extract 3 g and sodium chloride 3 g/l of distilled water. The cells were culti-

Table 1. Experimental and predicted values of growth data.

Sl. No	Time(hrs)	Biomass concentration(µg/ml)		
		Experimental data	Predicted by logistic equation	Predicted by GRNN
1	0	0.214	0.214	0.214
2	1	1.262	0.433	1.262
3	2	1.291	0.806	1.291
4	3	1.303	1.319	1.303
5	4	1.578	1.851	1.578
6	6	2.29	2.518	2.29
7	7	2.57	2.652	2.57
8	8	3	2.717	3
9	9	3	2.748	3
10	10	3	2.762	3
11	11	3	2.769	3
12	12	3	2.771	3
13	13	3	2.773	3
14	14	3	2.773	3
15	15	3	2.774	3
16	17	3	2.774	3
17	18.3	1.886	2.774	1.886
18	19.3	1.886	2.774	1.886

vated in this medium at 30°C on a shaker at 200 rpm for 24 h [13]. The growth data was taken using double beam spectrophotometer with which optical density was taken at 570 nm. The observations were noted each hour until the organism has reached the stationary stage of growth and the data were reported in **Table 1**.

2.4. Logistic Growth Model

Using the logistic model, the growth curve assumes a sigmoidal shape by plotting biomass vs. time. This shape can be predicted by combining the Monod equation with the growth equation and an equation for the yield of cell mass based on substrate consumption is given by

$$\frac{dX}{dt} = \frac{\mu_m S}{k_s + S} X \tag{1}$$

The specific growth rate is related to the amount of unused carrying capacity as

$$\mu_g = k\left(1 - \frac{X}{X_\infty}\right) \tag{2}$$

Thus,

$$\frac{dX}{dt} = kX\left(1 - \frac{X}{X_\infty}\right) \tag{3}$$

The integration of the equation yields [14],

$$X = \frac{X_0 e^{kt}}{1 - \frac{X_0}{X_\infty}(1 - e^{kt})} \tag{4}$$

where X_0 = initial concentration of biomass, g/l

X_∞ = concentration of biomass at infinite time, g/l

k = rate constant, h-1.

This is the logistic function relating biomass "X" with time "t" with unknown coefficients k and X_∞ which are to be estimated using non-linear least squares. However, non-linear least squares routine requires the initial guess values of k and X_∞. The guess value for X_∞ might be taken as 1.01 times the end value of biomass, while a guess value for k can be calculated by approximating the **Eq.3** for a pair of data points as follows:

$$k = \frac{\frac{1}{\overline{X}}\frac{\Delta X}{\Delta t}}{(1 - \frac{\overline{X}}{X_\infty})}$$

where $\overline{X}$ is the average of two data points, ΔX is the difference between the two data points, Δt is the corresponding difference in time. Non-linear regression routine, 'nlinfit' of MATLAB 7, was used to estimate the values of k and X_∞. The predicted biomass values were reported in **Table 1** as the fourth column.

2.5. Artificial Neural Networks

A neural network is a mathematical representation of the neurological functioning of the brain. It stimulates the brain learning process by mathematical modeling of the network structure of interconnected nerve cells. The essential requirement of neural network modeling was sufficient number of data as it operates directly on input-output data. Thus, ANN is purely data driven model made up of inter connected processing elements called neurons

that are arranged in layers. The most important of this modeling methodology is its ability to reduce the complexity of the network. A good introduction to the subject with respect to MATLAB usage is given by Demuth *et al.* [15].

The type of ANN used is the Generalized Regression Neural Networks (GRNN) which is mainly based on non-linear regression theory. ANN approximates any arbitrary function between input and output vectors, drawing function estimate directly from the training data. GRNN has four layers: input, a layer of radial centers, a layer of regression units and output. The radial layer units represent the centers of clusters of known training data. This layer must be trained by a clustering algorithm such as sub sampling. Thus, GRNN is a universal approximator for smooth function, so it should be able to solve any smooth function approximation problem given enough data.

Using MATLAB 7, the biomass values and time data were fitted by GRNN and predicted values were reported in **Table 1** as the fifth column.

3. RESULTS AND DISCUSSION

The experimental growth data was fitted by using both logistic equation and ANN. In logistic growth model, the parameter values (k and $1/X_\infty$) are obtained as 0.7946 and 0.3605 respectively using 'nlinfit' routine and using the parameter estimates the biomass values are predicted at different periods of times with neural networks, GRNN was used to predict the biomass values. Several iterations were conducted with different spread values ranging from 0.1 to 1.0. A larger spread leads to a large area around the input vector where first layer neurons will respond with significant outputs. If the spread is small the function is very steep, so that the neuron with the weight vector closes to input will have a much larger output than other neurons. Finally, with a spread value of 0.2, we could achieve the predicted values which are almost identical to the experimental values (**Figure 1**).

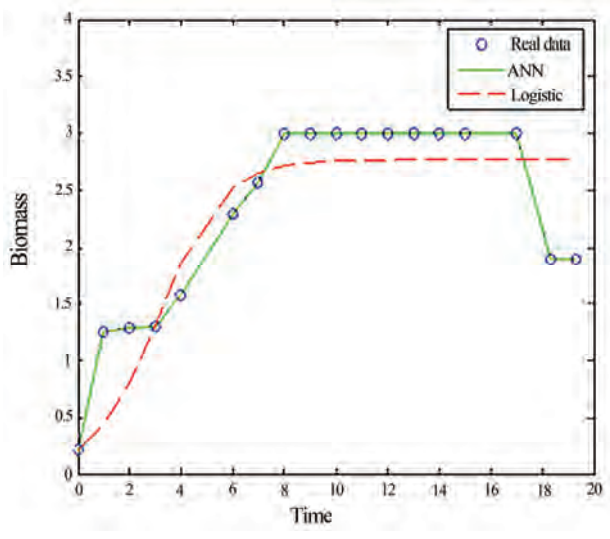

Figure 1. Growth data fitting with ANN & logistic equation.

Figure 1 represents the fitting of growth rate data using ANN and logistic equation. The solid line, dotted line, the circles represent the ANN curve, logistic curve and experimental data respectively. It is evident from **Figure 1** that ANN curve best fits with the experimental data curve when compared to logistic curve. Thus logistic equation is not adequate in fitting the data.

4. CONCLUSIONS

A comparative study has been made for the fitting of growth rate data of *Yarrowia lipolytica* NCIM 3589 using logistic equation and GRNN respectively. It is found that logistic equation is poor in fitting the growth data when compared to ANN. Thus ANN was found to be superior in describing the growth characteristics of the organism.

REFERENCES

[1] Dujon, B., Sherman, D., Fischer, G., Durrens, P., Casaregola, S., Lafontaine, I., De Montigny, J., Marck, C., Neuve´glise, C., Talla, E., Goard, N., Frangeul, L., Aigle, M., Anthouard, V., Babour, A., Barbe, V., Barnay, S., Blanchin, S., Beckerich, J.M., Beyne, E., Bleykasten, C., Boisrame, A., Boyer, J., Cattolico, L., Confanioleri, F., De Daruvar, A., Despons, L., Fabre, E., Fairhead, C., Ferry-Dumazet, H., Groppi, A., Hantraye, F., Hennequin, R., Jauniaux, N., Joyet, P., Kachouri, R., Kerrest, A., Koszul, R., Lemaire, M., Lesur, I., Ma, L., Muller, H., Nicaud, J.M., Nikolski, M., Oztas, S., Ozier-Kalogeropoulos, O., Pellenz, S., Potier, S., Richard, G.F., Straub, M.L., Suleau, A., Swennen, D., Tekaia, F., Wesolowski-Louvel, M., Westhof, E., Wirth, B., Zeniou-Meyer, M., Zivanovic, I., Bolotin-Fukuhara, M., Thierry, A., Bouchier, C., Caudron, B., Scarpelli, C., Gaillardin, C., Weissenbach, J., Wincker, P. and Souciet, J.L. (2004) Genome evolution in yeasts. *Nature*, **430**, 35-44.

[2] Barth, G. and Gaillardin, C. (1996) *Yarrowia lipolytica* in: nonconventional yeasts in biotechnology (Wolf, K., Ed.), *A Handbook*, Springer, Berlin, Heidelberg, New York, pp. 313-388.

[3] Barth, G. and Gaillardin, C. (1997) Physiology and genetics of the dimorphic fungus *Yarrowia lipolytica*. *FEMS Microbiology Reviews*, **19**, 219-237.

[4] Barth, G., Beckerich, J.M., Dominguez, A., Kerscher, S., Ogrydziak, D., Titorenko, V. and Gaillardin, C. (2003) Functional genetics of *Yarrowia lipolytica* In: (de Winde, J.H., Ed.), *Functional Genetics of Industrial Yeasts*, Springer, Berlin, Heidelberg, New York, 227-271.

[5] Dominguez, A., Ferminan, E., Sanchez, M., Gonzalez, F.J., Perez-Campo, F.M., Garcia, S., Herrero, A.B., San Vicente, A., Cabello, J., Prado, M., Iglesias, F.J., Choupina, A., Burguillo, F.J., Fernandez-Lago, L. and

Lopez, M.C. (1998) Non-conventional yeasts as hosts for heterologous protein production. *International Microbiology*, **1**, 131-142.

[6] Nicaud, J.M., Madzak, C., van den Broek, P., Gysler, C., Duboc, P., Niederberger, P. and Gaillardin, C. (2002) Protein expression and secretion in the yeast *Yarrowia lipolytica*. *FEMS Yeast Research*, **2**, 371-379.

[7] Madzak, C., Gaillardin, C. and Beckerich, J.M. (2004) Heterologous protein expression and secretion in the nonconventional yeast *Yarrowia lipolytica*: a review. *Journal of Biotechnology*, **109**, 63-81.

[8] Dominguez, A., Ferminan, E. and Gaillardin, C. (2000) *Yarrowia lipolytica*: an organism amenable to genetic manipulation as a model for analyzing dimorphism in fungi. *Contributions to Microbiology*, **5**, 151-172.

[9] Titorenko, V.I., Smith, J.J., Szilard, R.K. and Rachubinski, R.A. (2000) Peroxisome biogenesis in the yeast *Yarrowia lipolytica*. *Cell Biochemistry and Biophysics*, **32**, 21-26.

[10] Titorenko, V.I. and Rachubinski, R.A. (2001) Dynamics of peroxisome assembly and function. *Trends in Cell Biology*, **11**, 22-29.

[11] Kerscher, S., Drose, S., Zwicker, K., Zickermann, V. and Brandt, U. (2002) *Yarrowia lipolytica*, a yeast genetic system to study mitochondrial complex I. *Biochimica et Biophysica Acta*, **1555**, 83-91.

[12] Kurtzman, C. and Fell, J., Eds., (1998). The yeasts: a taxonomy study, Elsevier, Amsterdam.

[13] Imandi, S.B., Bandaru, V.V.R., Somalanka, S.R. and Garapati, H.R. (2007). Optimization of medium constituents for the production of citric acid from byproduct glycerol using doehlert experimental design. *Enzyme and Microbial Technology*, **40**, 1367-1372.

[14] Shuler M.L. and Kargi, F. (2002). Bioprocess engineering-basic concepts, 2nd Edition, Prentice-Hall of India pvt ltd, New Delhi.

[15] Demuth H., Beale M. and Hagan M. (2006). Neural network toolbox for use with MATLAB. *Neural Network Toolbox*, IEE Savoy Place, London.

Advances in Bioscience and Biotechnology, 2010, 1, 51-54 **ABB**
doi:10.4236/abb.2010.11008 Published Online April 2010 (http://www.SciRP.org/journal/abb/).

Applications of exponential decay and geometric series in effective medicine dosage

Chinnaraji Annamalai

Indian Institute of Technology Kharagpur, Kharagpur, India.
Email: anna@iitkgp.ac.in

Received 10 March 2010; revised 18 March 2010; accepted 20 March 2010.

ABSTRACT

The problem facing by physicians is the fact that for most drugs there is a minimum concentration below which the drug is ineffective, and a maximum concentration above which the drug is dangerous. Thus, this paper discusses the effective medicine dosage and its concentration in bloodstream of a patient. For analysis of dose concentration and mathematical modelling of minimum and maximum concentration of a drug administered intravenously, the EDM (Exponential Decay Model) and GSF (Geometric Series and its Formula) are the powerful mathematical tools. In the present research study, these two mathematical tools were used to predict the dose concentration of a drug in bloodstream of a patient.

Keywords: Bloodstream; Dose Concentration; Exponential Decay; Geometric Series; Medicine

1. INTRODUCTION

One of the physician's responsibilities is to give medicine dosage for a patient in an effective manner. In this research study, the effective medicine dosage and its concentration in bloodstream of a patient are discussed in detail using two mathematical techniques: one is EDM (Exponential Decay Model) and other one is GSF (Geometric Series and its Formula). The EDM is very useful technique for simulating the dose concentration of a drug over time and GSF plays a vital role in modelling the minimum and maximum concentration of a drug administered intravenously.

2. EXPONENTIAL GROWTH AND DECAY

Exponential growth and decay are rates; that is, they represent the change in some quantity over time.

2.1. Exponential Growth Model

A quantity say Q is said to be subject to exponential growth, $Q(t)$, if the quantity Q increases at a rate proportional to its value over time t. Symbolically, this can be expressed as follows:

$$\frac{dQ(t)}{dt} \quad \alpha \quad Q(t)$$

That is, $\frac{dQ(t)}{dt} = kQ(t)$, which is a differential equation.

where $\frac{dQ(t)}{dt}$ is the rate of change of quantity Q over time t, $Q(t)$ is the value of the quantity Q at time t, and k is a positive number called the growth constant.

Now, we can find solution for the differential equation

$$\frac{dQ(t)}{dt} = kQ(t)$$

By rearranging this equation, we get

$$\frac{dQ(t)}{Q(t)} = kdt$$

and then, by integrating this equation, we have

$\ln Q(t) = kt + c$ where c is the constant of the integration.

By simplifying this equation, we get

$$Q(t) = e^{kt+c} = e^{kt}e^{c}.$$

We can obtain $e^{c} = Q(0)$ by evaluating the equation $Q(t) = e^{kt}e^{c}$ at $t = 0$ and $Q(0)$ is the initial value of the quantity Q that is denoted by Q_0 for our convenience.

Therefore, $Q(t) = Q_0 e^{kt}$, which is called the Exponential Growth Model.

2.2. Exponential Decay Model (EDM)

A quantity Q is said to be subject to exponential decay, $Q(t)$, if the quantity Q decreases at a rate propor-

tional to its value over time t. Symbolically, this can be expressed as follows:

$$\frac{dQ(t)}{dt} \quad \alpha \quad Q(t)$$

That is, $\frac{dQ(t)}{dt} = -kQ(t)$ where the negative sign '–' means the decrease in the quantity Q over time t.

By solving this differential equation, we obtain $Q(t) = Q_0 e^{-kt}$, which is called the Exponential Decay Model (EDM).

Remarks: In general, e^x and e^{-x} are exponential functions.

2.3. Geometric Series and its Formula (GSF)

Traditionally, geometric series played a key role in the early development of calculus, but today, the geometric series have many key applications in medicine, biochemistry, informatics, etc.

Usually, a geometric series is the sum of the terms of the geometric sequence:

$$a, ar, ar^2, ar^3, \cdots, ar^n, \cdots .$$

Now, the sum of the geometric sequence of n terms is denoted by

$$S = \sum_{j=0}^{n-1} ar^j = a + ar + ar^2 + ar^3 + \cdots + ar^{n-1}$$

where S denotes the sum, a the first term, r the ratio, and n the number of terms.

$$rS = ar + ar^2 + ar^3 + \cdots + ar^{n-1} + ar^n .$$

When $r \geq 1$,

$$(r-1)S = a(r^n - 1) \Rightarrow S = \frac{a(r^n - 1)}{(r-1)} \quad (r \neq 1).$$

and

when $(-1 < r < 1)$ or $(|r| < 1)$,

$$(1-r)S = a(1-r^n) \Rightarrow S = \frac{a(1-r^n)}{(1-r)},$$

where $r \neq 1$

$$\sum_{j=0}^{\infty} ar^j = \frac{a}{(1-r)} \quad (|r| < 1)$$

$$\sum_{j=0}^{n-1} r^j = 1 + r + r^2 + r^3 + \cdots + r^{n-1} .$$

In the geometric series, the first term shows $a = 1$.

Thus, $\sum_{j=0}^{\infty} r^j = \frac{1}{(1-r)}$ when $|r| < 1$

3. EDM AND GSF IN EFFECTIVE MEDICINE DOSAGE

In this section, we discuss about the effective medicine dosage using Exponential Decay Model (EDM) and Geometric Series and its Formulae (GSF). Let us consider a patient is given the same dose of a medicine at equally spaced time intervals. The dose concentration in the bloodstream decreases as the drug is broken down by the body. However, it does not disappear completely before the next dose is given. Let us understand the exponential decay model for the concentration of a drug in a patient's bloodstream. It is assumed that the drug is administered intravenously and that the concentration of the drug in the bloodstream jumps almost immediately to its highest level, *i.e.* the concentration of the drug decays exponentially.

Now, we use the function $Q(t)$ to represent a dose concentration at time t and Q_0 to represent the concentration just after the dose is administered intravenously. Then the exponential decay model is formulated by

$$Q(t) = Q_0 e^{-kt}$$

where k is the decay constant or a property of the particular drug being used.

Now, let us consider that $Q(t)$ be the first dose concentration at time t and that Q_0 the concentration at time t = 0 just after the first dose is administered intravenously. Suppose that at $t = c$, a second dose of the drug is given to the patient. The concentration of the drug in the bloodstream jumps almost immediately to its highest level $Q(c)$ and then the concentration is diffused so rapidly throughout the bloodstream over time (**Figure 1**).

The expression $Q(t) = Q_0 e^{-kt}$ is valid as long as only a single dose is given [1]. However, suppose that, at $t = c$, a second dose is given and that the amount of thedrug administered is the same as the first dose. Ac-

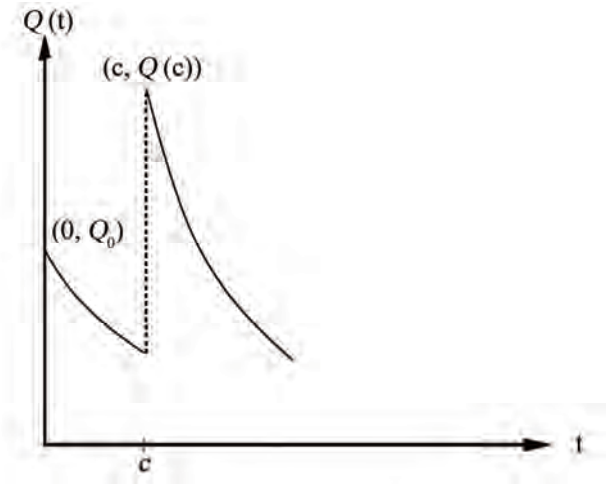

Figure 1. Dose consideration.

cording to the exponential decay model, the concentration will jump immediately by an amount equal to Q_0 when the second dose is given. However, when the second dose is given, there is still some of the drug in the bloodstream remaining from the first dose. This means that to compute the concentration just after the second dose, we have to add the value Q_0 to the concentration remaining from the first dose (**Figure 1**). During the time between the second and third doses, the concentration decays exponentially from this value. To find the concentration after the third dose, the same process must be repeated.

At $t = c$, the dose concentration is calculated as $Q(c^-) = Q_0 e^{-kc}$ just before the second dose is administered intravenously.

Here, $Q(c^-) = \lim_{t \to c^-} Q(t)$.

When the second dose is administered intravenously, the concentration jumps by an increment Q_0 , *i.e.* the concentration just after the second dose given is

$$Q(c^+) = Q_0 + Q(c^-) = Q_0 + Q_0 e^{-kc} = Q_0\left(1 + e^{-kc}\right).$$

Note that $Q(c^-)$ denotes 'just before the new dose is administered' and $Q(c^+)$ denotes 'just after the new dose is administered'.

The concentration then decays from this value according to the exponential decay rule [2], but with a slight twist. The twist is that the initial concentration is at $t = c$, instead of $t = 0$. One way to handle this is to write the exponential term as $e^{-k(t-c)}$ so that at $t = c$, the exponent is 0. If we do this, then we can write the concentration as a function of time as

$$Q(t) = Q_0\left(1 + e^{-kc}\right)e^{-k(t-c)}$$

This function is only valid after the second dose is administered and before the third dose is given. That is, for $c \le t < 2c$.

Now, suppose that a third dose of the drug is given at $t = 2c$. The concentration just before the third dose is given would be $Q(2c^-)$, which is

$$Q(2c^-) = Q(c^+)e^{-kc} = Q_0\left(1 + e^{-kc}\right)e^{-kc}$$

$$i.e.,\ Q(2c^-) = Q_0\left(e^{-kc} + e^{-2kc}\right)$$

When the third dose is given, the concentration would jump again by Q_0 and the concentration just after the third dose would be

$$Q(2c^+) = Q_0 + Q(2c^-) = Q_0\left(1 + e^{-kc} + e^{-2kc}\right)$$

Now, suppose that a forth dose of the drug is given at $t = 3c$. The concentration just before the forth dose is given would be $Q(3c^-)$, which is

$$Q(3c^-) = Q(2c+)e^{-kc} = Q_0\left(e^{-kc} + e^{-2kc} + e^{-3kc}\right)$$

When the third dose is given, the concentration would jump again by Q_0 and the concentration just after the third dose would be

$$Q(3c^+) = Q_0 + Q(3c^-) = Q_0\left(1 + e^{-kc} + e^{-2kc} + e^{-3kc}\right)$$

Let us consider the process is continued up to n-th dose,

$$i.e.\ \overbrace{0,1,2,3,\cdots}^{n-doses}\ \overbrace{n-1}$$

The concentration just before the *n-th* dose of the drug would be

$$Q((n-1)c^-) = Q_0 \sum_{j=1}^{n-1} e^{-jkc} \qquad (1)$$

The concentration just after the n-th dose of the drug would be

$$Q((n-1)c^+) = Q_0 \sum_{j=0}^{n-1} e^{-jkc} \qquad (2)$$

Let $r = e^{-kc}$

Note that $0 < r < 1$, since k and c are both positive constants.

From the geometric series (1) and (2), we formulate as

$$Q((n-1)c^-) = Q_0 \sum_{j=1}^{n-1} e^{-jkc} = Q_0\left(\frac{r - r^n}{1 - r}\right) \qquad (3)$$

and

$$Q((n-1)c^+) = Q_0 + Q((n-1)c^-) = Q_0 \sum_{j=0}^{n-1} e^{-jkc} = Q_0\left(\frac{1-r^n}{1-r}\right) \qquad (4)$$

The **Eqs.3** and **4** are formulae for the partial sum of a geometric series.

Suppose a treatment for a patient is continued indefinitely. Then the **Eq.4** becomes

$$Q((n-1)c^+) = \lim_{n\to\infty} Q_0\left(\frac{1-r^n}{1-r}\right) = Q_0\left(\frac{1}{1-r}\right)$$

$\left(\because\ 0 < r < 1\right)$.

Now, we conclude from the results that the minimum concentration is the concentration just before the second dose is given,

i.e. $Q_{\min} = Q_0 r$

and that the maximum concentration is the concentration just after the last dose is given, *i.e.*

$$Q_{\max} \le \left(\frac{Q_0}{1 - r}\right)$$

4. DISCUSSION

For example, a patient is injected a particular drug. Just

after the drug is injected, the concentration is 1.5 mg/ml (milligrams per milliliter). After four hours the concentration has dropped to 0.25 mg/ml.

Here, $Q(4) = 0.25$ at t = 4 and $Q_0 = 1.5$ at t = 0. So, $Q(t) = Q_0 e^{-kt} \Rightarrow 0.25 = 1.5 e^{-4k}$.

To find k, Maple commands were used [8].

Result: k = 0.4479398673.

A problem facing physicians is the fact that for most drugs, there is a concentration, m, below which the drug is ineffective and a concentration, M, above which the drug is dangerous. Thus, the concentration $Q(t)$ must satisfy the condition: $m \le Q(t) \le M$. For example, suppose that for the drug in the experiment [8] the maximum safe concentration is 5 mg/ml, or M = 5, and the minimum effective concentration is 0.6 mg/ml, or m = 0.6. Then the initial dose must not produce a concentration greater than 5 mg/ml.

5. CONCLUSIONS

In the research study, the EDM (Exponential Decay Model) and GSF (Geometric Series and its Formula) discuss in detail for effective medicine dosage. Especially the two techniques have been used for analysis of dose concentration in bloodstream of a patient and modelling of minimum and maximum concentration of a drug administered intravenously.

REFERENCES

[1] Geometric series and effective medicine dosage. *Mathematical Science*, Worcester Polytechnic Institute. http://www.math.wpi.edu/Course_Materials/MA1023D09/Labs/drug.pdf

[2] Exponential decay and effective medicine dosage, Published by Mathematical Science, Worcester Polytechnic Institute. http://www.math.wpi.edu/Course_Materials/MA1022C97/Labs/lab2_part1/node6.html

Advances in Bioscience and Biotechnology, 2010, 1, 55-59 **ABB**
doi:10.4236/abb.2010.1109 Published Online April 2010 (http://www.SciRP.org/journal/abb/).

A comparative investigation of interaction between metal ions with L-methionene and related compounds such as alanine, leucine, valine, and glycine in aqueous solution

S. A. A. Sajadi

Sharif University of Technology, Institute of Water & Energy, Tehran, Iran.
Email: sajadi@sharif.ac.ir

Received 7 February 2010; revised 25 February 2010; accepted 5 March 2010.

ABSTRACT

The acidity and stability constants of M-L (M: M^{2+}; L: Met, L-methionine) complexes, determined by potentiometric pH titrations, were used to make a comparative investigation. The stability constants of the 1:1 complexes formed between M^{2+} and L^{-}, were determined by potentiometric pH titration in aqueous solution (I = 0.1 M, $NaNO_3$, 25°C). The order of the stability constants was reported. It is shown that regarding to M ion – binding properties, vital differences on complex bilding were considered. It is demonstrated that in M-L complexes, M ion is coordinated to the carboxyl group, is also able to bild macrochelate over amine group. The aforementioned results demonstrate that for M (Met) complex, the stability constants are also largely determined by the affinity of Cu ion for amino group. It is indicated that this additional interaction with amino groups can influence the character of some amino acid complexes in biological systems.

Keywords: Methionine; Metal Ion; Potentiometric Titration; Acidity and Stability Constants

1. INTRODUCTION

The α-amino and α-carboxyl groups of amino acids play prominent roles in metal ion binding. There are many examples of side chain functional groups that also interact with metal ions. Peptides interact with metal ions primarily through side chain functional groups, although there are many examples of peptide amide nitrogen which are functioning as donor atoms with certain metal ions [1]. Many physiologically important peptides function as metal complexes. Methionine is an essential amino acid, which is one of the two sulfur-containing amino acids (**Figure 1**). The side chain is quite hydrophobic and methionine is usually found buried within proteins. unlike cysteine, the sulfur of methionine is not highly nucleophilic, although it will react with some electrophilic centers. It is generally not a participant in the covalent chemistry that occurs in the active centers of enzymes. The thiol ether can be chemical linkage of the sulfur in methionine. We can compare this terminology with that of the oxygen containing ethers. The sulfur of methionine, as with that of cysteine, is prone to oxidation. The first step, yielding methionine sulfoxide, can be reversed by standard thiol containing reducing agents. The second step yields methionine sulfone, and is effectively irreversible. It is thought that oxidation of the sulfur in a specific methionine of the elastase inhibitor in human lung tissue by agents in cigarette smoke is one of the causes of smoking-induced emphysema [2]. Data on the complexation of essential metal ions and the bioactive ligands methionine and cysteine give insight into many physicochemical processes. The significance of these amino acids is enhanced by the fact that they display independent therapeutic activity [3]. Exposure of the HIV-2 protease to H_2O_2 resulted in conversion of the two methionine residues (Met-76 & Met-96) to methionine sulfoxide as determined by amino acid analytical and mass spectroscopy [4]. Based on above mentioned essential role of Met is interesting to study the interaction between other metal ions with Met [5-8]. The interesting question is also, is there any interaction between sulfur group and metal ions. In other words, is it possible to detect the last mentioned interaction in aqueous solution?

2. EXPERIMENTAL

2.1. Materials

The L-methionine (extra pure) was purchased from Merck, Darmstadt, Germany. The nitrate salt of Na^{+}, Mn^{2+}, Co^{2+}, Cu^{2+}, and Zn^{2+} (all pro analysi) were from Merck. Potassium hydrogen phthalate and standard solutions of sodium hydroxide (titrasol), nitric acid, EDTA and of the buffer solutions of pH 4.0, 7.0 and 9.0 were all from Merck. All solutions were prepared with de-ionized water. Water was purified by Milil-Q water purification

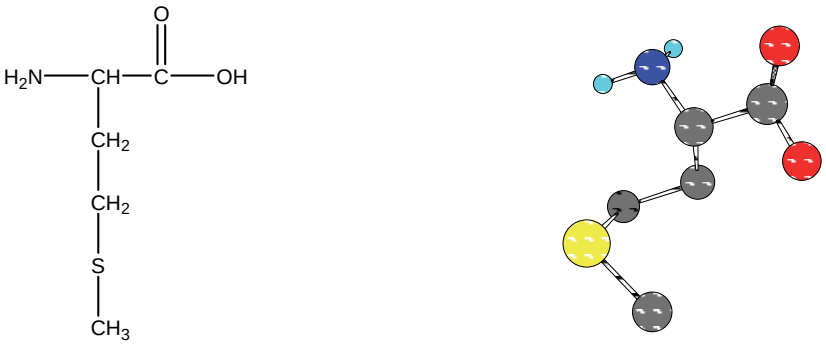

Figure 1. Chemical structure (2D & 3D) of L-methionine.

system, de-ionized and distillated.

2.2. pH Titrations

2.2.1. Reagents

Carbonate-free sodium hydroxide solution 0.03 M was prepared and standardized against sodium hydrogen phthalate and a standard solution of nitric acid 0.54 mM. M(II) nitrate solution (0.6 mM) was prepared by dissolving the above substance in water and was standardized with standard solution of EDTA 0.1 M (triplex).

2.2.2. Apparatus

All pH titrations were performed using a Metrohm 794 basic automatic titrator (Titrino), coupled with a thermostating bath Hero at 25℃ (± 0.1℃) and a Metrohm combined glass electrode (Ag/AgCl). The pH meter was calibrated with Merck standard buffer solutions (4.0, 7.0 and 9.0).

2.2.3. Procedure

For the determination of acid dissociation constants of the ligand Met, an aqueous solution (0.6 mM) of the protonated ligand was titrated with 0.03 M NaOH at 25℃ under nitrogen atmosphere and ionic strength of 0.1 M, $NaNO_3$. For the determination of binary (a ligand and M^{2+}) system, the ratios used were 1:1, M(II): Ligand and 1:1, M(II): Met, 0.6 mM. This solution was titrated with 0.03 M NaOH under the same conditions mentioned above. Each titration was repeated seven times in order to check the reproducibility of the data.

2.2.4. Calculation

The acid dissociation constants, $K^{H}_{H_2(Met)}$ and $K^{H}_{H(Met)}$ for $H_2(Met)^+$ were calculated by an algebraic method. The equilibria involved in the formation of 1:1 complex of Met and a divalent metal ion may be expressed as **Eqs.3** and **4**.

3. RESULTS AND DISCUSSION

The potentiometric pH-titrations (25℃, 0.1 M, $NaNO_3$) were carried out to obtain the acidity and stability constants which are summarized in **Tables 1** and **2**.

Table 1. Negative logarithm of the acidity constants of Met: L-methionine at 25°C, 0.1 M, $NaNO_3$*, **Eqs.1** and **2**.

No.	Species	pKa	Site
1	$H_2(Met)^+$	2.80±0.02	$-CO_2H$
2	$H(Met)^{\pm}$	9.85±0.01	$-NH_2$

*The given errors are three times the standard error of the mean value or the sum of the propabable systematic errors.

Table 2. Logarithm of the stability constants of binary complexes of M^{2+} at 25°C, 0.1 M, $NaNO_3$*, **Eq.4**. Met: methionine and related compounds such as Alanine, Leucine, Valine, and Glycine.

No.	Ligand	log $K^{M}_{M(L)}$			
		Mn^{2+}	Co^{2+}	Cu^{2+}	Zn^{2+}
1	Alanine[a]	3.24	4.82	8.18	5.16
2	Leucine[a]	2.15	4.49	7.00	4.92
3	Valine[a]	2.84	–	7.92	5.00
4	Glycine[a]	3.20	5.23	8.22	5.16
5	Methionine[a]	2.77	4.12	7.87	4.37
6	Methionine[b]	3.59±0.05	3.85±0.08	7.96±0.02	4.46±0.06

a) from [7]; b) from this work, *the given errors are three times the standard error of the mean value or the sum of the propabable systematic errors.

3.1. Acidity Constants

Methionate (Met̃), $^-O_2CCH(NH_2)CH_2CH_2SCH_3$, is a two-basic species, and thus it can accept two protons, given $H^2(Met)^+$, for which the following de-protonation equilibria are hold:

$$H_2(Met)^+ \rightleftharpoons H^+ + H(Met)^{\pm} \quad (1)$$

$$K^{H}_{H_2(Met)} = [H(Met)^{\pm}][H^+]/[H_2(Met)^+] \quad (2)$$

$$H(Met)^{\pm} \rightleftharpoons H^+ + Met^- \quad (3)$$

$$K^{H}_{H(Met)} = [Met^-][H^+]/[H(Met)^{\pm}] \quad (4)$$

The two proton in $H_2(Met)^+$ are certainly bound at the terminal acetate and amino groups, *i.e.*, it is released from $^-O_2CCH(NH_2)CH_2CH_2SCH_3$ according to equilibrium (1)

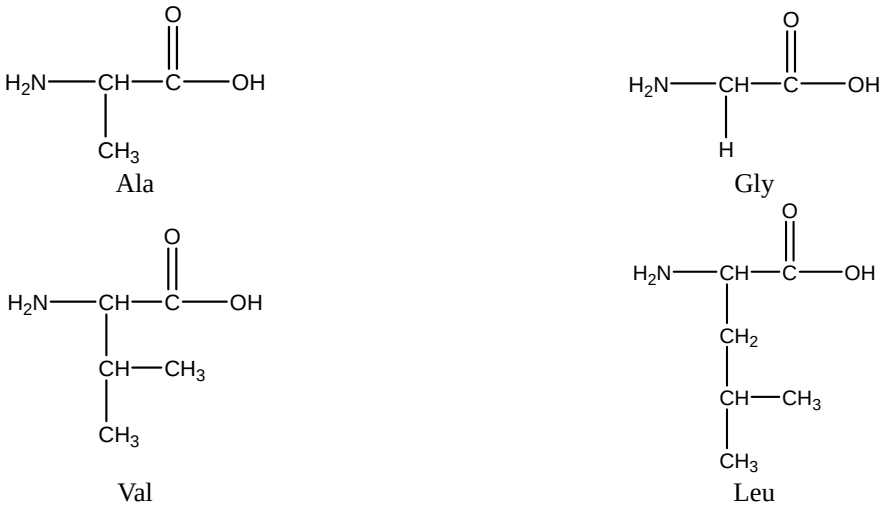

Figure 2. Chemical structure of Alanine (Ala), Glycine (Gly), Valine (Val), and Leucine (Leu).

& (2). It is known as zwitter-ion. It is also closed to the de-protonation of acetate groups which occurs at the terminal acetate groups of aspartic acid [7,8].

3.2. Stability of Binary and Ternary Complexes

If we abbreviate for simplicity associating metal ions with M^{2+}, then one may write the following two equlibria of (3) & (4):

$$M^{2+} + H(Met)^{\pm} \rightleftharpoons M(H;Met)^{2+} \quad (5)$$

$$K^{M}_{M(H;Met)} = [M(H;Met)^{2+}]/[M^{2+}][H(Met)^{\pm}] \quad (6)$$

$$M^{2+} + (Met)^{-} \rightleftharpoons M(Met)^{+} \quad (7)$$

$$K^{M}_{M(Met)} = [M(Met)^{+}]/[M^{2+}][Met^{-}] \quad (8)$$

The experimental data of the potentiometric pH titrations may be completed by considering the above-mentioned equilibria (1) through (4), if the evaluation thereof is not carried into the pH range, where hyrdoxo complex formation occurs. No constant could be determined for the $K^{M}_{M(H;Met)}$. The data were collected every 0.1 pH unit from the lowest pH which could be reached in the experiment to the beginning of the hydrolysis of $M(aq)^{2+}$.

3.3. Potentiometric Analysis

The chemical structures of some related amino acid are shown in **Figure 2**. Also we noticed right away that all these amino acids consist of organic part R, carboxyl- and amino-groups. Just in Met we distinguish the thioether group, which can influence the character of Met or not, as we will consider as follows.

The results of all potentiometric pH-titration, *i.e.* acidity and stability constants, were summarized below in **Tables 1** and **2**. The de-protonated amino acid Met^{-} can accept two protons, to give the acid $H_2(Met)^{+}$. The first

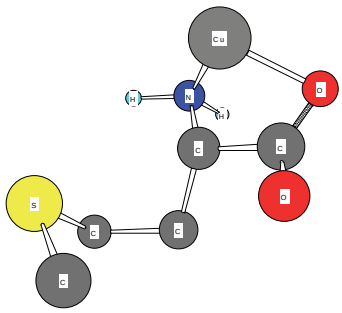

Figure 3. Schematic structures of the species with interactions according to equilibrium (5) for Cu–Met. The structure in the right part of the figure was drawn with the program CS Chem 3D, version 3.5, from Cambridge Software Corporation.

one of these two protons is released from carboxylate group; its pKa is shown in **Table 1**. However, now $Met^{\pm}$ can release one more proton from neutral -NH_3 group, which is the second acidity constant (**Table 1**). The measured acidity constants in this work show good agreement with the same value received by other authors [7,9-12]. However, the carboxyl group is a far stronger acid than the amino group [13].

The stability constants of the binary complexes, such as M–Met were refined separately using the titration data of this system in a 1:1, ligand: M^{2+} ratio in the same conditions of temperature and ionic strength (according **Eqs.3** and **4**), as they were in good agreement with reported value [7,12]. We didn't received reseanable results for $K^{M}_{M(H;Met)}$. All the stability constants of **Table 2** show the usual trend [14-17].

The stability constants of the binary complexes, such as Cu(Met) (**Figure 3**) were refined separately using the titration data of this system in a 1:1, ligand:Cu^{2+} ratio in

the same conditions of temperature and ionic strength

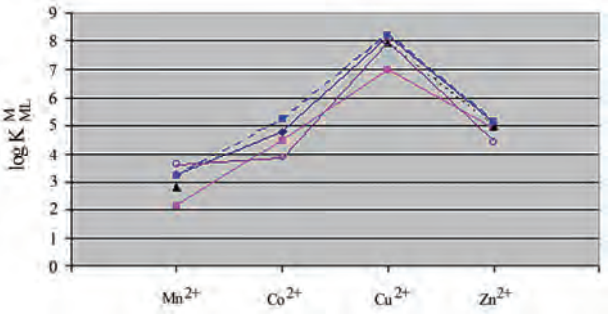

Figure 4. Irving-Williams sequence-type plot for the 1:1 complexes of Mn^{2+} to Zn^{2+} with some amino acids (see **Table 2**). ■: Leucine, ▲: Valine, ♦: Alanine, ●: Glycine, O: Methionine.

(according **Eqs.3** and **4**), as they were in good agreement with reported value [12,17].

The experimental results are summarized in the **Table 2**. The sequence shows the same Irving-Williams sequence. Also in **Table 2** were listed the second stability constants of some related amino acids such as alanine, leucin, valine, and glycine.

If we compare these amino acids with each other, we see that they consist of three similar parts. They consist of an organic rest, a carboxyl-, and an amine group. The major difference is the presence of S-group in Met. When we compare the stability constant of these amino acids, we see that all of them show similar values. This means that stability of these amino acids is dependent on the interactions of metal ions with carboxyl-and amino-groups. In other words, it has nothing to do with interactions with the S group. These results are also shown in **Figure 3** again. It is evident, that the stability constant shows the identical magnitude. If in M-Met would have seemed some additional interactions, would be observed an increase in stability. However, this was not observed, which means that there is no interaction between the metal ion to sulfur ether.

Also we noticed right away that these thermodynamic constants follow the Irving-Williams sequence (**Figure 4**). All the stability constants of **Table 2** show the usual trend. The obtained order is $Ca^{2+} < Mg^{2+} < Mn^{2+} < Co^{2+} < Cu^{2+} > Zn^{2+}$. It is expected that all these metal ions build a chelate with amino acids over carboxyl- and amine groups, which can be seen in **Figure 3**. In **Figure 3** is shown the structure of Met-complex with Cu^{2+}. We see that Cu binds to carboxyl group on the one hand, and on other hand to amine group. Hard and borderline metal ions show a tendency for interaction with the two mentioned groups.

The ether sulfur is a very weak base. The protonation occurs only in strongly acidic solutions with a pK of -6.2, *i.e.* much weaker than oxygen ether and ethanol Sulfur atoms are soft bases, and the most favorable interaction with borderline or soft metal ions. This softness is the basis for the interaction of thioehers with metal ions. It is expected that the ether sulfur best with a soft metal ions interact, and for hard metal ions is expected, no significant interactions. Interactions with the ether in sulfure Met is even weaker. These results suggest that the thioether group of the complex does not contribute to the stability of the Met. Comparison of the coordination tendencies of tioeher group as part of bidetate and terdentate ligand offers us a greater tendency for thioether group as a donor atom of a bidentate ligand of lower stability constant than the third donor atom in a ligand terdentate clearly is greater stability constant. This tendency is for Cu, where the more favored tetragonal donor atoms occupy positions on the airwaves, and sulfur is increasingly forced to interact in an apical position, if at all. The thioehre group does not contribute significantly to the stability of hard or borderline metal ions with. Chelate formation of Cu in the glycinate and a weak interaction of the thioether group in the apical position of one of these observations. That the interaction is weak has been reported by the lack of absorption in 400 nm by complexation of a thioether group in the tetragonal plane supports Cu. It was a success for the crystallographic that crystals mainly reflect the structural requirements for structures in solution for labile metal ions. Thus, as expected, the thioether group is not coordinated with a borderline metal ions in complexes met. A trans Met-Pt complex with bidentate chelation in with S and N has not been characterized [18]. Crystal structure also show S-and N-bidentate chelate formation with Pd and Pt [19,20]. Both N and S are bound in terdendate Pt Gly-Met-complex. These findings are in contrast to a complex of borderline terdendate GM-Cu, which were replaced a carboxylate O ether by S [21].

Metal ions may function to internally crosslink proteins. For example, at least ten motifs collectively known as zinc fingers have been described in nucleic acid–binding proteins. The M^{2+} allows relatively short stretches of polypeptide chain to fold into stable unites that can interact with nucleic acids. It is worth mention that a correct selection regarding to the kind of metal ions play a vital role in the biological system. This means the metal ions such as M^{2+}, which coordinate strongly to Met and bild macrochelate is not suitable for right application of metal-ligand interactions in biological systems. For a successful design of identical metal-ligand complexes with similar or better function, such as new drugs, the right selection of both components is significant.

REFERENCES

[1] L. Stryer, (1995) Biochemistry, 4th Edition, W.H. Freeman Company, New York.

[2] Bill, G., Rick, H., Ken, W. and Thomas, O.B. (2003) The biology project. Department of Biochemistry and Molecular Biophysics, University of Arizona.

[3] Suzukin, O. and Navarin, M.S. (1965) *Antibiotiki*, **6,** 562.
[4] Davis, D.A., *et al.* (2000) *Biochemical Journal*, **342(2)**, 305-311.
[5] IUPAC-IUBMB Joint Commission on Biochemical Nomenclature. Nomenclature and symbolism for amino acids and peptides. *Recommendations on Organic & Biochemical Nomenclature, Symbols & Terminology etc.*, 17 May 2007.
[6] Nelson, D.L. and Cox, M.M. (2000) Lehninger, principles of biochemistry, 3rd Edition, Worth Publishing, New York.
[7] Martel, A.E. (2006) Critical stability constants of metal complexes, **26**, Plenum Press, New York.
[8] Sajadi, S.A.A., Alamolhoda, A.A. and Alavi, A.N. (2009) Scientica Iranica, in Press.
[9] Handbook of Chemistry & Physics 55, D-129, 1975.
[10] Miranda, J.L. and Felcman, J. (2003) Polyhedron, **22(2)**, 225-233.
[11] Felcman, J. and Miranda, J.L. (1997) *Journal of Brazilian Chemical Society*, **8**, 575.
[12] IUPAC Stability Conatants Database, Release 3, version 3.02, (1998) coplied by Pettit, L.D. and Powel, H.K.J. Academic Software Timble, UK.
[13] Sigel, H., Zuberbuehler, A.D. and Yamauchi, O. (1991) *Analytica Chimica Acta*, **255**, 63.
[14] Ali, S., Sajadi, A., Song, B. and Sigel, H. (1998) *Inorganica Chimica Acta*, **283,** 193-201.
[15] Sajadi, S.A.A., Song, B., Gregan, F. and Sigel, H. (1999) *Inorganica Chimica*, **38(3)**, 439-448.
[16] Sajadi, S.A.A., Song, B., Gregan, F. and Sigel, H. (1997) *Bulletin of the Chemical Society of Ethiopia*, **11(2)**, 121-130.
[17] Voet, D. (1997) *Biochemistry*, John Wiley, 560.
[18] Volshtein, L.M. Krylova, L.F. and Mogilevkina, M.F. (1967) *Russian Journal of Inorganic Chemistry*, **12**, 832.
[19] Warren, R.C., McConnell, J.F. and Stephenson, N.C. (1970) *Acta Crystallographica*, **B26**, 1402.
[20] Freeman, H.C. and Golomb, M.L. (1970) *Chemical Communications*, 1523.
[21] Bear, C.A. and Freeman, H.C. (1976) *Acta Crystallographica*, **B32**, 2534.

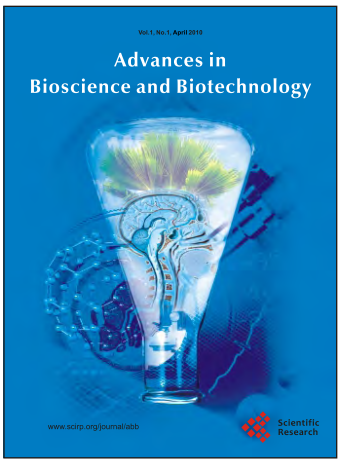

Call for Papers

Advances in Bioscience and Biotechnology (ABB)

http://www.scirp.org/journal/abb

ABB is an international journal dedicated to the latest advancement of biosciences. The goal of this journal is to provide a platform for scientists and academicians all over the world to promote, share, and discuss various new issues and developments in different areas of biosciences. All manuscripts must be prepared in English, and are subject to a rigorous and fair peer-review process. Accepted papers will immediately appear online followed by printed hard copy.

Editor-in-Chief

Prof. Jinfu Wang Zhejiang University, China

Editorial Board

Subject Coverage

This journal invites original research and review papers that address the following issues in materials sciences and applications. Topics of interest include, but are not limited to:

- Biochemistry
- Botany
- Cytobiology
- Developmental Biology
- Ecology
- Genetics
- Inorganic and Analytic Chemistry
- Microbiology
- Molecular Biology
- Neurobiology
- Organic Chemistry
- Physics
- Zoology

We are also interested in short papers (letters) that clearly address a specific problem, and short survey or position papers that sketch the results or problems on a specific topic. Authors of selected short papers would be invited to write a regular paper on the same topic for future issues of the ***ABB***.

Notes for Intending Authors

Submitted papers should not have been previously published nor be currently under consideration for publication elsewhere. Paper submission will be handle electronically through the website. All papers are refereed through a peer review process. Authors are responsible for having their papers checked for style and grammar prior to submission to ABB. For more details about the submissions, please access the website.

Website and E-Mail

http://www.scirp.org/journal/abb **E-mail: abb@scirp.org**

Advances in Bioscience and Biotechnology, 2010, 1, 1-59
Published Online April 2010 in SciRP (http://www.SciRP.org/journal/abb/).

TABLE OF CONTENTS

Volume 1 Number 1 **April 2010**

9771833171009 01